CHARACTERIZATION OF GRANULAR MATERIALS AND COMPACTION METHODS AND APPLICATION IN DESIGN OF TRANSPORTATION INFRASTRUCTURE

A Dissertation

by

POURA ARABALI

Submitted to the Office of Graduate and Professional Studies of
Texas A&M University
in partial fulfillment of the requirements for the degree of

DOCTOR OF PHILOSOPHY

Chair of Committee,	Robert L. Lytton
Committee Members,	Dallas Little
	Charles Aubeny
	Willa Chen
Head of Department,	Robin Autenrieth

December 2020

Major Subject: Civil Engineering

ABSTRACT

In this study, the characterization of soils and granular materials and their variation with the compaction method is investigated. Impact hammer compaction is the most prevalent method for sample fabrication of granular materials in the laboratory. Factors such as low precision of unconfined strength test and the presence of interface between layers can be downsides of this compaction method. In this research, an alternative laboratory compaction method for granular materials is proposed and studied. The effects of using Superpave gyratory compactors (SGC) on the compaction and engineering properties of unbound granular materials used in transportation infrastructure is investigated. An experimental program is performed on the specimens compacted with both the gyratory compactor and impact hammer. Unconfined compressive strength tests are conducted to investigate whether using gyratory compaction can improve the precision of this test. Furthermore, maximum dry density and optimum moisture content are determined from each compaction technique. Statistical analyses are also performed on the experimental results to compare maximum dry density, optimum moisture content, and compressive strength in the studied materials. Permanent deformation and resilient modulus testing and modeling, as pavement performance-related characteristics used in the mechanistic-empirical design of pavements, are performed on the specimens fabricated with these two procedures. Variation of these characteristics with the compaction method is studied. Moreover, filter paper test to measure the soil suction, laser particle size analyzer to obtain percent of fines content, Percometer to measure dielectric constant,

Methylene blue test, and Aggregate Imaging System (AIMS) tests are used. Therefore, the effects of material properties and compaction method are both investigated on the engineering behavior. The resilient modulus model incorporating suction, moisture conditions, and stress states is studied. Moreover, prediction models for the coefficients of the resilient modulus model are developed using the performance-related properties. The prediction models for the coefficients of the permanent deformation model are also developed using the performance related properties. Additionally, an equation for estimation of compaction energy is also developed to quantify the compaction effort required using gyratory compactor, that reveals substantial difference between base course materials. The results generally have shown that gyratory compactor produces a different mechanism of compaction from the impact hammer compaction. Furthermore, the prediction of conditions of granular materials using non-destructive testing techniques is investigated using the suction and dielectric constant. CT scanning also captures the difference between structure of the specimens compacted with the two methods.

DEDICATION

To my parents and family,

who believed in me and always supported me in my education.

And to my advisor, Dr. Robert Lytton, who guided me towards critical and creative thinking, and for his endless support, advice, patience, and his dedication to the students' learning and professional development.

ACKNOWLEDGEMENTS

I would like to express my sincere gratitude to Dr. Robert Lytton, my academic advisor and committee chair for his constant guidance, advice, and support throughout my doctorate degree education. Also, I would like to thank my committee members, Dr. Dallas Little, Dr. Charles Aubeny, Dr. Willa Chen, and special appointment, Dr. David Newcomb, for their guidance and advice throughout the course of this research. Moreover, I take this opportunity to express my sincere thanks to members of the research group of our project at Texas A&M Transportation Institute (TTI), Mr. Stephen Sebesta, Dr. Sang Ick Lee, and Dr. Maryam Sakhaeifar for their support and guidance through this research, especially in the experimental data collection efforts.

Moreover, I would like to express my deepest gratitude to knowledgeable TTI researchers, Dr. David Newcomb, Dr. Sheng Hu, Dr. Charles Gurganus, and Mr. Tom Freeman, for their support and advice throughout my Ph.D. education in several different projects.

Thanks also go to the department leadership, faculty, staff and my friends and colleagues for their support and making my time at Texas A&M University a unique experience. Finally, thanks to my parents and family for their endless support, patience, and devotion.

CONTRIBUTORS AND FUNDING SOURCES

Contributors

This work was supervised by a dissertation committee consisting of Professor Robert Lytton of Zachry Department of Civil and Environmental Engineering as the committee chair, Professor Dallas Little and Professor Charles Aubeny from Zachry Department of Civil and Environmental Engineering, Professor Willa Chen from Department of Statistics, and special appointment, Dr. David Newcomb form the Texas A&M Transportation Institute.

Funding Sources

Graduate study was supported by graduate assistantship from Texas A&M University System, Texas A&M Transportation Institute, and Texas A&M University, and also awards and scholarships from the Association of Former Students of Texas A&M University.

TABLE OF CONTENTS

Page

LIST OF FIGURES

Page

LIST OF TABLES

Page

1. INTRODUCTION

1.1. Background

Compaction tests need to be conducted in the laboratory prior to their application in the field in order to determine the maximum dry density (MDD) and optimum moisture content (OMC) of granular materials [1]. Several compaction techniques have been used to compact soils and base materials in the laboratory, including static, vibratory, impact, and kneading compaction. Impact compaction has been the most prevalent laboratory compaction technique for soils and granular materials for a long time. It was the first laboratory compaction technique with standardized testing procedures. The standard Proctor test was developed in the early 1930s for building earth dams [2]. Standard and modified Proctor compaction tests have been used for compaction of soils with the impact hammer in AASHTO T99 and AASHTO T180. However, the unconfined compressive strength test may not have sufficient precision in the specimens prepared with the impact hammer [3]. Thus, the specimens made with the impact compaction method may not provide the desirable repeatability and reproducibility in the strength test.

Another issue with the impact hammer compaction is layer interface between the lifts. The materials are compacted in several layers, resulting in layer interface barriers. Higher air void contents exist at the interface between layers [3]. It can adversely affect the strength test results. Non-uniform distribution of air voids and poor bonding between

layers may lead to stress concentration. Another concern is that the impact hammer compaction method may result in misrepresentative samples for some materials for the performance tests conducted based on the mechanistic-empirical (M-E) pavement design guide. Therefore, taking into account the concerns and downsides of the impact hammer compaction, interest remains in the development of alternative methods for compaction of granular materials in the laboratory.

Gyratory Compaction can be an option for laboratory compaction of unbound granular materials. Superpave gyratory compactor (SGC) has been widely used in asphalt industry in the recent years for the laboratory compaction of asphalt concrete mixtures based on the Superpave asphalt mix design and Strategic Highway Research Program (SHRP) [4, 5]. In this compaction method, compaction takes place through simultaneous action of compressive pressure exerted on the materials and shear forces created by the gyration of the mold about its vertical axis. It is worth noting that many laboratories in this field already have a gyratory compactor for their asphalt concrete applications. Thus, those who would like to use the gyratory compaction for soils and base materials may not need to purchase a separate machine.

Literature about using the gyratory compactor for the compaction of soils and base materials is sparse. Satisfactory results with using SGC were observed in some of these limited research works. Some studies concluded that gyratory compaction could simulate field compaction more accurately than the impact compaction [6, 7, 8]. Normal pressure induced on the materials along with the self-adjusting kneading action generated in the gyratory compaction simulates the loading of the moving traffic exerted

on the pavement [6, 9]. Ping et al. [6] evaluated the laboratory and field compaction, implementing both the impact and gyratory compaction methods for sandy soils. They concluded that the gyratory compaction leads to more dependable results than the impact compaction in the laboratory with regard to moisture- dry density relations [6]. Li et al. [9] implemented gyratory compactor to investigate the relations between water content, density, compaction energy, and shear forces in geomaterials. That research concluded that gyratory compaction could produce higher values of dry density than the impact compaction [9]. Mokwa et al. [10] carried out a feasibility study into the implementation of the gyratory compactors for soils. The incentive of that study was that only impact loading is the compaction force in the modified Proctor test in the laboratory, while a combination of vertical pressure, vibration, and kneading lead to the soil compaction in the field. Mokwa et al. [10] concluded that the MDD in the moisture-density curves obtained from the gyratory compaction is not very different from the MDD determined from the standard and modified Proctor tests. They also found that the most effective method for increasing the density of non-cohesive granular materials is raising the number of gyrations. However, increasing the normal pressure is the most effective way of boosting the density of fine-grained soils [10].

Compaction method may affect the engineering characteristics and behavior of the granular materials, since different forces and motions take place in the gyratory and impact compaction. An experimental program is required to investigate the gyratory compaction and compare the results between the SGC and the impact hammer compaction. Precision and variability of unconfined strength test between the specimens

prepared with the impact hammer and SGC can be compared. One of the main objectives of this research is to investigate if the compaction with SGC results in higher precision in the unconfined strength test compared to the impact compaction. Furthermore, moisture dry density curves can be compared between these two methods. Statistical analysis can be conducted on the Maximum dry density and optimum moisture content results. Moreover, the performance-related properties of the unbound materials in the specimens compacted with both of the compaction methods can be studied. Rutting or permanent deformation is one of the major pavement distresses which may occur in unbound flexible base courses. Thus, one of the significant characteristics in the assessment and prediction of pavement performance is the permanent strain of geomaterials [11]. There are different models and methods for prediction of the permanent strain of granular materials under load repetitions, including Tseng-Lytton model [12], mechanistic-empirical pavement design guide (MEPDG) model [13, 14], VESYS model [15], and Korkiala-Tanttu analytical-mechanistic calculation method [16].

Furthermore, the resilient modulus is the primary property of unbound materials used in the M-E pavement design [13, 14] for prediction of pavement responses to the loading. It is defined as the ratio of the maximum cyclic axial stress to the recoverable strain in one load cycle in a repeated loading. In this study, the permanent deformation and resilient modulus of the specimens compacted with the two compaction methods were investigated. Repeated load triaxial tests were conducted to study these behaviors. Two resilient modulus models were used to predict the resilient modulus using the

experimental data obtained from the repeated load triaxial tests and regression analysis. These models will be introduced in the next chapters.

Moreover, in order to more accurately predict the engineering properties of materials and estimate the regression coefficients of the prediction models of engineering characteristics, repeatable and performance-related properties of the materials were studied, obtained and applied. Methylene blue value (MBV) and percent fines content (PFC) can be used to characterize the fine particles of the granular materials [17, 18]. Methylene blue test and the test for measurement of PFC can be used to characterize the type and amount of moisture active clays in soils [17, 18, 19]. PFC is the output of the test with a laser particle size analyzer.

In addition, measurement of soil suction, matric suction, and total suction has proven to be a relatively difficult task [20]. It can be measured through experimental methods or can be predicted by available equations. Soil suction can be measured through filter paper test or pressure plate test. Filter paper test is described in more details in later sections in this chapter.

1.2. Objectives

The main objective of this research is characterization of granular materials and their variation with the compaction method, and to propose a robust method of laboratory compaction and sample fabrication for granular materials utilized in the transportation infrastructure. Considering the concerns with the impact compaction as a traditional and prevalent method, the application of Superpave gyratory compactor

(SGC) for granular materials may result in a more suitable method of compaction and sample fabrication in the laboratory. For this purpose, the effects of gyratory compaction of unbound granular materials on engineering properties and behavior of materials are investigated. An experimental program is conducted on the materials compacted with both the new and traditional methods. Comparing the results of the experiments and using statistical analyses, it can be found whether the impact hammer and gyratory compaction are similar in their results. Moreover, the performance-related material properties used in the M-E pavement design such as resilient modulus and permanent deformation are investigated. Therefore, the effects of compaction method and material characterization on the pavement performance and design can be investigated. The experimental program is also conducted regardless of the fabrication method to measure the material properties, which are not dependent on the compaction method, and investigate the engineering behavior. Thus, the effect of both material properties and compaction technique can be investigated on the engineering behavior of materials. Prediction models to estimate the model parameters, used in the predictive models of material characteristics such as resilient modulus and the permanent deformation, are developed. These models can be dependent on performance-related properties, not just empirical results. Furthermore, another objective is to determine if the compaction with SGC can give a practical estimate of the level of compaction effort or energy required to compact different materials up to the determined targets. Moreover, the non-destructive testing was performed using Computed Tomography (CT) scanning and Percometer. CT scanning assists with understanding and comparison of the internal structure of the

unbound materials in both the gyratory and impact hammer compaction methods. Dielectric constant of soil and granular materials is measured with the Percometer, and the suction is measured with the filter paper test. This measured data along with the form of equation accounting for the relationship between these two properties test can lead to find the relation between these properties for the studied material. Then, these relationships can be used to estimate the conditions of the soil and other properties by having the data from the nondestructive evaluation techniques.

2. PERFORMANCE RELATED PROPERTIES OF GRANULAR MATERIALS AND EXPERIMENTAL PLAN

2.1. Background

This chapter discussed the application of gyratory compactor for compaction of soils and unbound granular materials. The performance related propertied of unbound granular materials are discussed. This chapter describes the experimental program, equipment, and materials, implemented in this study. The Compressive strength test, moisture dry density curve, permanent deformation, resilient modulus, suction and soil water characteristic curve are discussed. The experimental program also includes the nondestructive testing used in this study, which are the CT Scanning, and the measurements of dielectric constant.

There are different models for prediction of the permanent strain of granular materials under load repetitions including Tseng-Lytton model [12], mechanistic-empirical pavement design guide (MEPDG) model [13, 14], UIUC model [21], VESYS model [15], and a recently proposed mechanistic empirical rutting model incorporating stress state [22].

In this study, the permanent deformation and resilient modulus of the specimens compacted with the two compaction methods were investigated, and repeated load triaxial tests were conducted. Tseng Lytton model and VESYS models were used for regression analysis on the experimental data of the permanent strain obtained from

repeated triaxial loads. In order to characterize and predict the resilient modulus of these materials, the generalized model [13, 14], which is one of the most popular resilient modulus models, was used for fitting the experimental data of resilient modulus.

Additionally, another model of resilient modulus [18, 23] which incorporates both moisture conditions, suction, and stress states can be applied and the model coefficients were investigated. This model and the coefficients are discussed later in next chapter.

Methylene blue test and the laser particle analyzer test to measure the PFC were used to characterize the type and amount of fine particles and moisture active clays in soils [18, 17, 19]. PFC, as the output of a laser particle size analyzer, was used to detect the physical distribution of fine particle sizes. Therefore, the laser particle size analysis is used to provide the particle size distribution of fine particles from smallest to largest particle dimension. PFC is defined as the ratio of the amount of particles smaller than 2 μm to the particles passing sieve no. 200 (75 μm) [19].

Methylene blue has a big organic polar molecule with a positive charge. The negatively charged surfaces of clay minerals can adsorb this molecule [17]. The amount of adsorbed Methylene blue varies depending on the surface area of clay particles in the granular materials. If a higher amount of methylene blue is adsorbed to the clay particles, the Methylene blue solution becomes brighter [17]. Thus, the change in the color of the Methylene blue solution can be associated with the adsorbed methylene blue [17]. Therefore, the evaluation of the color change of the solution can be an indication of

the surface area of the clay particles. There are some traditional methods for performing methylene blue tests. The method described in ASTM C 837, used to determine the amount of active clay in fine-grained materials, has an empirical criterion. The traditional method specified in AASHTO T 330, used for qualitative identification of harmful clay particles of Smectite category, is time-consuming and special training [17]. A more recent Methylene blue test method proposed by W.R. Grace Corporation was used to determine the MBV of the granular materials [11, 18, 17], which has high repeatability and reproducibility [11, 18].

Soil suction was also investigated for the samples prepared with the gyratory compactor and the impact hammer. Filter paper was performed to measure the suction of these two series of samples. Soil water characteristic curves (SWCC) were also developed for the experimental data obtained from the filter paper test using the least mean square error. The difference between these two series of curves for these two compaction methods was investigated. Filter paper test is described in this chapter. Moreover, Aggregate Imaging System (AIMS) tests were performed to obtain the shape properties of the aggregates in the soil structure. Angularity, surface texture, and the sphericity were used and studied in this research. The Weibull distribution of these properties was also studied. The effect of the angularity, surface texture, and the sphericity on the behavior materials can be investigated.

2.2. Data Collection

The materials studied in this research and the SGC machine used for compacting and fabricating specimens of granular materials as well as the laboratory experiments are described in the following section. The tests are conducted on the specimens compacted with both the impact hammer and gyratory compactor. The results were compared between the samples fabricated with the gyratory compactor and the impact hammer.

2.3. Materials

In this study, six different unbound materials from different parts of Texas are used. The materials include five base materials and one subgrade soil. Base materials are named based on their location as Pharr, Waco, San Antonio, Atlanta, and Amarillo base materials, and the soil is US 82 subgrade soil. The particle size distribution of the studied base materials is shown in Figure 1. Physical properties and Atterberg limits of the studied materials are presented in Table 1. Many standards and specifications recommend that the plasticity of base and subbase course materials needs to be less than 6% [24]. All of the base materials studied in this research meet this recommendation. Pharr material is classified as sand based on the Unified Soil Classification System (USCS). Waco, San Antonio, Atlanta, and Amarillo are classified as gravel based on the USCS.

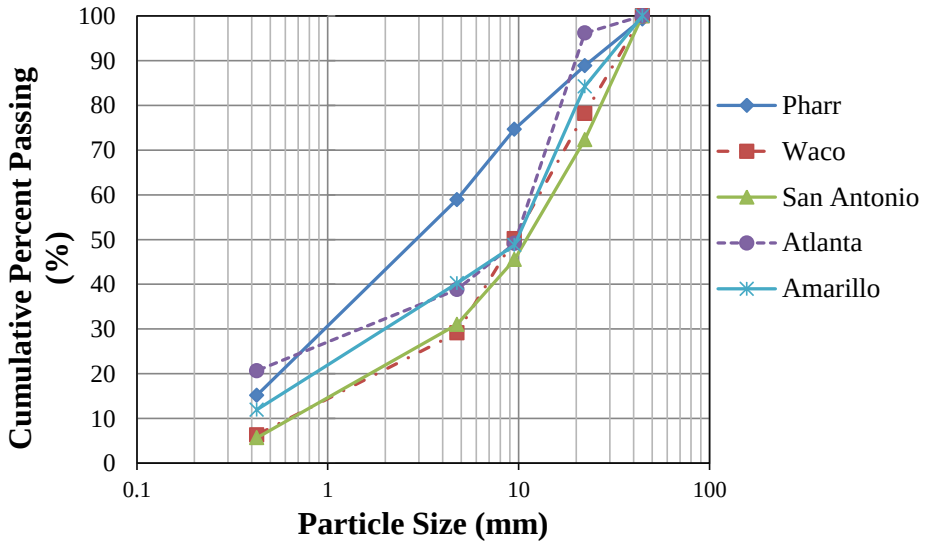

Figure 1. Particle Size Distribution in the Studied Base Course Materials

The specimens of the base materials prepared with the gyratory compaction have a diameter of 150 mm (5.91 in) and a height of 200 mm (7.87 in.). The specimens compacted with the impact hammer have 152.4 mm (6 in.) diameter and 203.2 mm (8 in.) height. The specimens of the subgrade material made with the impact hammer have 101.6 mm (4 in.) diameter and 152.4 mm (6 in.) height [25]. The specimens of the subgrade soil made with the gyratory compaction have 100 mm (3.94 in) diameter and 150 mm (5.91 in.) height.

Table 1. Physical Properties and Atterberg Limits of the Studied Materials

Material	Subgrade Soil	Pharr Base	Waco Base	Atlanta Base	Amarillo Base	San Antonio Base
Liquid Limit (%)	52.0	25.5	26.6	14.0	12	16.0
Plasticity Index (%)	33.0	4.8	5.8	2.5	N.A.	0.4
Main Term of Soil Classification based on USCS	Clay (C)	Sand (S)	Gravel (G)	Gravel (G)	Gravel (G)	Gravel (G)
Type of Fine Particles based on Atterberg Limits	CH	CL-ML	CL-ML	ML	Non-plastic	ML

2.4. Superpave Gyratory Compactor

The gyratory compactor used in this study is shown in Figure 2. Compaction parameters such as the angle of gyration and normal pressure can be changed by users in this machine. Users are able to set the angle of gyration from 0 to 1.5 degree and consolidation pressure from 200 to 999 kPa. Gyration rate is 30 gyrations per minute. In this study, the compaction pressure was initially set to 600 kPa. If a specimen did not reach the specified height after the maximum gyration number in the SGC, a new sample was compacted with an increased compaction pressure with the increment of 100 kPa. The consolidation pressure of 600 kPa has been used for compaction of Waco, Atlanta, Amarillo, and subgrade materials. The consolidation pressure of 800 kPa has been used for compaction of San Antonio and Pharr materials. The gyration angle is set to 1.25

degree for compaction of base materials with the mold diameter of 150 mm. The gyration angle is set to 1.16 degree for compaction of subgrade material with the mold diameter of 100 mm. Steps of application of gyratory compactor for compaction of granular materials are demonstrated in Figure 3.

Figure 2. Superpave Gyratory Compactor Used in this Research for Compaction of Granular Materials

(1)

(2)

(3)

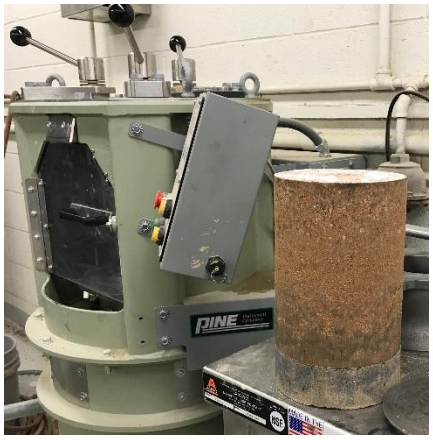

(4)

Figure 3. Steps of Compaction of Unbound Granular Materials using Gyratory Compactor

2.5. Compressive Strength Test

Unconfined compressive strength test was performed on the materials studied in this study. Both types of specimens compacted with the gyratory compactor and impact hammer are tested. This test was carried out based on Tex-117-E standard test procedure [26]. Variability and precision of the strength test results can be evaluated and compared between the samples made with the two compaction methods [25, 27]. Eight replicates were tested for each type of material while four replicates were tested for each compaction method. The precision of a test method allows the users of each method to evaluate its functionality and application in terms of variability and scatter of the test results [28, 29]. Statistical analysis for the equality of variance has been performed for comparison of the variance of the test data between these two sets of specimens. For this purpose, F-test on the pooled variance [30] has been conducted in this study.

2.6. Moisture- Dry Density Curves

Compaction tests were performed to obtain the maximum dry density (MDD) and optimum moisture content (OMC) for all of the materials for both the gyratory and impact hammer compaction methods [25, 27]. The test with impact hammer compaction was conducted based on Tex-113-E [31] and Tex-114-E [32] standard test procedures. Using the experimental data points, the OMC and MDD were found based on the tools implemented in the referred standard test methods of the Texas Department of Transportation. Statistical analyses have been conducted to investigate the effect of compaction method on the OMC and MDD [25, 33]. The objective of the statistical

analysis has been to investigate whether the OMC and MDD of the specimens determined from the SGC and impact hammer compaction are equivalent or different. Paired t-test has been conducted for this purpose.

2.7. Repeated Load Triaxial Tests for Characterization of Permanent Deformation

Repeated load triaxial tests were performed on four different base course materials in order to characterize their mechanical behavior in terms of permanent deformation and resilient modulus. The triaxial tests were performed on both of the specimens compacted with the gyratory compactor and impact hammer. A top-loading closed loop electro-hydraulic testing machine was used for these cyclic loading tests.

The cyclic axial loading had a haversine shaped load pulse with a loading period of 0.1 second and a rest period of 0.9 second. In preconditioning for permanent deformation test, 100 of axial load repetitions were applied with a confining pressure of 103.42 kPa (15 psi) and axial cyclic stress of 20.68 kPa (3 psi) while the contact stress was 20.68 kPa (3 psi). Therefore, the maximum axial stress in preconditioning was 41.37 kPa (6 psi). Then, the specimens were subjected to 10,000 cycles of axial load with the confining pressure of 68.95 kPa (10 psi) and axial cyclic stress of 137.90 kPa (20 psi) in the permanent deformation test, where the contact stress was 20.68 kPa (3 psi). Therefore, the maximum axial stress was 158.58 kPa (23 psi). Both sets of specimens made with the gyratory compactor and impact hammer have the diameter to height ratio of 0.75. The experimental data for permanent deformation test have been fitted with the

Tseng-Lytton model [12] and VESYS model [15] for the prediction of the permanent strain of the materials. Computation of plastic deformations in MEPDG is based on the model originally developed by Tseng and Lytton to calculate the permanent deformation of the aggregate layers with thickness *t* in the pavement structure [13, 34].

2.8. Repeated Load Triaxial Test for Measurement of Resilient Modulus

The resilient modulus is the primary property of unbound materials used in the M-E pavement design [13, 14] for prediction of pavement responses to the loading. It is defined as the ratio of the maximum cyclic axial stress to the recoverable strain in one load cycle in a repeated loading. In this study, the permanent deformation and resilient modulus of the specimens compacted with the two compaction methods are investigated, and repeated load triaxial tests are conducted. In order to characterize and predict the resilient modulus of these materials, the generalized model [13, 14], and Lytton Model incorporating both the moisture conditions and stress states [18], can be used for fitting the experimental data of resilient modulus.

As mentioned before, repeated load triaxial tests were performed for four of the base course materials in order to investigate the resilient modulus. Similar to the permanent deformation test, these tests were conducted on both of the specimens compacted with the gyratory compactor and impact hammer. These tests were performed in a top-loading closed loop electro-hydraulic machine. The cyclic axial loading had a haversine shaped load pulse with a loading period of 0.1 second and a rest period of 0.9 second. In this study, standardized test procedure and loading sequences in the National

Cooperative Highway Research Program (NCHRP) 1-28A [14] were applied for the resilient modulus tests. Therefore, the confining pressure, contact stress, cyclic stress, maximum stress, and number of load repetitions in the 30 applied loading sequences were set based on this test procedure. The loading sequences and stress states used in this study are presented in Table 2.

Specimen dimensions are similar to the ones used in the permanent deformation test. The generalized model developed in NCHRP 1-37A [13] has been used to characterize and predict the resilient modulus of these materials. The proposed resilient modulus model [18, 23] incorporating both moisture dependent and stress-dependent behavior of resilient modulus was also applied. The prediction models may be developed for the prediction of the model parameters based on the materials performance base properties.

Table 2. Loading Sequences for the Repeated Load Triaxial Test used in This Study for Resilient Modulus Testing

Sequence No.	Confining Pressure		Contact Stress		Axial Cyclic Stress		Maximum Axial Stress		No. of Load Repetitions
	kPa	psi	kPa	psi	kPa	psi	kPa	psi	
Pre-conditioning	103.5	15	20.7	3	207	30	227.7	33	1000
1	20.7	3	4.1	0.6	10.4	1.5	14.5	2.1	100

Table 2. Continued

Sequence No.	Confining Pressure		Contact Stress		Axial Cyclic Stress		Maximum Axial Stress		No. of Load Repetitions
	kPa	psi	kPa	psi	kPa	psi	kPa	psi	
2	41.4	6	8.3	1.2	20.7	3	29	4.2	100
3	69	10	13.8	2	34.5	5	48.3	7	100
4	103.5	15	20.7	3	51.8	7.5	72.5	10.5	100
5	138	20	27.6	4	69	10	96.6	14	100
6	20.7	3	4.1	0.6	20.7	3	24.8	3.6	100
7	41.4	6	8.3	1.2	41.4	6	49.7	7.2	100
8	69	10	13.8	2	69	10	82.8	12	100
9	103.5	15	20.7	3	103.5	15	124.2	18	100
10	138	20	27.6	4	138	20	165.6	24	100
11	20.7	3	4.1	0.6	41.4	6	45.5	6.6	100
12	41.4	6	8.3	1.2	82.8	12	91.1	13.2	100
13	69	10	13.8	2	138	20	151.8	22	100
14	103.5	15	20.7	3	207	30	227.7	33	100
15	138	20	27.6	4	276	40	303.6	44	100
16	20.7	3	4.1	0.6	62.1	9	66.2	9.6	100
17	41.4	6	8.3	1.2	124.2	18	132.5	19.2	100
18	69	10	13.8	2	207	30	220.8	32	100
19	103.5	15	20.7	3	310.5	45	331.2	48	100

Table 2. Continued

Sequence No.	Confining Pressure		Contact Stress		Axial Cyclic Stress		Maximum Axial Stress		No. of Load Repetitions
	kPa	psi	kPa	psi	kPa	psi	kPa	psi	
20	138	20	27.6	4	414	60	441.6	64	100
21	20.7	3	4.1	0.6	103.5	15	107.6	15.6	100
22	41.4	6	8.3	1.2	207	30	215.3	31.2	100
23	69	10	13.8	2	345	50	358.8	52	100
24	103.5	15	20.7	3	517.5	75	538.2	78	100
25	138	20	27.6	4	690	100	717.6	104	100
26	20.7	3	4.1	0.6	144.9	21	149	21.6	100
27	41.4	6	8.3	1.2	289.8	42	298.1	43.2	100
28	69	10	13.8	2	483	70	496.8	72	100
29	103.5	15	20.7	3	724.5	105	745.2	108	100
30	138	20	27.6	4	966	140	993.6	144	100

2.9. Percent Fines Content (PFC)

In order to more accurately predict the engineering properties of materials and estimate the regression coefficients in the prediction models of engineering characteristics, repeatable and performance-related properties of the materials can be studied and applied. Methylene blue value (MBV) and percent fines content (PFC) can

be used to characterize the fine particles of the granular materials [17, 18]. Methylene blue test and the test for measurement of PFC can be used to characterize the type and amount of moisture active clays in soils [18, 17, 19]. PFC, as the output of a laser particle size analyzer, can be used to detect the physical distribution of fine particle sizes. Therefore, the laser particle size analysis is used to provide the particle size distribution of fine particles from smallest to largest particle dimension. PFC is defined as the ratio of the amount of particles smaller than 2 μm to the particles passing sieve no. 200 (75 μm) [19]:

$$PFC = \frac{\%\ smaller\ than\ 2\ micron}{\%\ passing\ 75\ micron} \times 100 \quad (2\text{-}1)$$

As mentioned before, a laser particle size analysis was used to generate the particle size distribution of the fine particles from the smallest to largest particle dimension. In this test, a sample of materials smaller than sieve No. 200 (75 μm) is tested. A suspension of particles passing sieve No. 200 mixed with water is inserted into laser analyzer, as shown in Figure 4. The fine particles suspended in the solution are detected by the scattering laser. Then, a particle size distribution is generated and the curve for plotting cumulative percent passing versus each size is also produced [18, 17, 19]. Percent fines content (PFC) is defined as the ratio of the amount of the particles smaller than 2 μm to the amount of particles passing sieve no. 200 (smaller than 75 μm) [19].

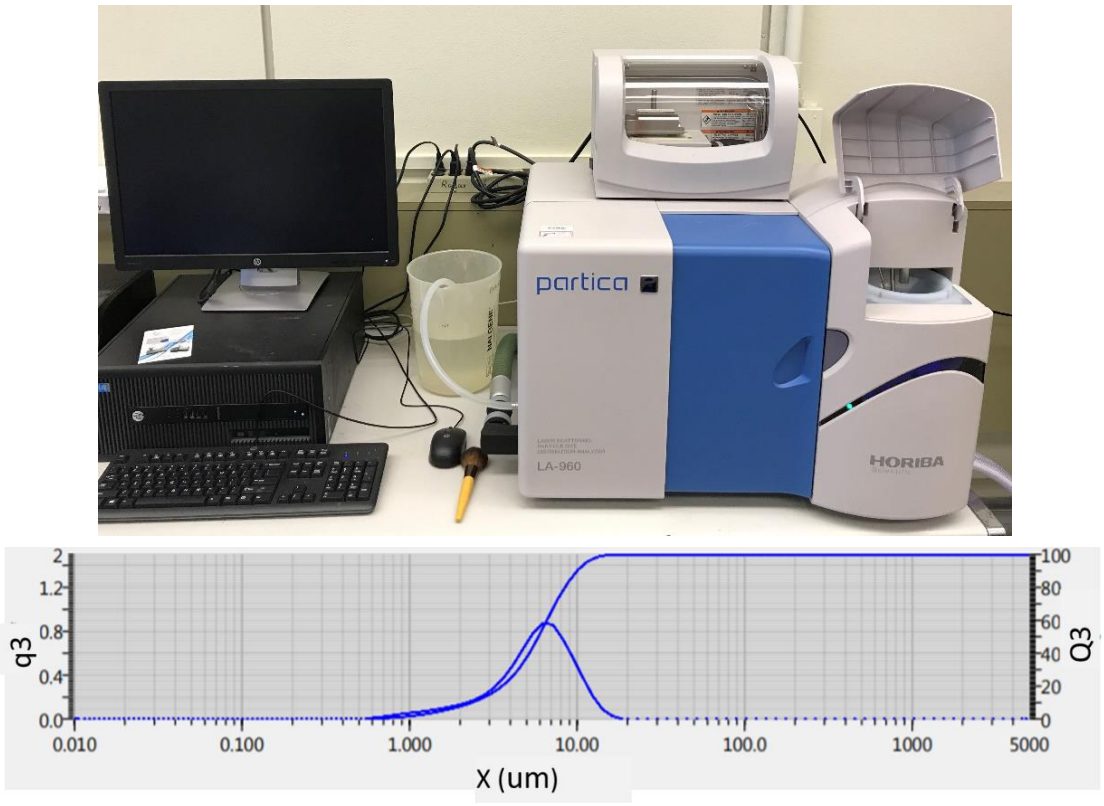

Figure 4. Laser Particle Size Analyzer Used in This Study and Sample Produced Data

2.10. Methylene Blue Test

Methylene blue value (MBV) and percent fines content (PFC) can be used to characterize the fine particles of the granular materials [17, 18]. Methylene blue test and the test for measurement of PFC can be used to characterize the type and amount of moisture active clays in soils [18, 17, 19]. Methylene blue has a big organic polar molecule with a positive charge. The negatively charged surfaces of clay minerals can

adsorb this molecule [17]. The amount of adsorbed Methylene blue varies depending on the surface area of clay particles in the granular materials. If a higher amount of methylene blue is adsorbed to the clay particles, the Methylene blue solution becomes brighter. Thus, the change in the color of the Methylene blue solution can be associated with the adsorbed methylene blue [17]. Therefore, the evaluation of the color change of the solution can be an indication of the surface area of the clay particles. There are some traditional methods for performing methylene blue tests. The method described in ASTM C 837, used to determine the amount of active clay in fine-grained materials, has an empirical criterion. The traditional method specified in AASHTO T 330, used for qualitative identification of harmful clay particles of Smectite category, is time-consuming and requires special training [17]. A more recent Methylene blue test method proposed by W.R. Grace Corporation can be used to determine the MBV of the granular materials [11, 18, 17], which has high repeatability and reproducibility [11, 18].

As mentioned before, the evaluation of the color change of the Methylene blue solution can be an indication of the surface area of the clay particles. The more recent Methylene blue test method proposed by W.R. Grace Corporation which has high repeatability and reproducibility [11, 18] is used to determine the Methylene Blue Value (MBV) of the granular materials [11, 18, 17]. The MBV of particles is determined using a colorimeter device [17]. This method is inexpensive, repeatable, and fairly simple. The color change of the methylene blue solution can be evaluated based on the principle of Beer's Law, using the colorimeter [17].

A sample size of 20 g of particles passing sieve size No. 4 is initially used in this test. This amount of materials is added to 30 ml of methylene blue solution in a plastic tube [17, 18]. This sample is shaken and mixed using a shaking machine for one minute. It is left for three minutes and shaken again for one more minute. Then, this solution is passed through a 2 μm filter. Subsequently, 130 ml of the filtered solution is mixed with the distilled water until the amount of total solution reaches 45 ml. Then, this solution is placed in a glass tube connected to the colorimeter. The MBV value is measured using the colorimeter. If the MBV value is less than 7 mg/g, then the measurement is valid. If the MBV value is higher than 7 mg/g, then the initial sample size needs to be reduced to 10 g [17].

This methylene blue test can be used to detect the plastic and non-plastic fines in soils. Fine particles are categorized into plastic and non-plastic fines based on their specific surface area (SSA). The MBV from Methylene blue test can distinguish these fine particles at a critical MBV of 7 mg/g [17].

2.11. Suction and Soil Water Characteristic Curve

The most significant state variables for the behavior of unsaturated soils are effective (net) stress ($\sigma - u_a$), and the matric suction (u_a - u_w). Soil suction is the state variable with the highest relevance to the mechanics of unsaturated soils [20]. Soil suction, which relates the moisture conditions in the soil to the engineering behavior is referred to the free energy state of the soil moisture [17]. Soil suction can refer to matric suction, osmotic suction, or total suction. One primary difference between the behavior

of saturated and unsaturated soils is that the relationship between soil suction and moisture content needs to be established in the unsaturated soils. The relationship between water content and soil suction is the soil-water characteristic curve (SWCC). SWCC is a function applied for the evaluation of the properties of unsaturated soils [20]. Combining soil suction and moisture content, SWCC can be used to estimate different parameters applied in describing the behavior of unsaturated soils [20, 35].

Measurement of soil suction, matric suction, and total suction has proven to be a difficult task [20]. It can be measured through experimental methods or can be predicted by available equations. Soil suction can be measured through filter paper test or pressure plate test. Filter paper test is described in later sections in the next chapter. Furthermore, it can be estimated using the equation developed by Fredlund and Xing [35, 36]:

$$\theta_w = C(h) \times \left(\frac{\theta_{sat}}{\left\{ln\left[exp(1)+\left(\frac{h}{a_f}\right)^{b_f}\right]\right\}^{cf}}\right) \quad (2\text{-}2)$$

$$C(h) = \left[1 - \frac{ln\left(1+\frac{h}{h_r}\right)}{ln\left(1+\frac{1.45\times100000}{h_r}\right)}\right] \quad (2\text{-}3)$$

where, θ_{sat} = saturated volumetric water content;

θ_w = volumetric water content;

h = matric suction; and

a_f, b_f, c_f, and h_r = regression coefficients.

There are some equations for predicting a_f, b_f, c_f, and h_r coefficients in MEPDG which are estimated based on the percent passing No. 200, Plasticity Index (PI), and

effective particle size with 60% passing (D60). Moreover, some more recent equations were developed for prediction of these coefficients using MBV and PFC [17, 19].

2.11.1. Filter Paper Test

The filter paper test method described in ASTM D5298-16 has been conducted to measure the matric suction and total suction in base course material samples. The soil suction is measured at specified moisture content in the specimen. The samples are kept in a sealed container for seven days in this test. The increased weight of the filter papers, placed on and in between soil specimens is measured by an accurate scale. The matric suction, total suction, and water content are determined using filter paper calibration curve [17, 37].

Filter paper test has been conducted on four of the studied base course materials to measure the total suction and matric suction at the specific moisture contents. Total suction and matric suction have been measured at two different moisture contents using the filter paper test. Four different series of samples (eight samples) have been made for each unbound material to include the two moisture content conditions and two compaction methods. One series of the test specimens were made at the optimum moisture content, and the others were made at a moisture content drier than the optimum moisture content. Two series of samples for each material were compacted using the two compaction methods for testing in this way. Some of the steps of this experimental process are demonstrated in Figure 5.

(1)

(2)

(3)

(4)

(5)

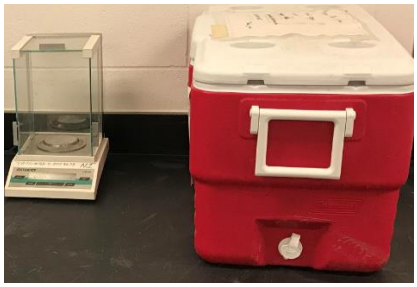

(6)

(7)

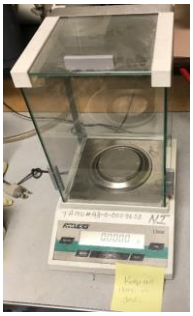

(8)

Figure 5. Filter Paper Test for Measurement of Suction [19]

2.12. Non-destructive Testing and Dielectric Constant

Engineering properties of the granular materials, such as modulus, are highly dependent on the moisture content. It is suggested that the moisture conditions of the soil be predicted through non-destructive testing using electrical measurements and devices. The Percometer, as shown in Figure 6, is a non-destructive instrument which measures dielectric constant (ε_r), electrical conductivity (J), and temperature (T) at the surface of a sample [19]. Each material has a unique dielectric constant. The dielectric constant depends on the material type.

Figure 6. Percometer to Measure the Dialectic Constant of Soil Surface

In this research, the dielectric constant of the specimens made for filter paper tests was measured using the Percometer. The dielectric constant of the specimens made with two compaction methods, each at two different moisture contents, was measured.

Then, using the CRIM model, the dielectric constant of the solid particles is calculated. Subsequently, using the CRIM model and calculated dielectric constant of solid particles, the dialectic constant of the sample in dry conditions (moisture content of 0%) and saturated conditions (degree of saturation equal to 1, s=1) are estimated.

The dielectric consent is measured with Percometer, and the soil suction is determined through the filter paper test. The relationship between soil dielectric constant and soil suction can be investigated using the results of the Percometer measurements, CRIM model, and filter paper test data. The correlation between the soil suction and the dielectric constant of the soil can help predict the moisture content or conditions of the soil. Therefore, some materials properties can be assessed having an estimation of suction and moisture content. This method can be finally used for prediction of the dry density and moisture conditions of the granular materials in the field by having the dielectric constant from the nondestructive pavement evaluation technique, ground penetrating radar (GPR). Then, it can be determined which compaction method provides more realistic values for moisture-density curves, resilient modulus, and permanent deformation.

2.13. Aggregate Imaging System (AIMS) Test

Aggregate Imaging System (AIMS) equipment characterizes the morphology of the aggregates [38, 39, 40]. The properties of the coarse and fine particles have a significant effect on the performance of the unbound base and subbase layers and consequently the performance of the pavement structure. The AIMS equipment analyzes

the angularity, form, and surface texture of coarse aggregates, and the form and angularity of the fine particles [39]. Angularity, surface texture, and form play an important role in the performance of the unbound layers [38]. The form of coarse aggregates is analyzed based on the three-dimensional evaluation and analysis of the aggregates. It distinguishes between flat, elongated, or flat and elongated aggregates.

Angularity describes the variations of the aggregates at corners [39]. The angularity describes variation at the particle boundaries. It is analyzed by quantification of the gradient change on a particle boundary and is associated with the sharpness of particles at the corners on the two-dimensional images [41]. The relative range of angularity is from 0 to 10,000. A complete circle has an angularity value of 0. Surface texture describes the surface irregularities at a smaller scale which is too small to influence the overall shape [39], and defines the relative roughness or smoothness of the aggregate surface. The surface texture has a range of 0 to 1000. A polished and smooth surface has a surface texture value close to 0.

Sphericity is one of the indices used to characterize the form of aggregate as a function of the three-dimensional shape of the particle [38]. Sphericity demonstrates the overall three-dimensional shape of the aggregates [27]. Sphericity is calculated according to the following equation [39]. The range of sphericity index is between 0 to 1. Sphericity index value of one indicates that the particle has equal dimension similar to the cubical shape.

$$Sphericity = \sqrt[3]{\frac{d_I \, d_S}{d_L^2}} \tag{2-4}$$

where $d_{S=}$ the particle shortest dimension,

$d_{I=}$ the particle intermediate dimension, and

$d_{L=}$ the longest dimension.

In this study, the aggregates retained on sieves, 7/8 in, 3/8 in, and sieve No. 4 were tested in the AIMS device. The angularity, surface texture, and sphericity indices of these coarse aggregates were measured. The AIMS device used in this study is shown in Figure 7.

Figure 7. Aggregate Imaging System (AIMS) Device Used in This Study

Since the aggregate structure is composed of different aggregate sizes, the composite index is calculated to reflect the AIMS indices of the aggregate blend:

$$\text{Composite Index} = \frac{\sum_{i=1}^{n} \text{index}_i\,(a_i)}{\sum_{i=1}^{n}(a_i)} \quad (2\text{-}5)$$

where, *composite index* = the composite angularity, texture, or sphericity of the blended aggregate mixture,

a_i = volumetric percentage of the aggregate size *i* in the aggregate structure of the material, and

$index_i$ = angularity, texture, or sphericity of the aggregate size *i*.

2.14. Computed Tomography (CT) Scanning

The Computed Tomography (CT) scanning was performed on the specimens compacted with gyratory compactor and impact hammer for the nondestructive evaluation of the internal structure of the compacted specimens. The CT scanning was carried out in the Petrophysical Imaging Laboratory in the Department of Petroleum Engineering at Texas A&M University. The porosity versus depth curve of the specimens has been provided for both series of compacted specimens, which demonstrates the porosity distribution through the height of the specimen.

The CT scanner equipment provided images of cross sections of the specimens (tomography), compacted with either the impact hammer or gyratory compactor. The Petrophysical Imaging Laboratory in the Petroleum Engineering Department has a state-of-the-art Aquilion^{TM} RXL CT Scanner [27, 33], as shown in Figure 8. The CT scanner used in this study captured tomographic images of the cross sections of the specimens every 0.3 mm through the height of each sample. The researchers can investigate inside the specimen

nondestructively and identify the voids within the sample by data processing of the data produced by the CT scanner about the sample internal structure.

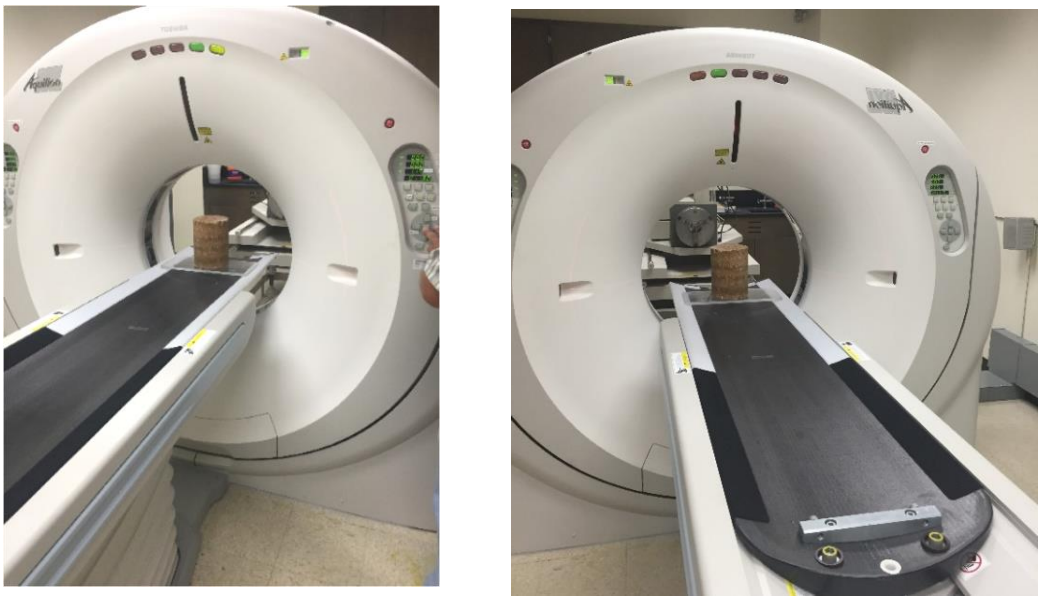

Figure 8. CT Scanning of the Fabricated Specimens with the Gyratory and Impact Hammer Compaction

3. DATA ANALYSIS AND MODELING OF MATERIALS BEHAVIOR AND EFFECTS OF GYRATORY COMPACTION

3.1. Introduction

In this section, the results of the experimental program conducted to investigate the performance related properties of materials are presented and discusses. The results are compared between the materials compacted with gyratory compactor and impact hammer. Compressive strength test, moisture dry density curve, permanent deformation, resilient modulus, suction and soil water characteristic curve are investigated for the materials fabricated with these compaction methods. The AIMS test results and the Weibull distribution, percent fines content, and Methylene Blue Value are also presented. These properties are used in the modeling of the mechanical behavior of the materials. A compaction energy equation has been developed for the gyratory compaction, which can distinguish between the compaction effort required for different materials.

3.2. Compressive Strength Test

The results of the unconfined compressive strength test are presented in Table 3 and Figure 9. The test results indicate that the coefficient of variation (COV) and the standard deviation of the compressive strength are lower in the samples prepared with the gyratory compactor than the ones compacted with the impact hammer. The COV is a

better way for evaluating the variability of the test results herein, since the materials have different ranges of average compressive strength. Thus, gyratory compaction can result in lower variability in terms of COV. The comparison between COV of unconfined strength test results is shown in Figure 10. One reason for lower COV in the specimens prepared with the SGC might be that the gyratory compaction can provide more uniform specimens, and the interface between layers was minimized.

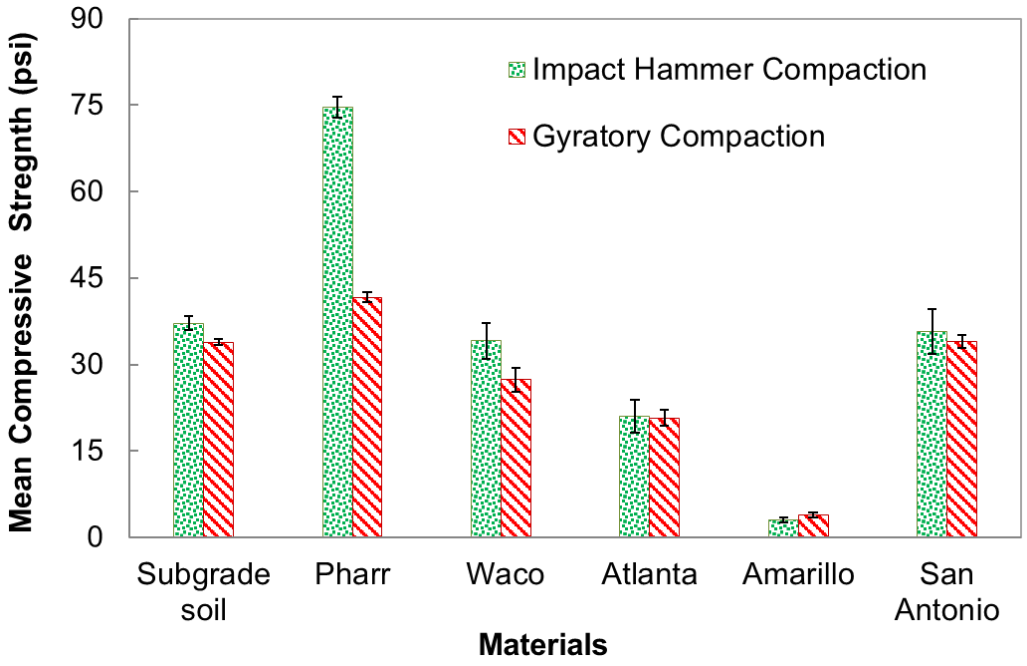

Figure 9. Compressive Strength Test Results for Two Laboratory Compaction Methods

Table 3. Unconfined Compressive Strength Test Results of Materials Compacted with Impact Hammer and SGC

Material	US 82-Subgrade		Pharr- Base		Waco- Base		Atlanta-Base		Amarillo-Base		San Antonio-Base	
Compaction Method	IH*	SGC	IH	SGC	IH	SGC	IH	SGC	IH	SGC	IH	SGC
Average Compressive Strength (psi)**	37.12	33.84	74.62	41.66	34.15	27.36	21.02	20.71	3.05	3.87	35.73	34.07
Standard Deviation (psi)	2.42	1.04	3.62	1.63	6.21	4.10	5.06	2.43	0.82	0.91	7.85	2.23
COV (%)	6.54	3.06	4.86	3.92	18.19	14.97	24.07	11.73	26.99	23.58	21.98	6.53
Standard Error	1.21	0.52	1.81	0.82	3.11	2.05	2.92	1.40	0.41	0.46	3.93	1.11

* IH: Impact Hammer Compaction.

** 1 psi= 6.89476 kPa.

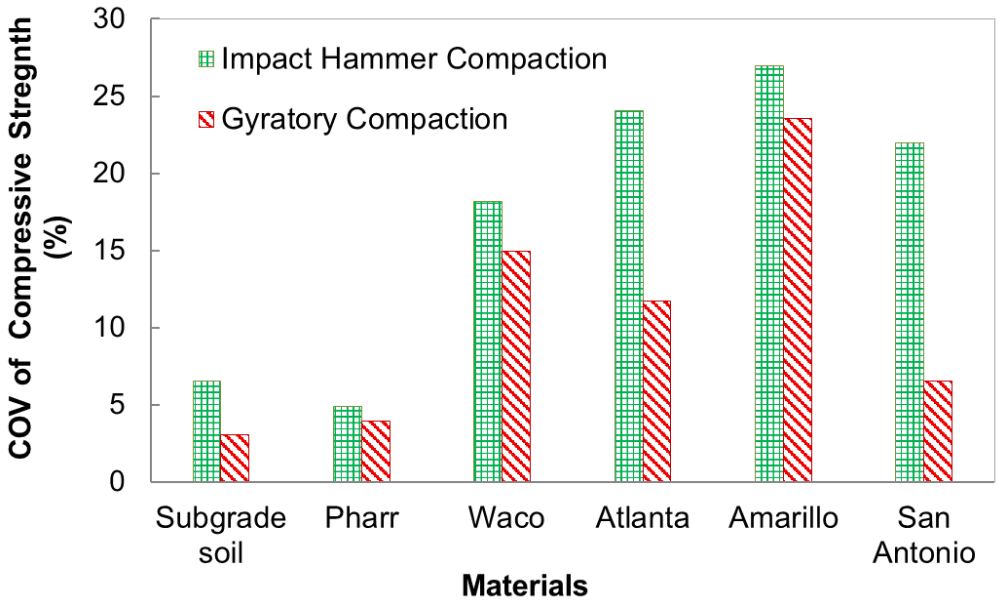

Figure 10. Coefficient of Variation of Compressive Strength Test Results

3.3. Statistical Analysis

Statistical analysis has also been performed for the strength test data to evaluate and compare the variability of the test data between the specimens made with these two compaction methods. Statistical analysis for equality of variance in strength test has been conducted. F-test on pooled variance has been performed and, the variance of these two sets of test data has been compared. The results of the F-test on pooled variance are shown in Table 4. In this statistical test, the null hypothesis (H_0) assumed that the variance of unconfined strength was statically equal for the samples compacted with the SGC and impact hammer. The alternative hypothesis stated that the variance of unconfined strength of the SGC-compacted samples was lower than the hammer-

compacted samples. This is a one-tailed statistical test with a confidence level of 95%. The results of the statistical test indicated that the variance of the strength test data in the hammer compacted samples was statically higher than the ones made with the impact compaction. Therefore, gyratory compaction could help reduce the variability of the strength test in these datasets.

Table 4. Results of the Statistical Analysis for Compressive Strength Test

Material	Pharr Base		Waco Base		Atlanta Base		Amarillo Base		San Antonio Base		US 82-Subgrade	
Compaction Method	IH*	SGC	IH	SGC	IH	SGC	IH	SGC	IH	SGC	IH	SGC
Average Compressive Strength (psi) **	74.62	41.67	34.16	27.36	21.02	20.71	3.05	3.87	35.73	34.07	37.13	33.84
Variance	13.13	2.67	38.61	16.77	25.60	5.91	0.68	0.83	61.69	4.95	5.89	1.07
Pooled Variance	7.899		27.690		15.752		0.754		33.304		3.483	
Pooled Variance-Impact hammer-$S_p^2{}_{IH}$***	24.16											
Pooled Variance-SGC-$S_p^2{}_{SGC}$ ***	5.32											
F-statistic	2.27											

* IH: Impact Hammer.

** 1 psi= 6.89476 kPa.

*** $S_p^2{}_{IH}$ and $S_p^2{}_{SGC}$ = Pooled variance in for hammer and SGC compacted samples, respectively.

3.4. Moisture- Dry Density Curves

The OMC and MDD of the studied materials were determined based on Tex-113-E and Tex-114-E test procedures and moisture- dry density relations. The results are presented in Table 5. In this table, the coefficient of determination (R^2) in the regression analysis for obtaining moisture –dry density curves is also shown. The high R^2 values indicated how well the observed data fit the moisture- dry density curves derived from the regression analysis in both gyratory and impact compaction techniques.

Table 5. Moisture- Dry Density Curve Results for Impact Hammer and Gyratory Compaction

Material	Impact Hammer Compaction			SGC Compaction		
	Optimum Moisture Content (%)	Maximum Dry Density (pcf)	R^2	Optimum Moisture Content (%)	Maximum Dry Density (pcf)	R^2
Pharr-Base	12.78	112.62	0.95	13.58	118.36	0.96
Waco- Base	8.21	130.95	0.96	8.96	132.07	0.99
Atlanta- Base	6.67	134.30	0.83	6.91	135.46	0.83
Amarillo- Base	5.19	138.63	0.70	6.53	141.29	0.99
San Antonio- Base	6.48	137.47	1.00	7.87	137.96	0.99
US 82-Subgarde	20.39	100.29	0.99	22.18	99.29	0.99

* 1 pcf= 16.01846 kg/m^3

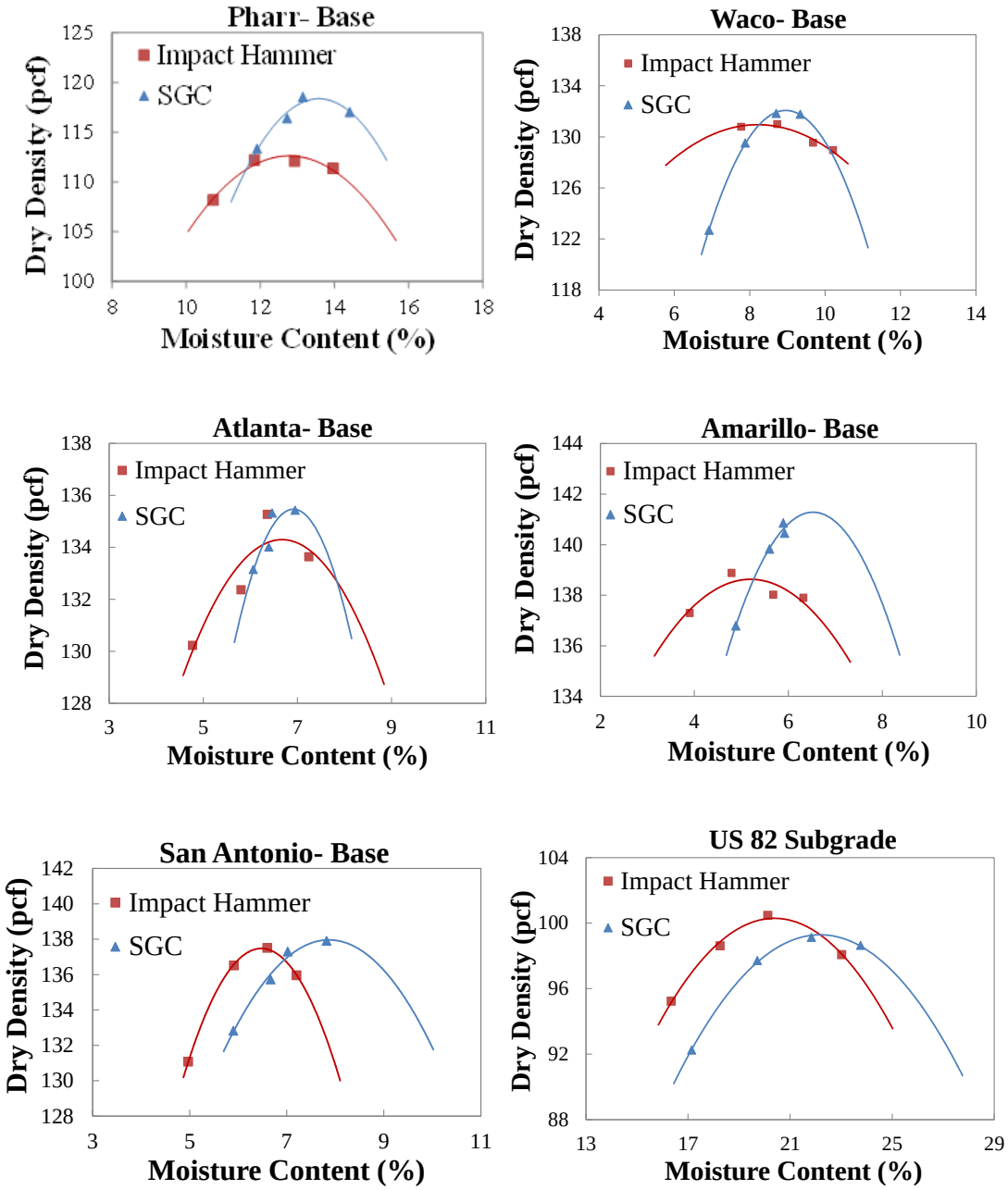

Figure 11. Moisture-Dry Density Curves for Impact Hammer and Gyratory Compaction

3.5. Statistical Analysis

Paired t-test has been performed to statistically compare the OMC and also MDD between the tested materials compacted with the impact hammer and gyratory compaction. In the paired *t*-test performed on the OMC data, the null hypothesis assumed that the OMC values obtained from the gyratory and impact hammer compaction were the same. The alternative hypothesis stated that the OMC obtained from the SGC is higher than the one from the impact hammer. The data support the alternative hypothesis which stated that the OMC determined from the impact hammer compaction was lower than the OMC obtained from the SGC compaction. The confidence level of this test was 95%. If the paired t-test was conducted on only base materials, the same finding would be reached. The null hypothesis in the paired t-test for the evaluation of the MDD in base materials was that the MDD from the impact hammer compaction was the same as the one obtained from the SGC compaction. The alternative hypothesis stated that the MDD obtained from the impact compaction was lower than the MDD from the gyratory compaction. The data supported the alternative hypothesis, stating that the MDD obtained from the gyratory compaction was higher than the one from the impact compaction in the base course materials.

3.6. Material Properties

Measurement of the material properties with laser particle size analyzer and Methylene blue test are presented in the table below. The PFC and MBV of the base course materials can be found in this table. Moreover, the percent of materials smaller

than 75 microns (P200) is also presented using prediction equations [19]. The measurements of P200 in the laboratory can also be performed.

Table 6. Materials Properties of Base Course Materials

Material	Percent Fine Content (PFC)	Methylene Blue Value (MBV)	P200
Pharr Base	4.16	13.98	12.06
Waco Base	12.34	18.19	8.09
Atlanta Base	3.52	0	9.54
Amarillo Base	8.24	-	10.28
San Antonio Base	7.19	9.22	8.99

3.7. Soil Water Characteristic Curve

The filter paper test was conducted on four of the base course materials to measure the total suction and matric suction at the specific moisture contents. The coefficients of the soil water characteristic curve (SWCC) model have been obtained for these base course materials using experimental data and regression analyses. SWCC of these base course materials has been generated for these materials using the root mean square error and minimizing the error. SWCC has been obtained for one of the base

course materials and each compaction method is plotted in Figure 12. Additionally, the prediction models using the performance base properties [17, 19] have been used for prediction of the SWCC curves of these materials. The MBV- based and pfc- based prediction models have been applied for these materials, and the predicted SWCC have been plotted in addition to the experimental SWCC obtained from curve-fitting and regression analysis. It can be estimated using the equation developed by Fredlund and Xing [35]:

$$\theta_w = C(h) \times \left(\frac{\theta_{sat}}{\left\{\ln\left[\exp(1)+\left(\frac{h}{a_f}\right)^{b_f}\right]\right\}^{cf}}\right) \quad (3\text{-}1)$$

$$C(h) = \left[1 - \frac{\ln\left(1+\frac{h}{h_r}\right)}{\ln\left(1+\frac{1.45\times100000}{h_r}\right)}\right] \quad (3\text{-}2)$$

where, θ_{sat} = saturated volumetric water content;

θ_w = volumetric water content;

h = matric suction; and

a_f, b_f, c_f, and h_r = regression coefficients.

There are some equations for predicting a_f, b_f, c_f, and h_r coefficients in MEPDG which are estimated based on the percent passing No. 200, Plasticity Index (PI), and effective particle size with 60% passing (D60). Moreover, some more recent equations developed for prediction of these coefficients using MBV and PFC have been used [17, 19].

Table 7. Coefficients of SWCC Curves for the Base Course Materials Using Regression Analysis and Filter Paper Test Data

Base Material	Compaction Method	a_f	b_f	C_f	hr
Pharr Base	Impact Hammer	9.67444	0.784513	0.7866	3000
	Gyratory Compactor	9.99763	0.801028	0.493821	3000
Waco Base	Impact Hammer	3.171	1.0057	1.052	3000
	Gyratory Compactor	3.988	1.0197	0.977	3000
Atlanta Base	Impact Hammer	10.0096	0.94350	0.86766	3000
	Gyratory Compactor	14.4885	1.26988	0.69186	2999.999
San Antonio Base	Impact Hammer	9.99873	1.06161	1.09090	3000
	Gyratory Compactor	8.52092	0.74097	0.46994	3000

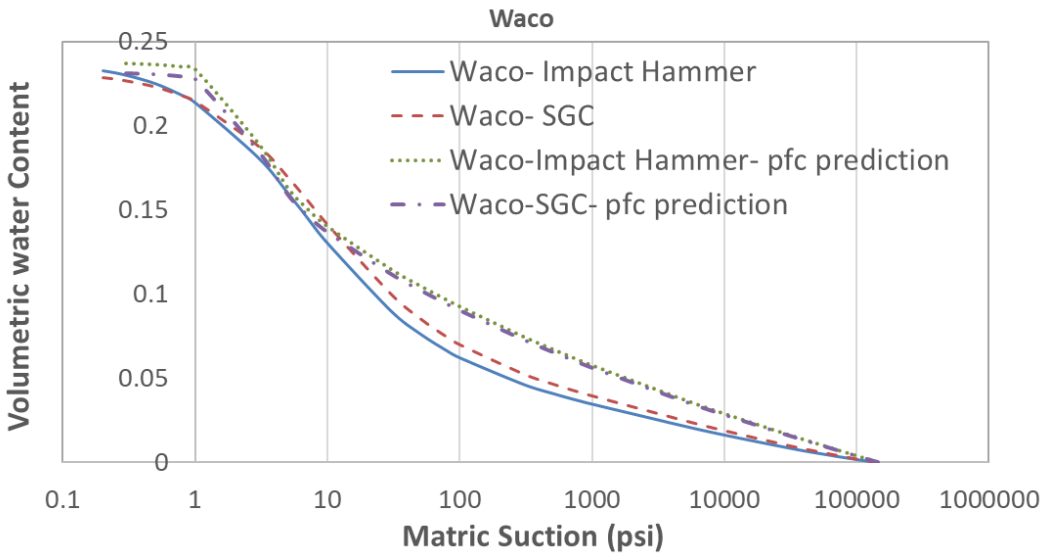

Figure 12. Experimental SWCC for Two Compaction methods and Predicted SWCC Based on Material Properties for Waco Base Course Material

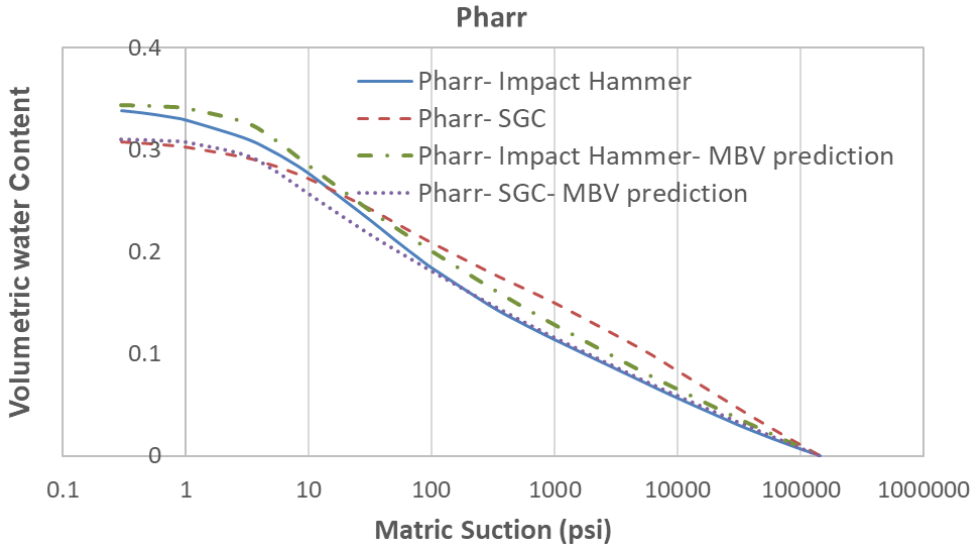

Figure 13. Experimental SWCC for Two Compaction methods and Predicted SWCC Based on Material Properties for Pharr Base Course Material

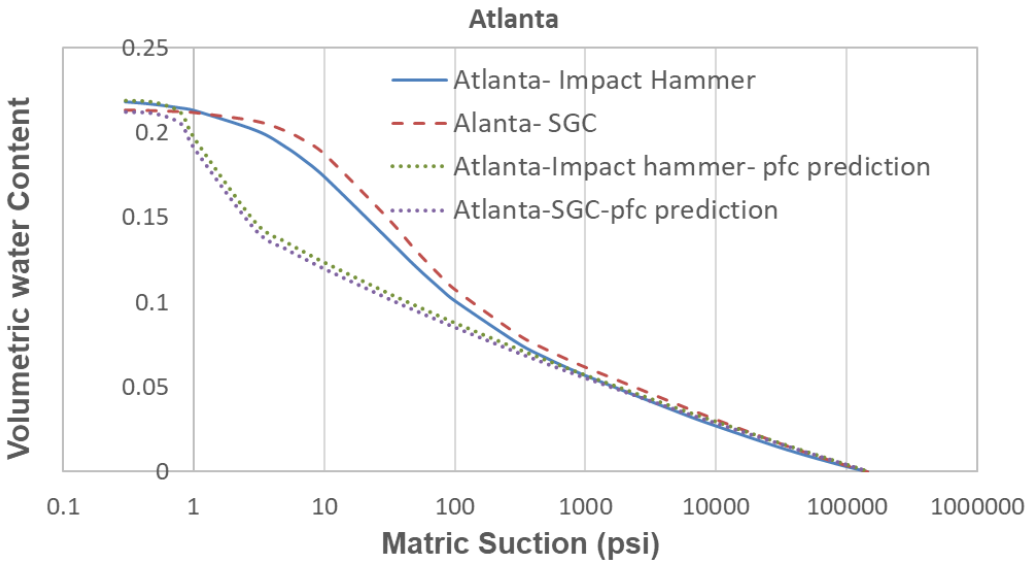

Figure 14. Experimental SWCC for Two Compaction methods and Predicted SWCC Based on Material Properties for Atlanta Base Course Material

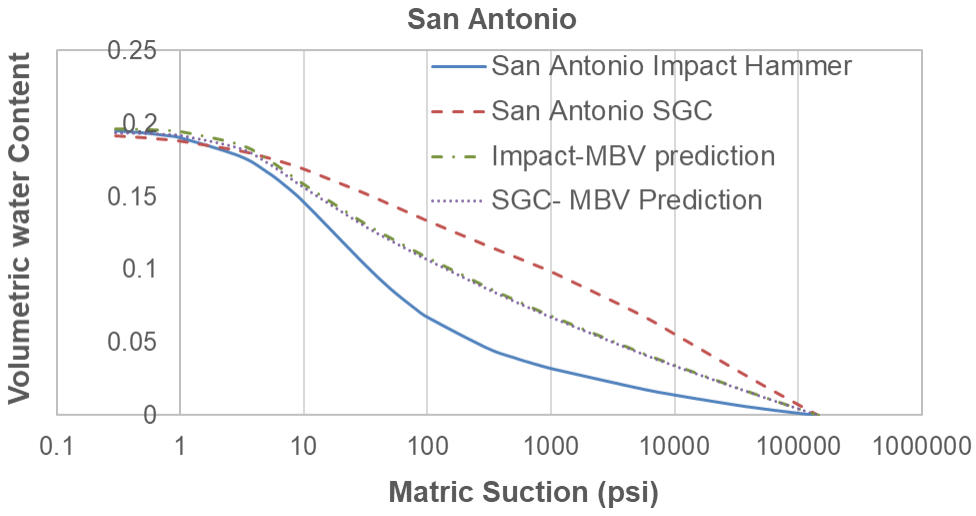

Figure 15. Experimental SWCC for Two Compaction methods and Predicted SWCC Based on Material Properties for San Antonio Base Course Material

3.8. Aggregate Imaging System (AIMS) Test Results

In this study, the angularity, surface texture, and sphericity indices of the coarse aggregates of the studied materials were measured. The aggregates retained on sieves, 7/8 in, 3/8 in, and sieve No. 4 were tested in the AIMS device. The angularity, surface texture, and sphericity indices of these coarse aggregates of the studied materials were measured. Then, the data measured in the AIMS device were fitted in a well-known distribution to characterize and quantify the angularity, texture, and sphericity indices. The cumulative Weibull distribution has been used in this study, expressed in the following equation:

$$P(x, a, \lambda) = 1 - e^{-(x/\lambda)^a} \quad (3\text{-}3)$$

where, $P(x, a, \lambda)$ = cumulative probability,

x = composite angularity, texture, or sphericity index,

λ = scale parameter, and

a = shape parameter.

The experimental results from the AIMS testing were used for curve-fitting against the cumulative Weibull distribution using the least mean square error. The shape parameter and scale parameter of the Weibull distribution for each material are presented in Table 8 for each material for angularity, texture, and sphericity indices. The Weibull distributions of each index are plotted in **Error! Reference source not found.** to Figure 19 for each granular material.

Table 8. Weibull Distribution Coefficients for the Aggregate Indices Obtained from AIMS Test

Material	Angularity		Texture		Sphericity	
	a_A	λ_A	a_T	λ_T	a_S	λ_S
Waco	3.978	3553.0	2.367	138.2	10.216	0.696
Pharr	3.801	3147.0	3.457	147.9	7.841	0.748
Atlanta	5.012	2800.7	2.721	193.5	7.433	0.739
San Antonio	4.565	2998.3	2.310	126.8	8.943	0.684

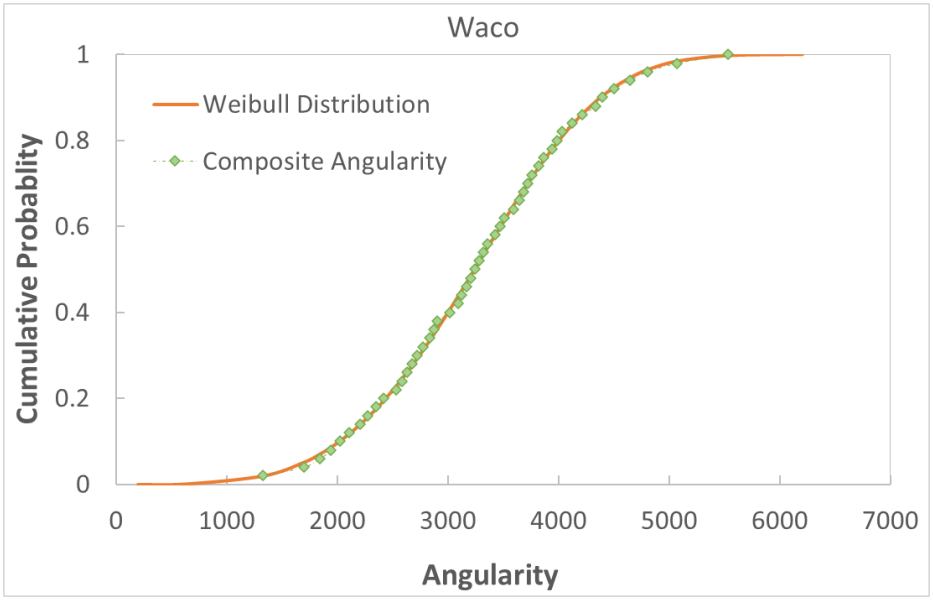

Figure 16. Weibull Distribution of Angularity, Texture, and Sphericity for Waco Base Course Material

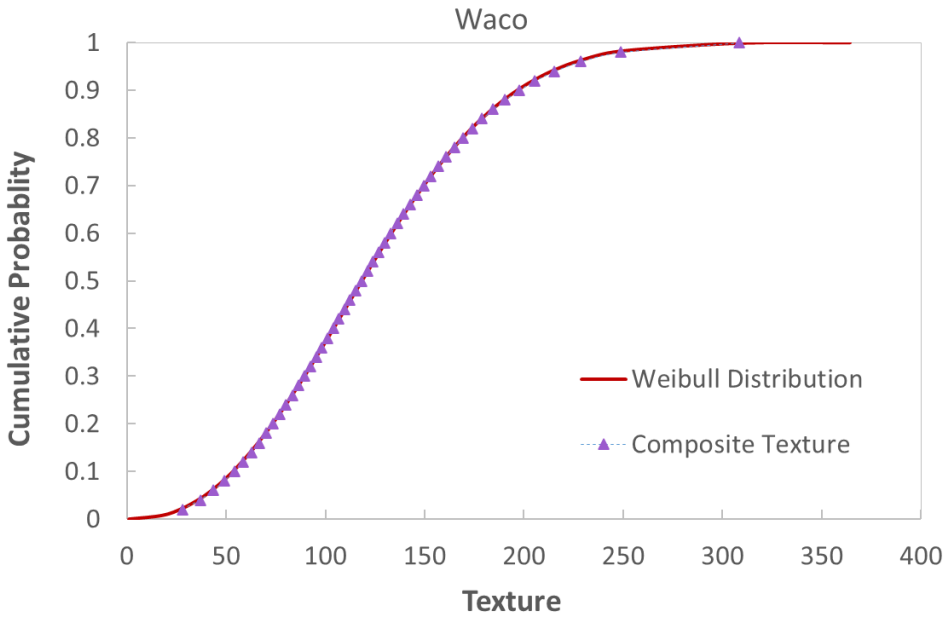

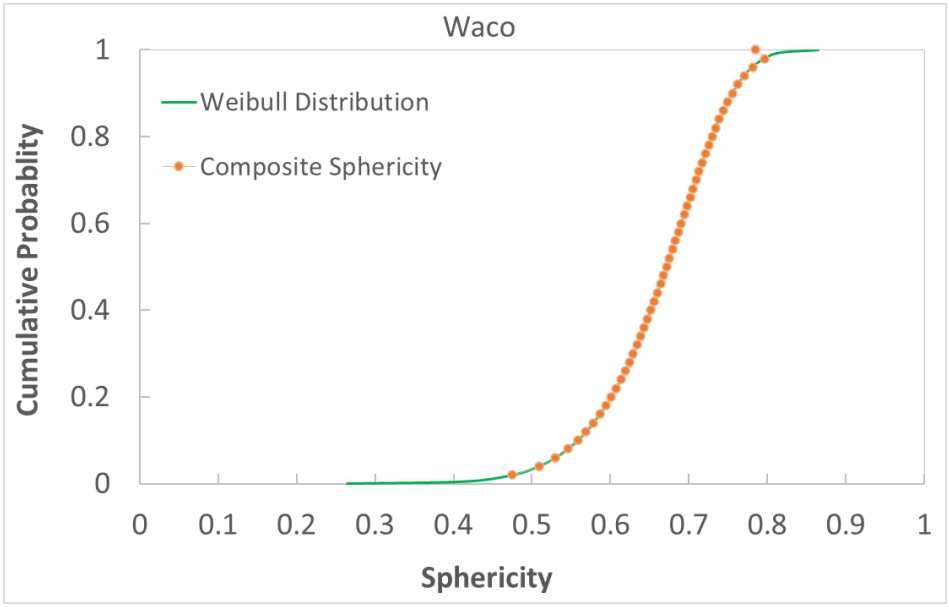

Figure 16. Continued

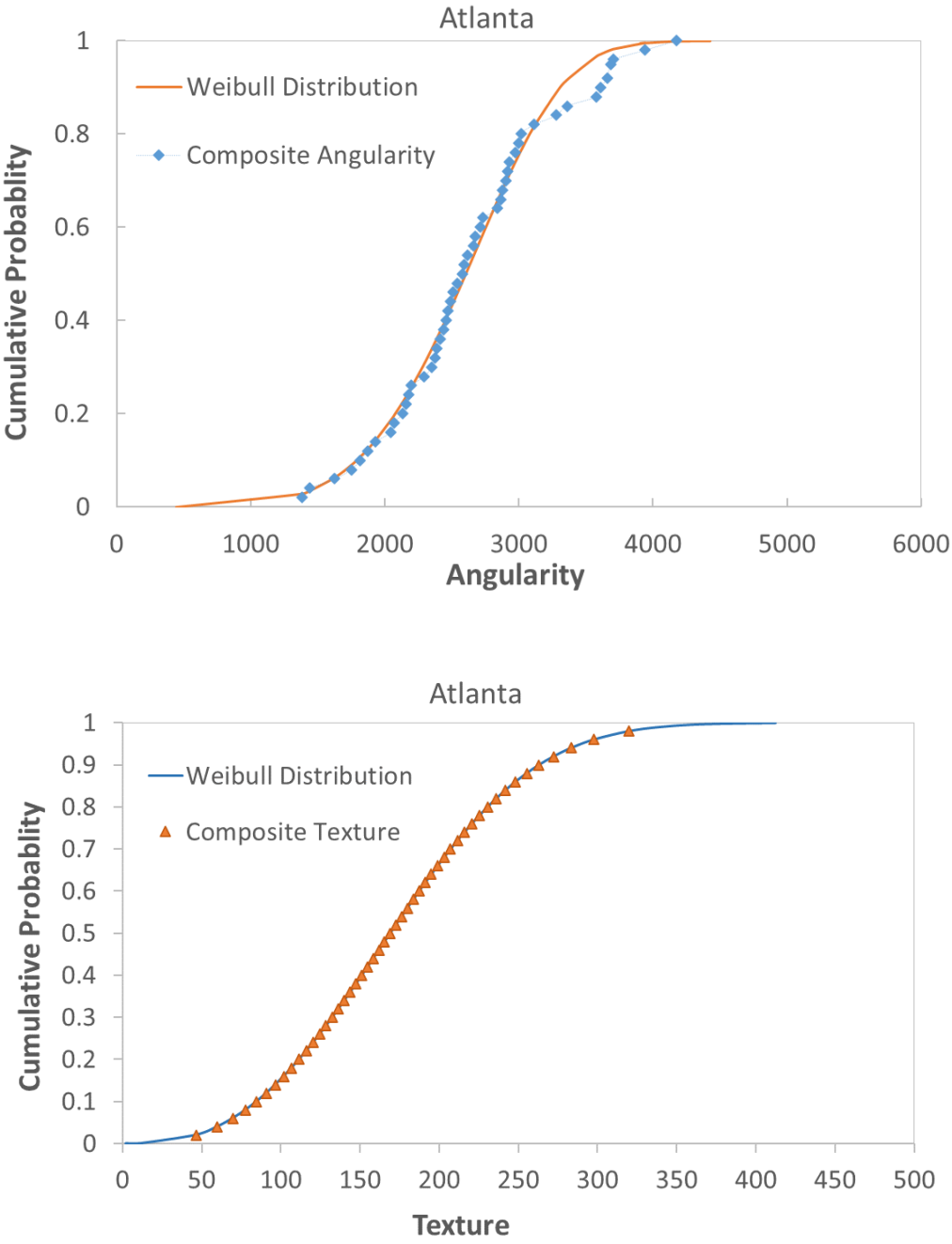

Figure 17. Weibull Distribution of Angularity, Texture, and Sphericity for Atlanta Base Course Material

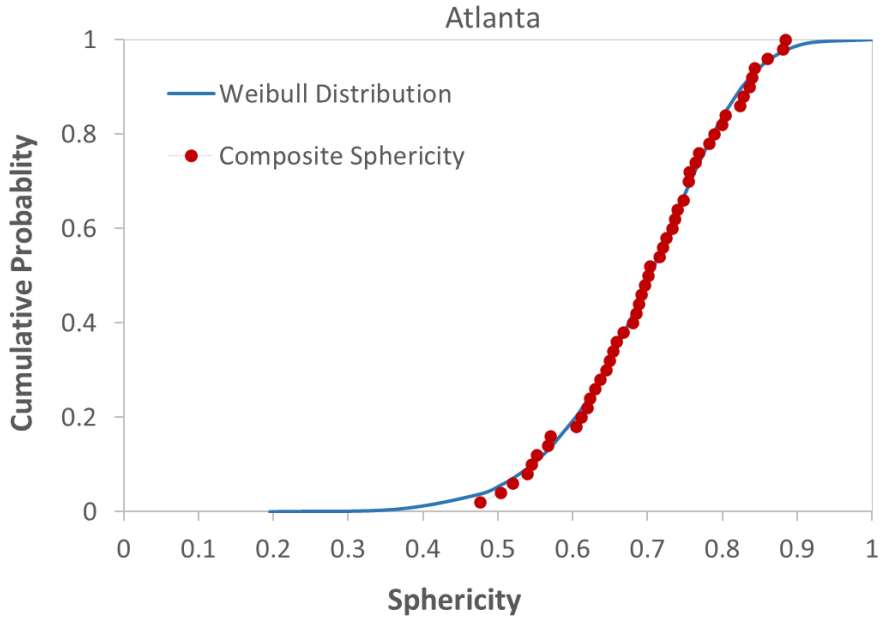

Figure. 17. Continued

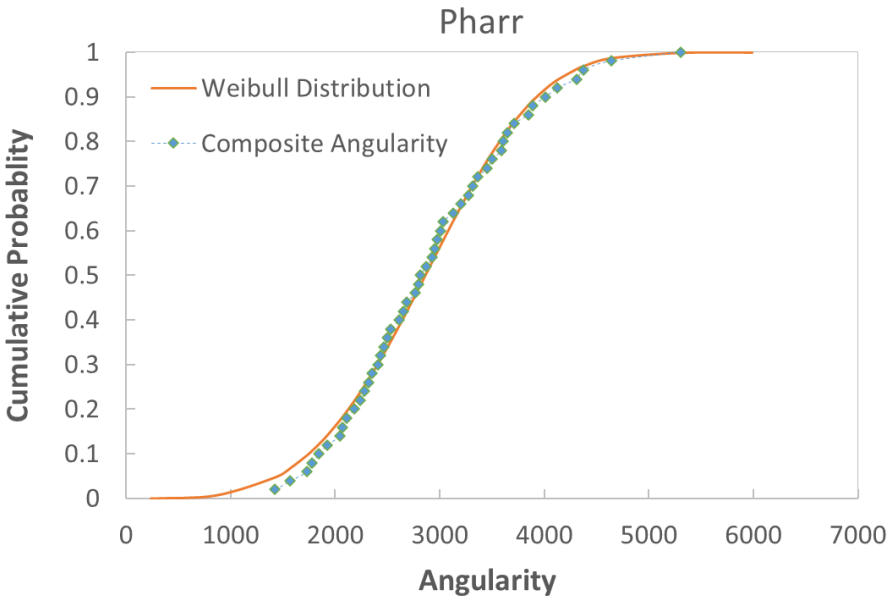

Figure 18. Weibull Distribution of Angularity, Texture, and Sphericity for Pharr Base

Course Material

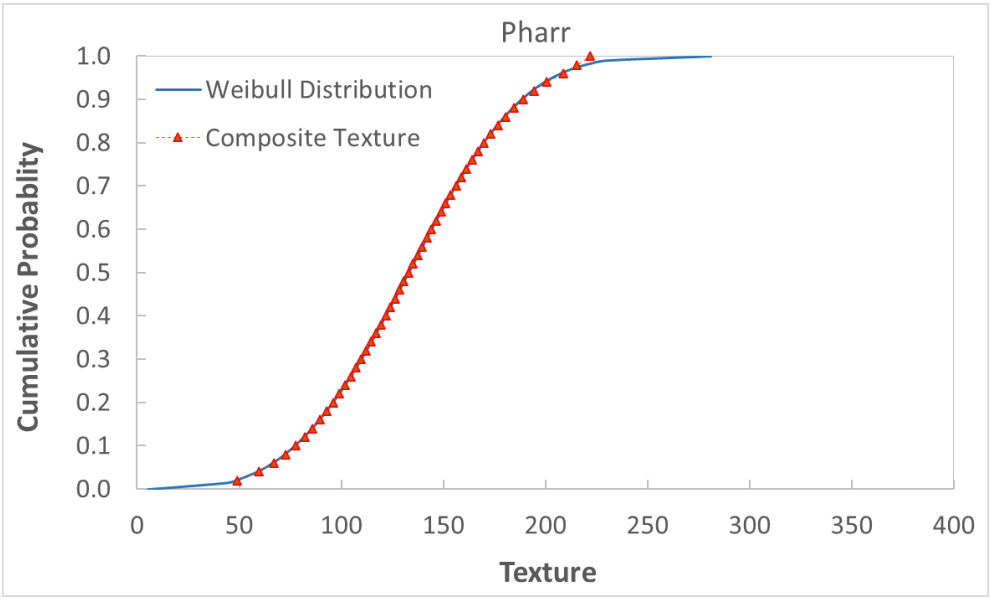

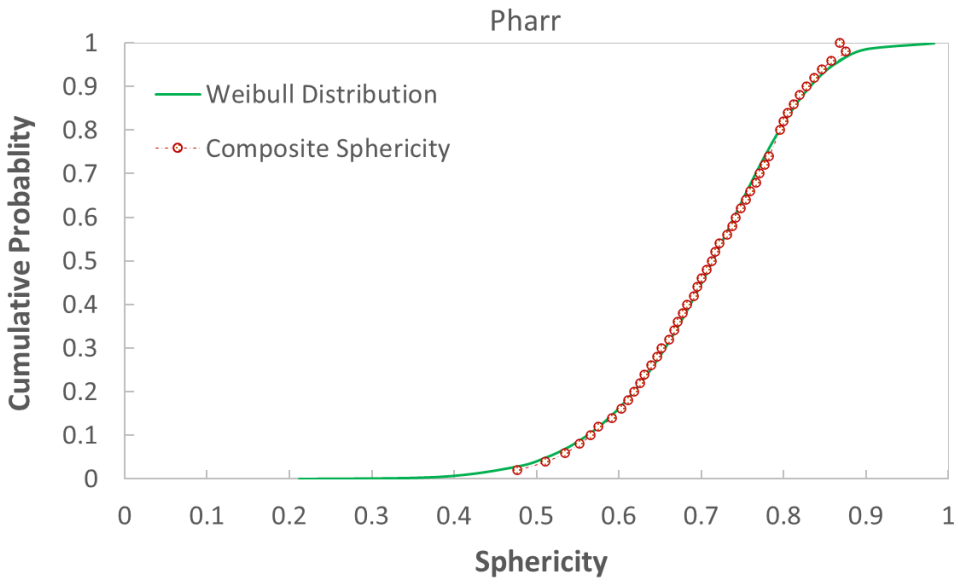

Figure 18. Continued

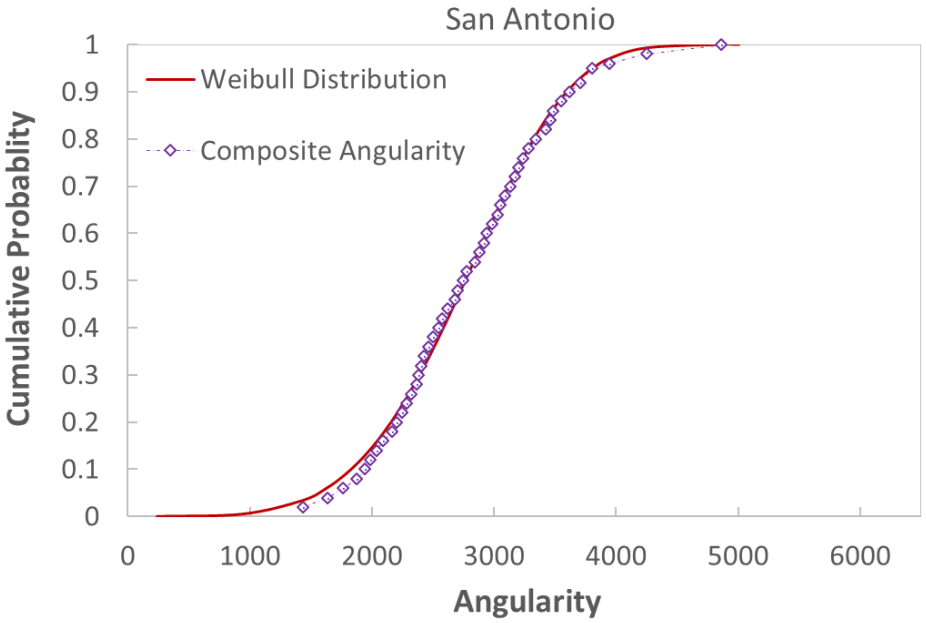

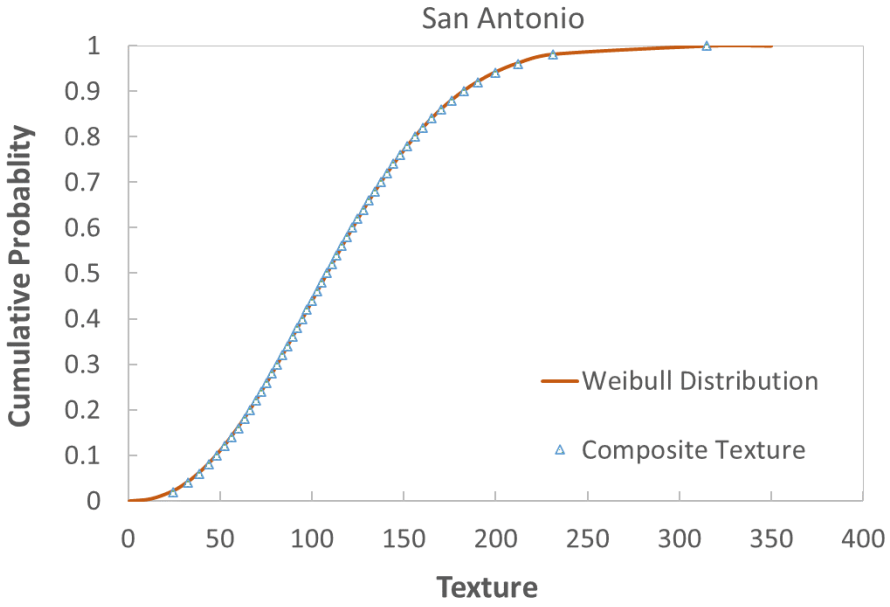

Figure 19. Weibull Distribution of Angularity, Texture, and Sphericity for San Antonio Base Course Material

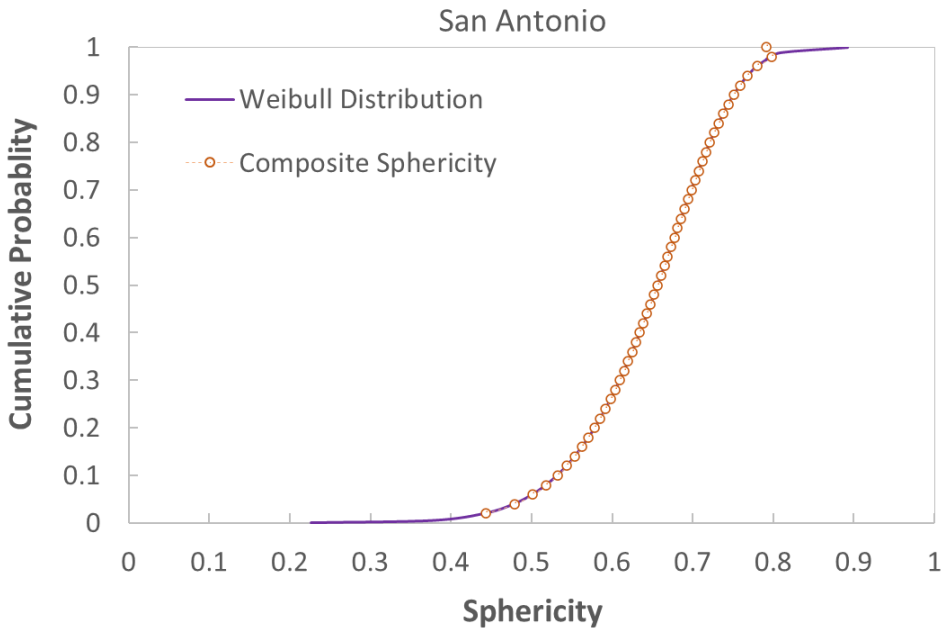

Figure 19. Continued

3.9. Particle Size Distribution Parameters

In this study, the aggregate gradation of the studied materials was determined using sieve analysis as mentioned in section 2.3. The particle size distribution has been presented in Figure 1. The data measured in the particle size distribution curve was fitted in the well-known cumulative Weibull distribution to further characterize and quantify the aggregate gradation. The cumulative Weibull distribution has been presented in equation (3-3). The experimental results from the aggregate gradation were used for curve-fitting against the cumulative Weibull distribution using the least mean square

error. The scale parameter, λ, and shape parameter, *a*, in the cumulative Weibull distribution were obtained for the studied materials.

Gradation scale parameter, λ_G, and gradation shape parameter, a_G, obtained using regression analysis has been presented in Table 9. The shape parameter is also compared among the different studied materials in Figure 20, and scale parameter is compared among the studied materials in Figure 21. The Pharr base course has the lowest gradation shape parameter, a_G, and lowest Gradation scale parameter, λ_G. It indicates that this granular material has the best well graded particle size distribution among these materials. It also indicates that it has generally smaller particle sizes compared to other materials. These are in accordance with the observation from the particle size distribution curves presented in Figure 1, and in line with the fact that it was classified as sand, while the other base course materials were classified as gravel. Moreover, the San Antonio and Waco base course materials have highest values of Gradation scale parameter, λ_G, and gradation shape parameter, a_G. It indicates that these materials may have the least well-graded particle size distribution among the studied materials. It is in accordance with the observation from the particle size distribution curves presented in Figure 1.

Table 9. Weibull Distribution Coefficients for the Aggregate Particle Size Distribution

Material	Gradation Shape parameter, a_G	Gradation Scale parameter, λ_G
Waco Base	0.995	13.73
Pharr Base	0.612	5.54
San Antonio Base	0.995	15.24
Atlanta Base	0.886	10.68
Amarillo Base	0.843	11.86

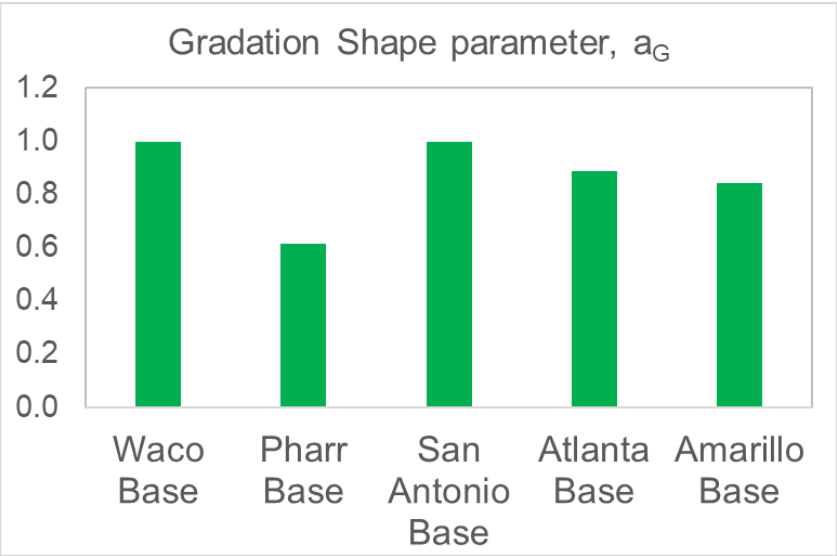

Figure 20. Gradation Shape Parameter as the Weibull Distribution Coefficient for the Particle Size Distribution

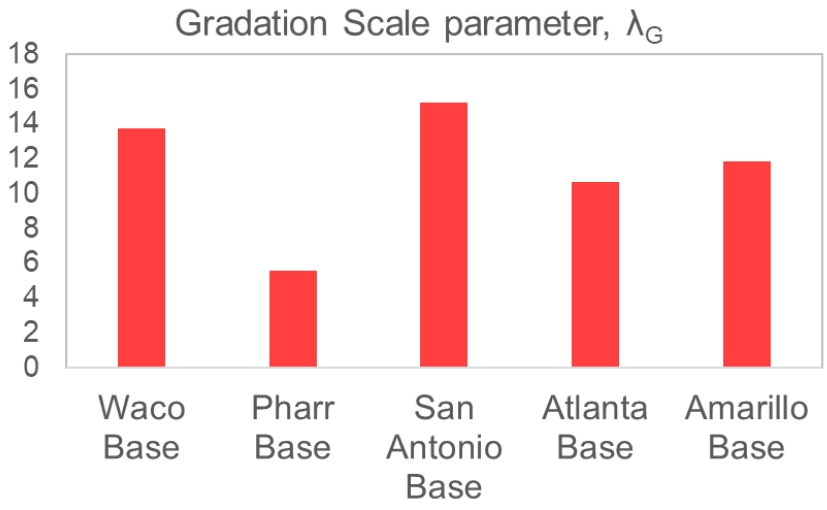

Figure 21. Gradation Scale Parameter as the Weibull Distribution Coefficient for the Aggregate Size Distribution

3.10. Permanent Deformation

One of the significant characteristics in the assessment and prediction of pavement performance is the permanent strain of geomaterials [11]. There are different models for prediction of the permanent strain of granular materials under load repetitions including Tseng-Lytton model [12], mechanistic-empirical pavement design guide (MEPDG) model [13, 14], UIUC model [21], VESYS model [15], and a recently proposed mechanistic empirical rutting model incorporating stress state [22]. Tseng Lytton model and VESYS models are used for fitting the experimental permanent strain data. Tseng-Lytton model and VESYS model are expressed in Equations 3-4 and 3-5, respectively:

$$\varepsilon^{p} = \varepsilon_0^{p} e^{-(\rho/N)^{\beta}} \quad (3\text{-}4)$$

where, ε^p = permanent strain;

N = number of load cycles;

ε_0^p = maximum permanent strain;

β = shape factor; and

ρ = scale factor.

β, ρ, and ε_0^p = three unknown parameters.

VESYS permanent strain model is also used in this study:

$$\varepsilon_p(N) = \mu\, \varepsilon_r\, N^{-\alpha} \quad (3\text{-}5)$$

where, ε_p = permanent strain;

ε_r = resilient strain at 200th load repetition;

N = number of load cycles; and

α, μ= permanent deformation parameters.

3.10.1. Permanent Deformation Testing and Modeling

The experimental results of the repeated load triaxial test on San Antonio, Waco, Pharr, and Atlanta base course materials, are plotted in Figure 22, Figure 23, Figure 24, and Figure 25, respectively. The permanent strain formed in the samples due to the repeated loading is plotted up to 10,000 load cycles. Lower permanent strain was

observed in the specimens made with the gyratory compaction compared to impact compaction in all of these base materials except for the Pharr base course.

3.10.2. Permanent Deformation Models

The experimental data have been fitted with Tseng-Lytton and VESYS permanent deformation models to obtain the model coefficients using the least mean square error method. The experimental results and the permanent strains are plotted in Figure 22, Figure 23, Figure 24, and Figure 25 for San Antonio, Waco, Pharr, and Atlanta base course materials, respectively. The results of the regression analyses are also presented in this section. The modeling results and predicted permanent strains from the Tseng-Lytton model versus experimental results are also presented in the same figures, Figure 22 to Figure 25, for these materials.

The coefficients of the Tseng-Lytton model determined for the studied materials are shown in Table 10. The maximum permanent strain, ε_0^p , has higher values in the impact hammer compaction compared to the gyratory compaction (SGC) in all of the materials except for Pharr material, as shown in Table 10.

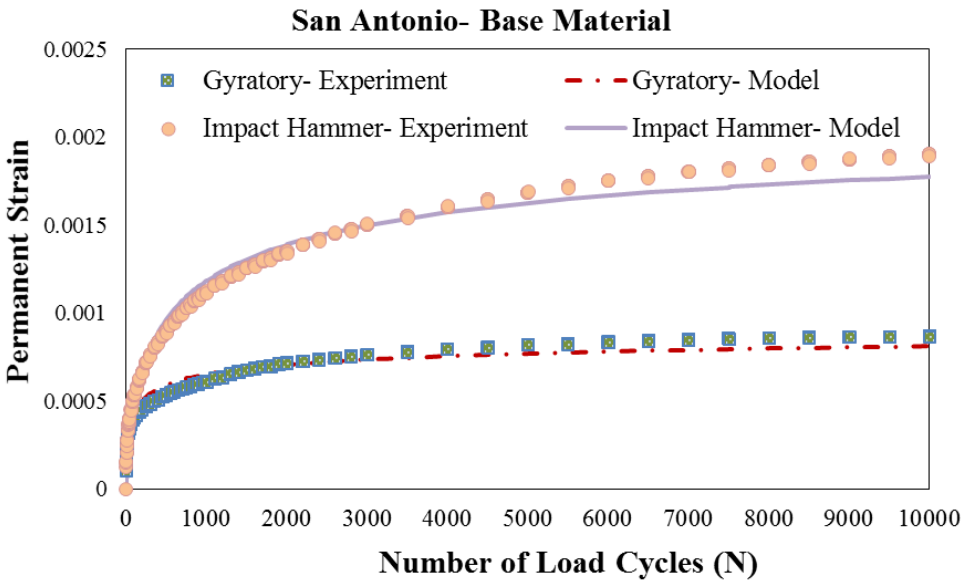

Figure 22. Experimental Results of Permanent Deformation Test for San Antonio Base Material and Modeling with Tseng-Lytton Model

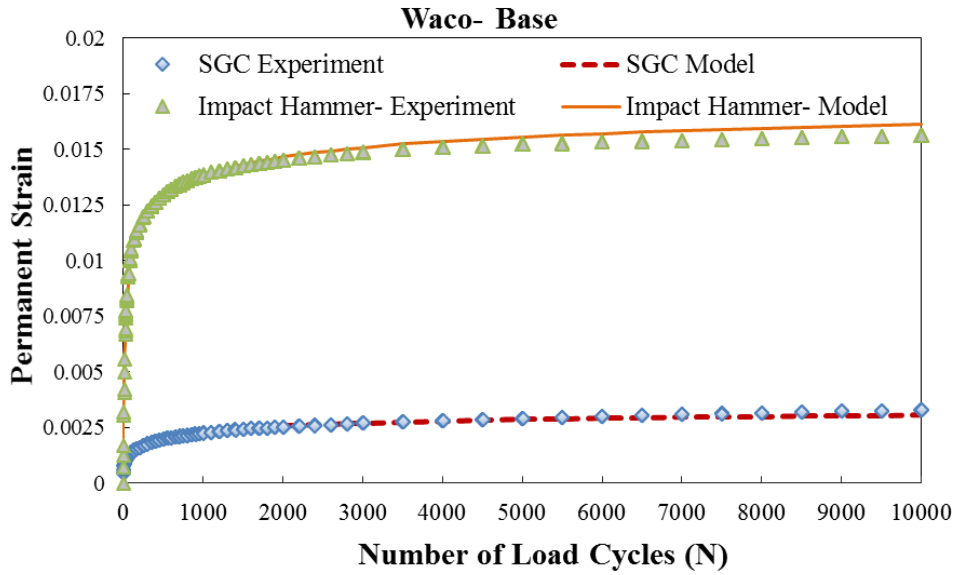

Figure 23. Experimental Results of Permanent Deformation Test for Waco Base Material and Modeling with Tseng-Lytton Model

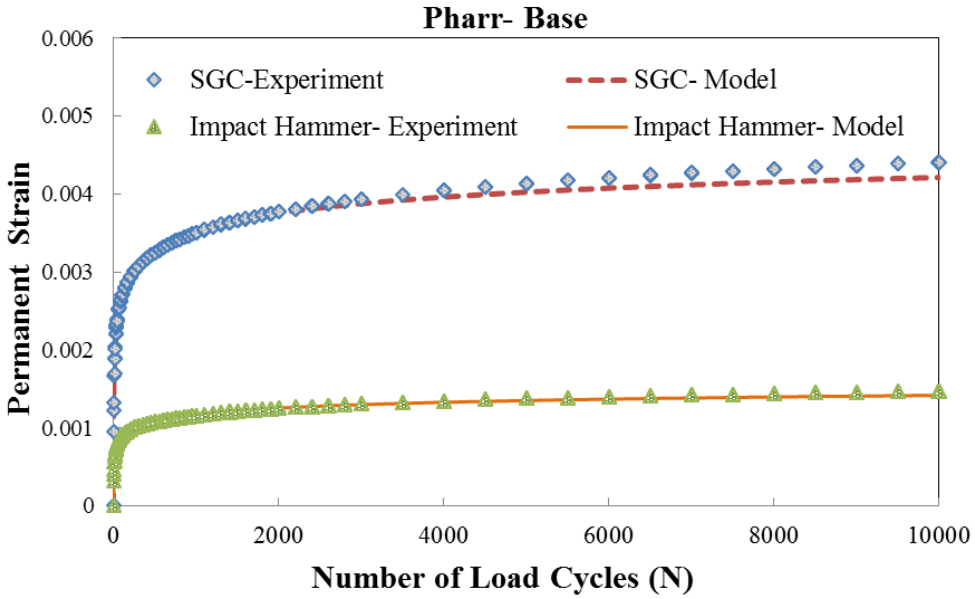

Figure 24. Experimental Results of Permanent Deformation Test for Pharr Base Material and Modeling with Tseng-Lytton Model

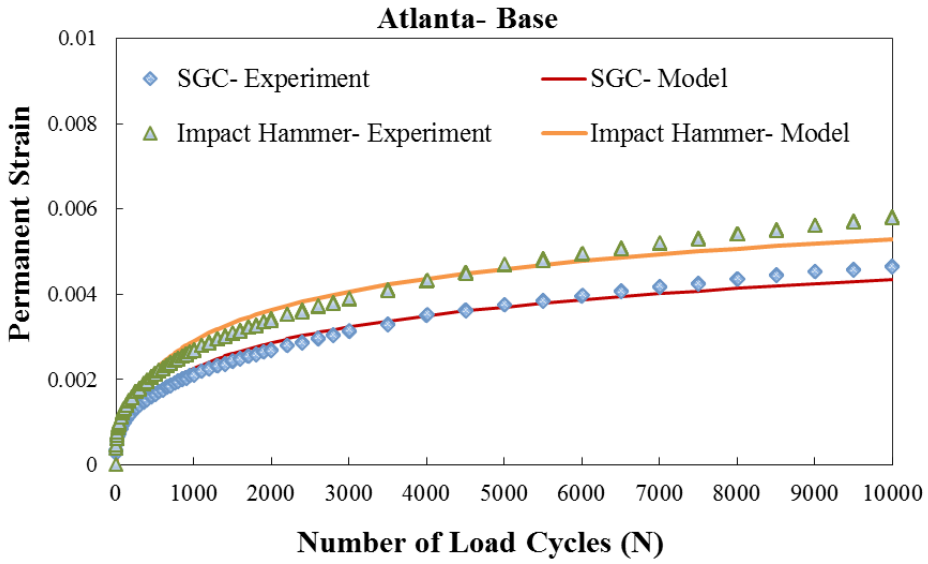

Figure 25. Experimental Results of Permanent Deformation Test for Atlanta Base Material and Modeling with Tseng-Lytton Model

Table 10. Coefficients of Tseng-Lytton Model for Prediction of Permanent Strain of the Studied Materials

Base Material	Compaction Method	β	ρ	ε_0^p	R^2
Pharr	Impact Hammer	0.178	36.93	0.0020	0.98
	Gyratory Compactor (SGC)	0.169	26.60	0.0060	0.97
Waco	Impact Hammer	0.321	21.89	0.0185	0.96
	Gyratory Compactor (SGC)	0.272	145.42	0.0042	0.96
Atlanta	Impact Hammer	0.285	2177.88	0.0101	0.97
	Gyratory Compactor (SGC)	0.265	2727.07	0.0085	0.95
San Antonio	Impact Hammer	0.370	391.50	0.0024	0.99
	Gyratory Compactor (SGC)	0.282	61.54	0.0010	0.99

Moreover, the experimental results of the permanent strains were also used to find the coefficients of the VESYS prediction model. The coefficients of the VESYS model determined for the studied materials are shown in Table 11. The predicted results of permanent strain using VESYS model versus the experimental permanent strains obtained from testing data are presented in Figure 26, Figure 27, Figure 28, and Figure 29 for San Antonio, Waco, Pharr, and Atlanta base course materials, respectively.

Table 11. Coefficients of VESYS Model for Prediction of Permanent Strain of the Studied Materials

Base Material	Compaction Method	VESYS Model			
		ε_r *at 200th load cycle (microstrain)*	α	μ	R^2
Pharr	Impact Hammer	642	0.891	0.089	0.99
	Gyratory Compactor (SGC)	825	0.893	0.211	0.99
Waco	Impact Hammer	410	0.931	1.423	0.96
	Gyratory Compactor (SGC)	272	0.822	0.417	0.99
Atlanta	Impact Hammer	496	0.657	0.170	0.99
	Gyratory Compactor (SGC)	419	0.645	0.150	0.99
San Antonio	Impact Hammer	205	0.731	0.217	0.99
	Gyratory Compactor (SGC)	156	0.819	0.191	0.98

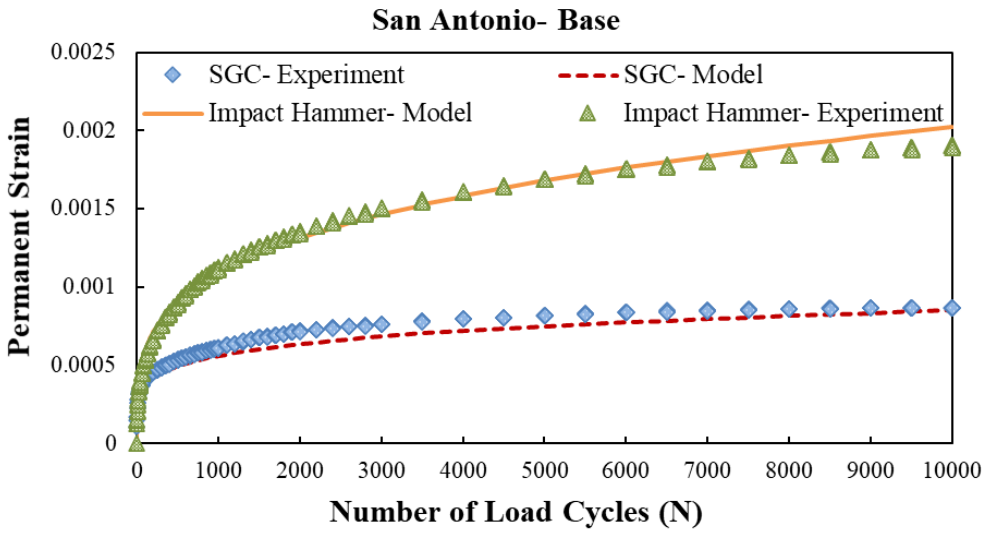

Figure 26. Permanent Deformation Test Results for San Antonio Base Material and Modeling with VESYS Model

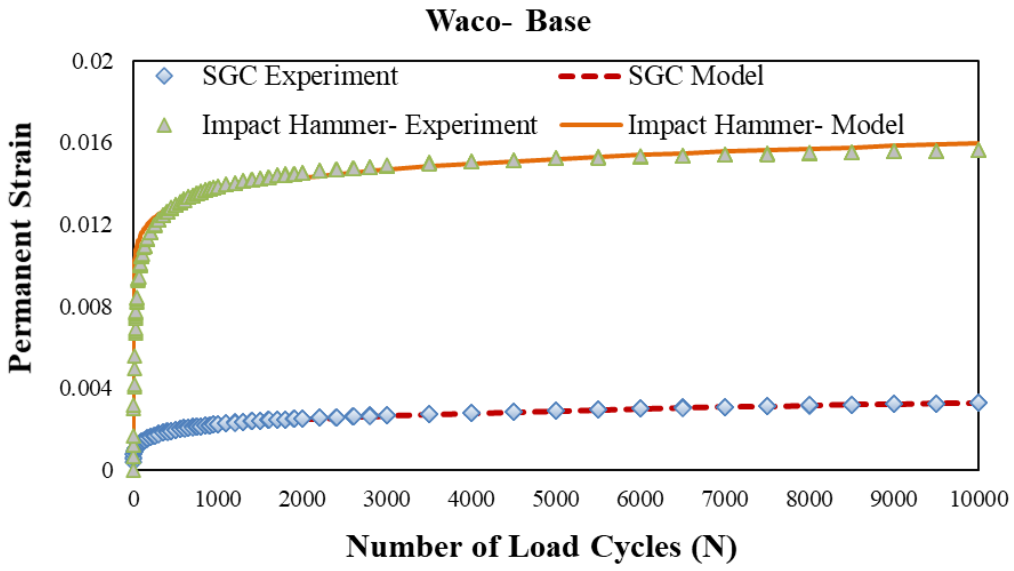

Figure 27. Permanent Deformation Test Results for Waco Base Material and Modeling with VESYS Model

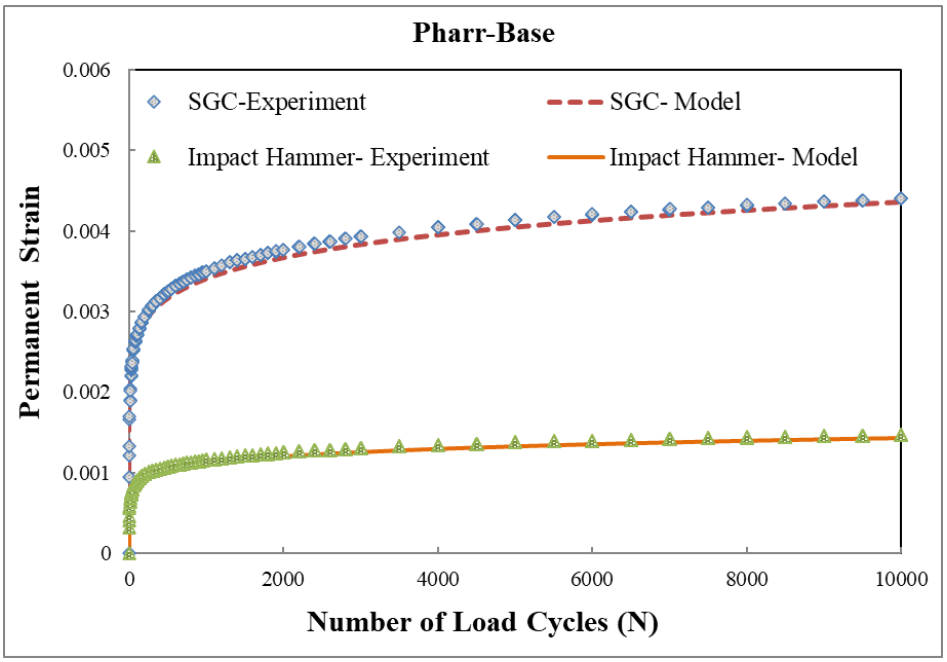

Figure 28. Permanent Deformation Test Results for Pharr Base Material and Modeling with VESYS Model

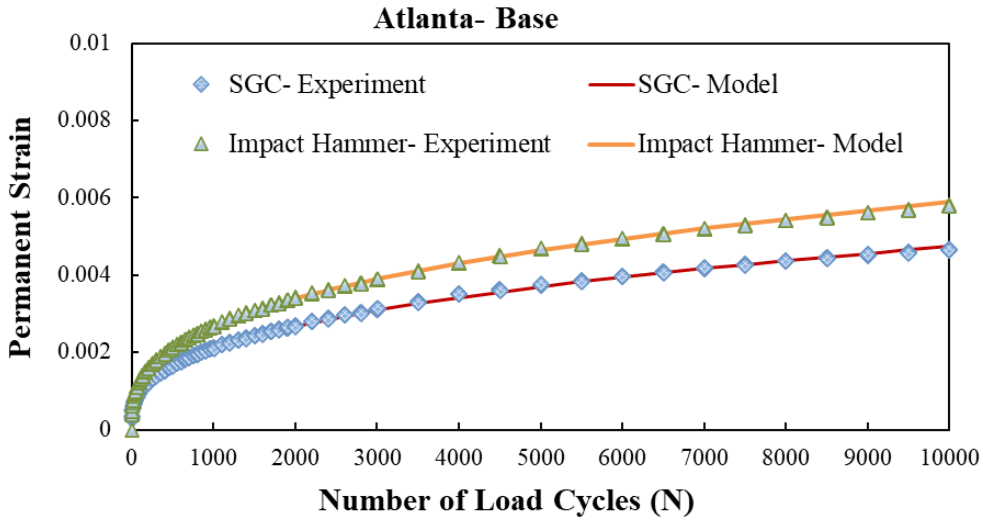

Figure 29. Permanent Deformation Test Results for Atlanta Base Material and Modeling with VESYS Model

3.10.2.1. Multivariable Regression Analysis for Coefficients of Permanent Deformation Model

Multivariable Regression Analysis has been performed using R programming Software [42] and RStudio [43] to investigate the relation between the performance-related properties of base course materials and the coefficients ε_0^p, ρ, and β of the Tseng-Lytton permanent deformation model. The properties considered in the prediction models for ε_0^p, ρ, and β coefficients are the maximum dry density (γ_d), Percent fines Content (pfc), Methylene Blue Value (MBV), moisture content (ω_c) , aggregate angularity, texture, and sphericity in terms of the parameters of the Weibull distribution. The AIMS parameters are angularity scale parameter ($\boldsymbol{\lambda_A}$), angularity shape parameter (a_A), texture scale parameter ($\boldsymbol{\lambda_T}$), texture shape parameter (a_T), sphericity scale parameter ($\boldsymbol{\lambda_S}$), and sphericity shape parameter (a_S). The materials properties considered in the development of coefficients ε_0^p, ρ, and β in this study in the Tseng-Lytton model are presented in Table 12 for the materials fabricated with both the gyratory compaction and impact hammer compaction methods.

The dry density, angularity, texture, and shape indices from AIMS test, percent fines content (pfc), and the moisture content were considered the variables in the development of the prediction models for the coefficients ε_0^p, ρ, and β of the resilient modulus model based on the statistical analysis performed by Gu et al. [44] within their data points. The correlation tables were formed in the R program in this study which included the correlation between different input variables with each other, and also the

output parameter, the permanent strain. The input variables parameters with lower correlation with each other and higher correlation value with the output parameters have been selected. The value of correlation between maximum dry density and moisture content was high according to the R programming results. Therefore, it is not logical to use them together in the same equations, and they can be used in the separate equations.

Table 12. Materials Properties used in the Multivariable Regression Analysis for coefficients k_1, k_2, k_3 of Resilient modulus Model

Material	Compaction Method	Angularity		Texture		Sphericity		pfc	MBV	γ_{Dry} (lb/ft^3)	Water Content (%)
		a_A	λ_A	a_T	λ_T	a_s	λ_S				
Waco	Hammer	3.98	3553	2.37	138	10.216	0.696	12.34	18.19	130.95	8.21
Waco	SGC	3.98	3553	2.37	138	10.216	0.696	12.34	18.19	132.07	8.96
Pharr	Hammer	3.80	3147	3.46	147	7.841	0.748	4.16	13.98	112.62	12.78
Pharr	SGC	3.80	3147	3.46	147	7.841	0.748	4.16	13.98	118.36	13.58
Atlanta	Hammer	5.01	2800	2.72	193	7.433	0.739	3.52	0	134.3	6.67
Atlanta	SGC	5.01	2800	2.72	193	7.433	0.739	3.52	0	135.46	6.91

Table 12. Continued

Material	Compaction Method	Angularity		Texture		Sphericity		pfc	MBV	γ_{Dry} (lb/ft^3)	Water Content (%)
		a_A	$\boldsymbol{\lambda_A}$	$\boldsymbol{a_T}$	$\boldsymbol{\lambda_T}$	$\boldsymbol{a_s}$	$\boldsymbol{\lambda s}$				
San-Antonio	Hammer	4.57	2998	2.31	126	8.943	0.684	7.19	9.22	137.47	6.48
San-Antonio	SGC	4.57	2998	2.31	126	8.943	0.684	7.19	9.22	137.96	7.87

The prediction equations for the coefficients ε_0^p, ρ, and β of the Tseng-Lytton permanent deformation model for the materials compacted with gyratory compactor are as follows:

$$\varepsilon_0^p = 0.2663 - 0.0147\, Ln(\lambda_T) + 0.0078\, pfc - 0.0280\, (a_s) \quad (3\text{-}6)$$

$$Ln(\rho) = -4516.583 + 378.911\, Ln(\lambda_A) - 9.6461\, pfc + 315.930\, Ln(\gamma_d) \quad (3\text{-}7)$$

$$\beta = 0.6691 - 0.0563\, Ln(\lambda_T) - 0.0169\, \omega_c + 0.0026\, pfc \quad (3\text{-}8)$$

The prediction models for the coefficients ε_0^p, ρ, and β of the permanent deformation model for the materials compacted with the impact hammer are as follows:

$$\varepsilon_0^p = 0.3617 - 0.0183\, Ln(\lambda_A) + 0.0120\, pfc - 0.0334\, (a_s) \quad (3\text{-}9)$$

$$Ln(\rho) = -584.119 + 45.870\ Ln(\lambda_A) - 1.6225\ pfc + 47.6357\ Ln(\gamma_d) \quad (3\text{-}10)$$

$$\beta = 1.3604 - 0.1734\ Ln(\lambda_T) - 0.0253\ \omega_c + 0.0019\ pfc \quad (3\text{-}11)$$

where, λ_A: angularity scale parameter,

λ_T: texture scale parameter,

a_S : Sphericity shape parameter,

pfc: Percent Fines Content,

γ_d: Maximum Dry Density (Pound Per Cubic Feet, pcf) and,

ω_c: moisture content (percent).

The angularity scale parameter, λ_A, affects the coefficient ρ and subsequently the value of permanent strain, ε^p, predicted from the model, as it contributes to the equation developed for scale factor, ρ, for both materials compacted with the gyratory compactor and the impact hammer. Increase of angularity of the aggregates raises the scale parameter, ρ, and thus, results in reduction of the permanent strain predicted by the Tseng-Lytton model in this regard for the same number of load repetitions. It is in accordance with the findings in the literature, stating that increasing the angularity of the aggregates decreases the permanent deformation of the granular materials [44, 45, 46]. It is worth noting that higher scale parameter, ρ, indicates that higher number of load repetitions are required to reach a certain level of permanent strain. The contribution of λ_A to the coefficient ρ, is higher in the materials produced by the gyratory compactor compared to the impact hammer.

Moreover, the angularity scale parameter, λ_A, affects ε_0^p in the materials compacted with the impact compaction. Increase of the λ_A lowers ε_0^p , and thus, results in reduction of the predicted permanent strain for the samples compacted with the impact hammer compaction.

The angularity scale parameter, λ_A, is replaced with the texture scale parameter (λ_T), in the ε_0^p equation for the materials compacted with gyratory compactor. It is one of the differences between these series of prediction models developed for the materials fabricated with the gyratory compaction and impact compaction. The increase of texture scale parameter (λ_T) reduces the ε_0^p , and therefore, results in decrease of the predicted permanent strain for samples compacted with the gyratory compaction. It is in accordance with the findings in the literature, stating that increasing the surface texture of the aggregates lowers the permanent deformation of the granular materials [44, 45, 46].

Furthermore, the percent fines content (*pfc*) affects the coefficients of the permanent deformation model. Increase of the *pfc* raises the ε_0^p , and decreases the scale parameter, ρ, in both the series of equations developed for the materials made with the gyratory compactor and impact hammer. Therefore, these changes of the two coefficients both result in the rise in the predicted permanent strain. It is in line with the expectation that higher fines content increases the potential of moisture absorption and leads to the higher permanent deformation in the aggregate layers. In addition, maximum dry density, γ_d, contributes to the equations developed for the scale parameter, ρ. Rise

in γ_d increases the ρ in both samples prepared with the impact hammer and gyratory compactor, which consequently reduces the predicted permanent strain for the same number of load repetitions.

Generally, the effect of change of angularity scale parameter, λ_A, and maximum dry density, γ_d, on scale parameter, ρ, is lower in the materials compacted with the impact hammer compared to the gyratory compactor. The coefficients of λ_A and γ_d in the model of scale parameter, ρ, are all higher for the gyratory compacted samples. The effect of aggregate and material properties on the ε_0^p, ρ, and β and consequently on the permanent deformation is a combined effect of properties. Therefore, it is a combination of properties which determine if the material ultimately would experience high or low permanent strain. Combination of aggregate properties and mixture properties determines if the materials has a low or high maximum permanent strain, ε_0^p, needs high or low number of load repetitions to reach a certain level of permanent strain, ρ, and has a sharp initial slope of strain at the beginning of loading, i.e., inverse effect of β. Angularity scale parameter, λ_A, and texture scale parameter, λ_T, are among the important factors that affect the coefficients and the parameters.

Angularity, texture, and pfc are among the important factors that affect the permanent deformation model. Generally, higher angularity scale parameter λ_A and texture scale parameter, λ_T affect the coefficients of the permanent deformation models in a way that lessens the predicted permanent deformation.

3.11. Resilient Modulus Testing and Modeling

The resilient modulus is the primary property of unbound materials used in the M-E pavement design [13, 14] for prediction of pavement responses to the loading. It is defined as the ratio of the maximum cyclic axial stress to the recoverable strain in one load cycle in a repeated loading. In this study, the permanent deformation and resilient modulus of the specimens compacted with the two compaction methods are investigated, and repeated load triaxial tests can be conducted. In order to characterize and predict the resilient modulus of these materials, the generalized model [13, 14], which is one of the popular resilient modulus models, can be used for fitting the experimental data of resilient modulus:

$$E_y = k_1 P_a \left(\frac{I_1}{P_a}\right)^{k_2} \left(\frac{\tau_{oct}}{P_a} + 1\right)^{k_3} \quad (3\text{-}12)$$

where, E_y = resilient modulus;

I_1 = first invariant of the stress tensor,

τ_{oct} = octahedral shear stress;

P_a = atmospheric pressure; and

k_1, k_2, k_3 = model coefficients.

Additionally, a model of resilient modulus [18, 23] which incorporates both moisture conditions and stress states is used and the model coefficients are obtained. This model is discussed later in this chapter.

The results of resilient modulus and regression coefficients corresponding to the generalized model are shown in Table 13. The predicted resilient modulus at the confining pressure of 5 psi (34.5 kPa) and deviatoric stress of 15 psi (103.4 kPa) are also presented in this table. The results indicate that the specimens compacted with gyratory compaction show higher resilient modulus than the ones compacted with the impact hammer compaction except for Pharr materials. It is similar to the results observed in the permanent deformation test.

Table 13. Resilient Modulus Generalized Model Coefficients for the Base Materials

Base Material	Compaction Method	k_1	k_2	k_3	M_r at 15 psi deviator stress & 5 psi confining pressure
Pharr	Hammer	1094.55	0.688	-0.476	21.80
	SGC	998.00	0.660	-0.481	19.44
Waco	Hammer	1359.66	0.798	-0.029	34.90
	SGC	1369.58	0.861	-0.259	37.50
Atlanta	Hammer	874.469	0.736	0.137	22.94
	SGC	1320.902	0.998	-0.693	30.15
San Antonio	Hammer	2284.035	0.877	-0.579	49.99
	SGC	1899.535	0.579	1.227	68.33

3.11.1. Resilient Modulus Model Incorporating Matric Suction

One of the unsaturated soil properties affected by soil suction is the resilient modulus. Modeling of the resilient modulus should incorporate both the moisture conditions and stress states [18, 23]. However, the generalized model does not incorporate soil moisture and saturation conditions. The model used in MEPDG applies the AASHTO model [47] which adopts an environmental parameter to incorporate the moisture dependence of the resilient modulus. Heath et al. [48] incorporated a normalized matric suction into the Uzan model [49] to predict the resilient modulus. Also, the variation of the resilient modulus with moisture conditions in granular materials is dependent on both the matric suction and degree of saturation [18, 23]. Therefore, a new model was developed [18] to address the stress dependence and moisture dependence behavior of the resilient modulus:

$$E_y = k_1 P_a \left(\frac{I_1 - 3\theta f h_m}{P_a}\right)^{k_2} \left(\frac{\tau_{oct}}{P_a}\right)^{k_3} \quad (3\text{-}13)$$

where, I_1 = first invariant of the stress tensor;

P_a = atmospheric pressure;

θ = volumetric water content;

h_m = matric suction in the aggregate matrix;

f = saturation factor, and $1 \leq f \leq 1/\theta$;

τ_{oct} = octahedral shear stress; and

k_1, k_2, and k_3 = model parameters.

Some prediction models using regression analysis were developed by Gu et al. [18] to determine the coefficients in the proposed resilient modulus model using material properties.

The coefficients of this model were obtained for each granular materials using the experimental data and the least mean square error method. The Solver Function in excel software was used to minimize the error. The coefficient k1, k2, and k3 were obtained for each set of materials compacted with gyratory compactor and impact hammer. The coefficients are presented in Table 14. The measured resilient moduli were computed from the data obtained from MTS machine for 30 loading sequences from NCHRP 1-28A report. Each loading sequence had a different confining pressure, contact stress, and axial cyclic stress. Therefore, 30 resilient moduli for each of these 30 stress states were calculated from experimental data for each material and each compaction method.

The Suction value for each of the materials and each compaction method can come from the SWCC for the moisture conditions of the specimens in the resilient modulus testing. In this study, the resilient modulus testing was conducted at the optimum moisture content of the specimens compacted with each compaction method. The matric suction was measured for the optimum moisture content of each compaction method. The SWCC of these materials were also developed. Thus, the matric suction is inserted into the resilient modulus model. The volumetric water content was also known for each set of specimens having the moisture content of the tested specimens, maximum dry density, and the specific gravity. The saturation factor, *f*, is an indicator of saturation

conditions [23, 50]. It is multiplied by volumetric water content, θ, and the matric suction, h_m, to account for the moisture stress state in the soil structure in the transition zone. The following equation is used for saturation factor [50], considering that $1 \leq f \leq 1/\theta$:

$$f = 1 + \frac{S-85}{15}\left(\frac{1}{\theta} - 1\right) \quad \text{(3-14)}$$

where, f = saturation factor;

S= degree of saturation (in percent);

θ = volumetric water content.

The predicted values of the resilient modulus for each stress state in the 30 loading sequences and the measure resilient modulus are plotted for each base course material and both gyratory and impact hammer compaction methods in Figure 30 to Figure 33. The predicted resilient modulus are plotted versus the experimental resilient modulus obtained from the repeated triaxial load tests for the 30 loading sequences for Atlanta, San Antonio, Pharr, and Waco base courses in Figure 30, Figure 31, Figure 32, and Figure 33, respectively. Each datapoint in these curves corresponds to a loading sequence used in this study.

Table 14. Coefficients of Resilient Modulus Model Incorporating Matric Suction for the Base Materials

Base Material	Compaction Method	k_1	k_2	k_3	*Suction at Optimum Moisture Content (kPa)*	*Volumetric Water Content*
Waco	Impact Hammer	2586.68	0.3996	0.001	-2.408	0.1721
	Gyratory Compactor	2338.65	0.4356	0.080	-19.573	0.1895
Atlanta	Impact Hammer	1057.48	0.7243	0.0143	-8.224	0.1442
	Gyratory Compactor	1209.10	0.6095	0.010	-209.694	0.1498
Pharr	Impact Hammer	962.20	0.4751	0.001	-215.293	0.2310
	Gyratory Compactor	1131.85	0.4173	0.003	-104.558	0.2575
San Antonio	Impact Hammer	2387.73	0.5986	0.003	-2.199	0.1432
	Gyratory Compactor	2273.06	1.0278	0.105	-44.100	0.1739

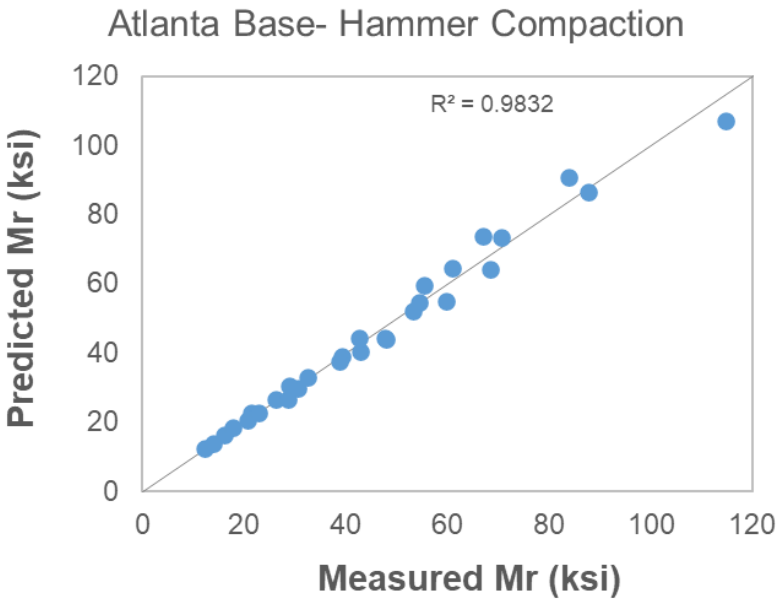

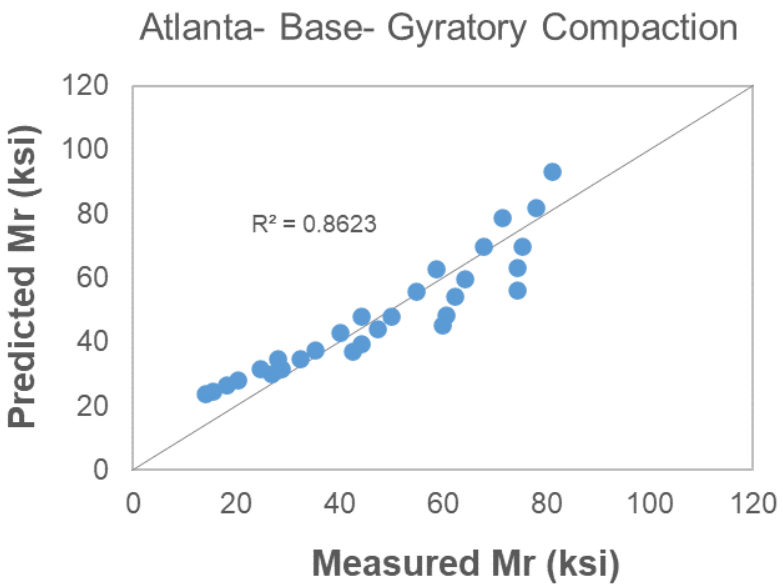

Figure 30. Experimental and predicted Resilient Modulus Data from the Model Incorporating both Suction and Stress States for Atlanta Base Course

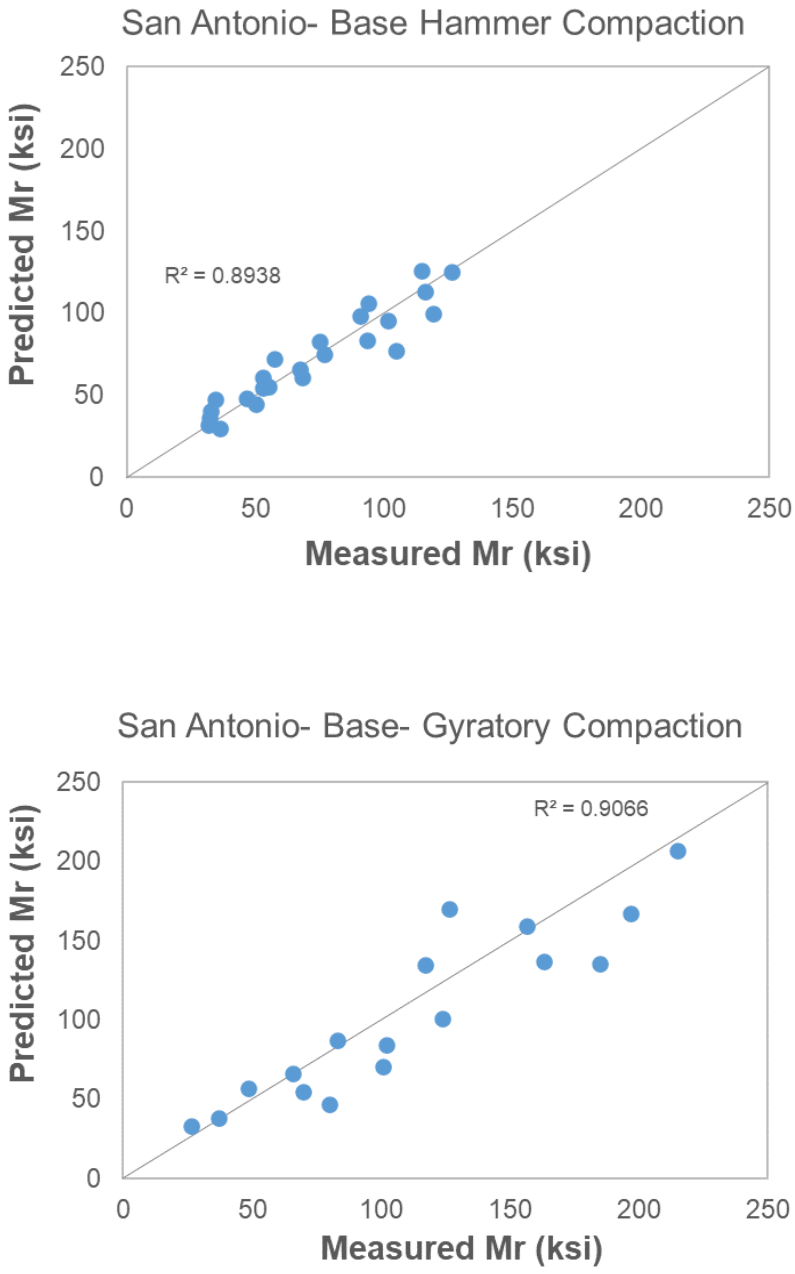

Figure 31. Experimental and predicted Resilient Modulus Data from the Model Incorporating both Suction and Stress States for San Antonio Base Course

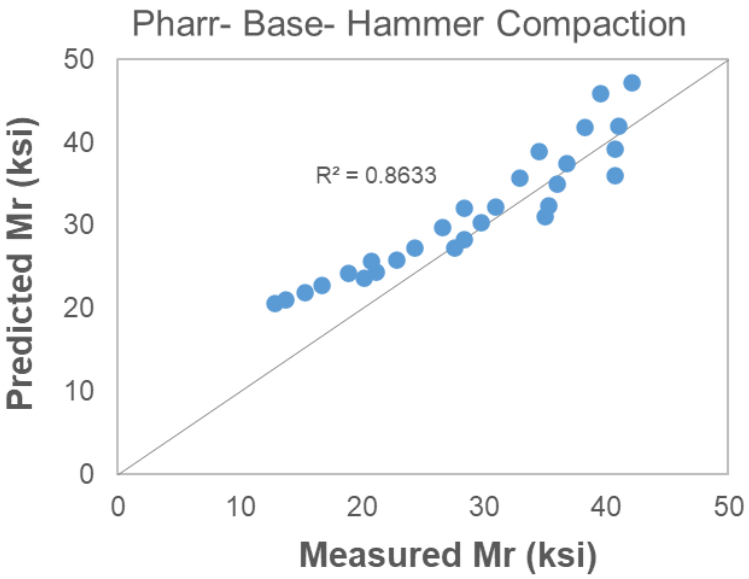

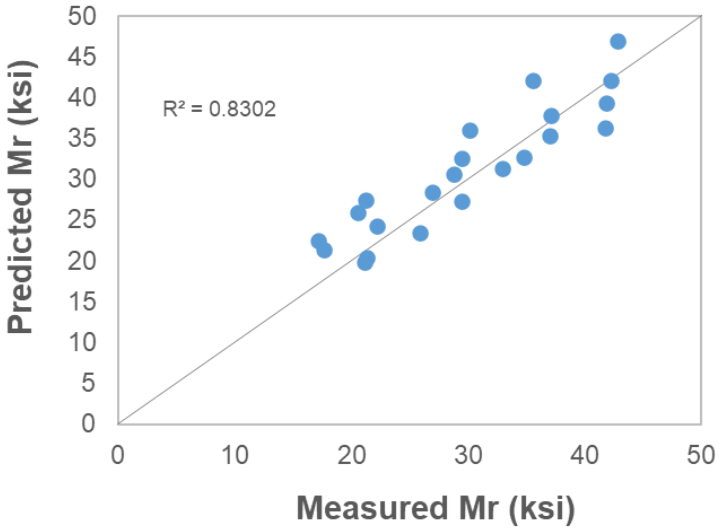

Figure 32. Experimental and predicted Resilient Modulus Data from the Model Incorporating both Suction and Stress States for Pharr Base Course

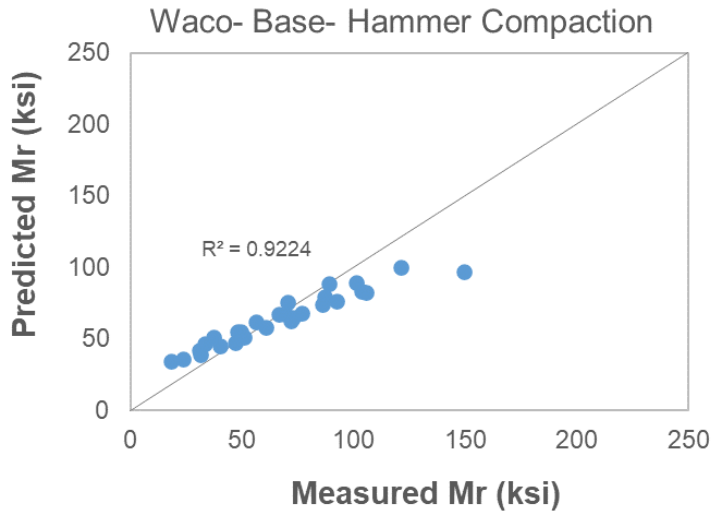

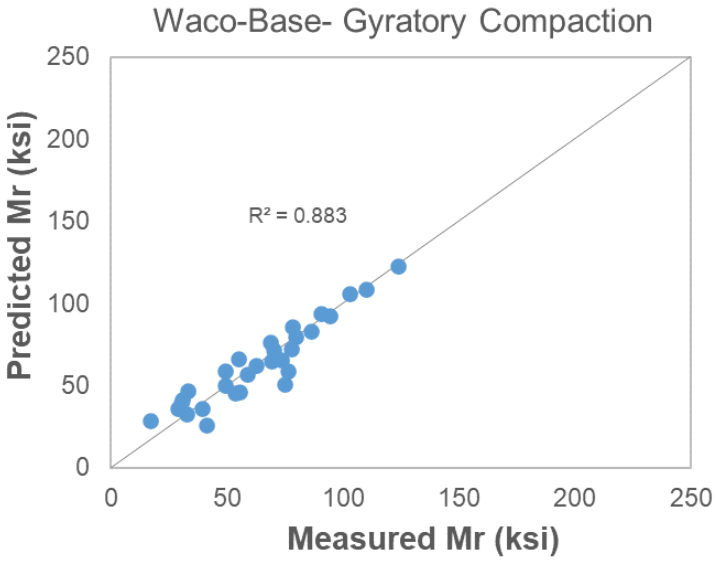

Figure 33. Experimental and predicted Resilient Modulus Data from the Model Incorporating both Suction and Stress States for Waco Base Course

3.11.1.1. Multivariable Regression Analysis for Coefficients of the Resilient Modulus Model

Multivariable regression analysis has been performed using R programming software to investigate the relation between the performance-related properties of materials and the k_1, k_2, and k_3 coefficients in the Resilient modulus model [23] incorporating suction, stress states, and moisture and saturation conditions. The properties considered in the prediction models for *k1*, *k2*, and *k3* are the maximum dry density (γ_d), pfc, MBV, aggregate angularity, texture, and sphericity in terms of the parameters in the cumulative Weibull distribution. These cumulative Weibull distribution parameters are angularity shape parameter (a_A), angularity scale parameter ($\boldsymbol{\lambda_A}$), texture shape parameter (a_T), texture scale parameter ($\boldsymbol{\lambda_T}$), sphericity shape parameter (a_S), and sphericity scale parameter ($\boldsymbol{\lambda_S}$). The material properties considered in the development of prediction models of coefficients k_1, k_2, and k_3 in this study in the following model in equation 3-12 are presented in Table 15 for the materials fabricated with both the gyratory and impact hammer compaction methods.

$$E_y = k_1 P_a \left(\frac{I_1 - 3\theta f h_m}{P_a}\right)^{k_2} \left(\frac{\tau_{oct}}{P_a}\right)^{k_3} \quad (3\text{-}12)$$

The dry density, angularity, texture, and shape indices from AIMS test, and percent fines content (pfc) were considered the significant variables in the development of the prediction models for the *k* coefficients based on the statistical analysis performed by Gu et al. [18] within their data points. Correlation tables were formed in the R program in this study which included the correlation between different input variables

with each other, and also the output parameter in this study. The input variable parameters with lower correlation with each other and higher correlation with the output parameters were selected.

Table 15. Materials Properties Used in the Multivariable Regression Analysis for Coefficients k_1, k_2, k_3 of Resilient Modulus Model

Material	Compaction method	Angularity		Texture		Sphericity		pfc	MBV	γ_{Dry} (lb/ft^3)
		a_A	λ_A	a_T	λ_T	a_s	λ_s			
Waco	Hammer	3.978	3553.0	2.367	138.2	10.216	0.696	12.34	18.19	130.95
Waco	SGC	3.978	3553.0	2.367	138.2	10.216	0.696	12.34	18.19	132.07
Pharr	Hammer	3.801	3147.0	3.457	147.9	7.841	0.748	4.16	13.98	112.62
Pharr	SGC	3.801	3147.0	3.457	147.9	7.841	0.748	4.16	13.98	118.36
Atlanta	Hammer	5.012	2800.7	2.721	193.5	7.433	0.739	3.52	0	134.3
Atlanta	SGC	5.012	2800.7	2.721	193.5	7.433	0.739	3.52	0	135.46
San-Antonio	Hammer	4.565	2998.3	2.310	126.8	8.943	0.684	7.19	9.22	137.47
San-Antonio	SGC	4.565	2998.3	2.310	126.8	8.943	0.684	7.19	9.22	137.96

The prediction models for the coefficients k_1, k_2, and k_3 in the resilient model for the materials compacted with the gyratory compactor are as follows:

$$Ln(k_1) = 2.2880 + 1.0728\ Ln(\lambda_A) - 9.9225\ (\lambda_s) + 0.7383\ Ln(\gamma_d) \quad (3\text{-}15)$$

$$k_2 = 12.0264 - 0.1890\ Ln(\lambda_A) - 13.0544\ (\lambda_s) - 0.0777\ pfc \quad (3\text{-}16)$$

$$k_3 = -1.1479\ +\ 0.4368\ Ln(\gamma_d) - 0.1887\ Ln(\lambda_t) + 0.00199\ pfc \quad (3\text{-}17)$$

where, the resilient modulus values from the model is in psi.

The prediction models for the coefficients k_1, k_2, and k_3 in the resilient model for the materials compacted with the impact hammer are as follows:

$$Ln(k_1)\ = -1.7222 + 1.6438\ Ln(\lambda_A) - 12.3820\ (\lambda_s) + 0.9765\ Ln(\gamma_d) \quad (3\text{-}18)$$

$$k_2 = 19.0565 - 2.4961\ Ln(\lambda_A) + 1.8170\ (\lambda_s) + 0.0393\ pfc \quad (3\text{-}19)$$

$$k_3 = -0.2917\ + 0.0362\ Ln(\gamma_d) +\ 0.0248\ Ln(\lambda_t) - 0.00046\ pfc \quad (3\text{-}20)$$

where, the resilient modulus values from the resilient model are in psi, and,

λ_A: angularity scale parameter,

λ_T: texture scale parameter,

λ_S: sphericity scale parameter

pfc: Percent Fines Content, and,

γ_d: Maximum Dry Density (Pound per Cubic Feet, pcf).

Therefore, it is a combination of properties which determines if the material ultimately would show high or low resilient modulus. Combination of aggregate properties and mixture properties determines if the materials have high or low k_1, k_2, *and*

k_3. Angularity scale parameter, λ_A, texture scale parameter, λ_T, sphericity scale parameter, λ_S, and *pfc* are among the important factors that affect the resilient modulus and the coefficients of the resilient modulus model. A sensitivity analysis has also been conducted. It indicated that the most important factor in the prediction models of resilient modulus model coefficient is the angularity scale parameter, λ_A, for the materials compacted with the gyratory compactor. Moreover, the sphericity scale parameter, λ_S, and angularity scale parameter, λ_A, are the most important factors in resilient modulus prediction models for the materials compacted with impact hammer.

The angularity scale parameter, λ_A, affects the coefficient k_1 and subsequently the resilient modulus value predicted from the model, as it contributes in the equations developed for k_1 for both materials compacted with the gyratory compactor and the impact hammer. The coefficient k_1 increases with rise of angularity scale parameter, λ_A in the both of these series of materials. Therefore, the value of the resilient modulus predicted from the resilient modulus model using the prediction models of the coefficients is supposed to increase. This observation is in accordance with the finding in the literature review that the higher angularity enhances the aggregate interlocking and ultimately increases the resilient modulus [51, 45, 52, 53].

The contribution of λ_A on the coefficient k_1 is almost the same in both series of materials produced by the gyratory compactor and impact hammer, with a slightly more contribution in k_1 in the hammer compacted samples. It is worth noting that the intercept of the equation of the coefficient k_1 in higher for the samples compacted with gyratory compactor, which leads to higher k_1 for the similar conditions and similar other

properties. The effect of gyratory compaction can also be reflected on the effect of maximum dry density, γ_d, in the equation for k_1. It is worth noting that the effect of material properties and compaction method are combined effects of multiple variables, as seen in the developed equations for the model coefficients. Increase of maximum dry density, γ_d, raises the coefficient k_1 and, subsequently, results in a higher predicted resilient modulus in both series of the samples compacted with the gyratory compactor and the impact hammer. The contribution of γ_d to the equations of k_1 is close for the samples compacted with gyratory compaction and impact hammer. The aggregate properties and material properties affect the coefficients k_2, and k_3 differently. The sphericity scale parameter and pfc affect the equations for k_2 differently for the gyratory compacted samples versus the impact hammer compact samples. Higher values of pfc result in the lower value of the predicted k_2 for gyratory compacted samples. This matter consequently leads to a reduction in the predicted amount of resilient modulus. It is in line with the presumption that the fine particles affect the mechanical behavior of granular matrix adversely. The different series of equations for the coefficients k1, k2, and *k3* in the resilient modulus model show the difference between these compaction methods.

The texture scale parameter, λ_T, also affects the coefficient k_3 and thus, it influences the resilient modulus value obtained from the model. It contributes to the equations developed for k_3 for both materials compacted with gyratory compactor and impact hammer. The contribution of texture scale parameter, λ_T, is higher in the equation developed for k_3 for the samples compacted with gyratory compactor than the

impact hammer. The increase of texture scale parameter, λ_T, reduces the coefficient k_3 for samples compacted with the gyratory compactor, and usually increases the predicted resilient modulus value in this study. We need to consider that the value of k_3 has been less than 1.0 in this study. Also, the base where the exponents k_3 affects in the resilient modulus model, which includes the octahedral shear stress (τ_{oct}) fraction, has been less than 1.0 for most of the loading sequences used in this study. Therefore, increase of texture scale parameter, λ_T, usually results in rise in the predicted resilient modulus values. It is in line with the findings in the literature stating that a rise of the aggregate texture index increases the friction and interlock between aggregates, and increases the resilient modulus.

The materials compacted with the gyratory compactor had been subjected to the shear stresses in the compaction process, and it is presumed that the aggregates with higher texture index could form a stronger structure with higher friction during the motions in the gyratory compaction. This presumption is in accordance with the equation developed for k_3 for the specimens produced by the gyratory compactor. The coefficient k_3, as the exponent to the normalized octahedral shear stress, impacts the role of the octahedral shear stress in the resilient modulus model. The gyratory compacted samples are subjected to shear stresses during the motions of the compaction process. The texture scale parameter, λ_T, has more contribution to the prediction model of k_3 for the specimens compacted with the gyratory compaction compared to the impact hammer compaction. Generally, higher angularity scale parameter λ_A and texture scale parameter,

λ_T affect the coefficients of the resilient modulus models in a way that increases the predicted resilient modulus.

3.11.2. Statistical Analysis of the Resilient Modulus Data

Statistical analyses were conducted on the experimental data of resilient modulus obtained from the repeated load triaxial tests using JMP software [54]. The experimental results of resilient modulus for the samples compacted with gyratory compactor and impact hammer were compared using the Paired t-test. Paired t-test was applied to these datasets, since each resilient modulus datapoint corresponded with a certain loading sequence. Therefore, each pair was associated with the datapoints for one loading sequence for the gyratory compacted and impact hammer compacted samples.

The mean of the difference between the two datapoints within each pair was analyzed. The confidence level of the test was 95%. The outputs of this statistical analysis can help evaluate the mean difference between the resilient modulus obtained from each set of specimens, and generally study the difference between these two datasets of resilient modulus. The results of the paired t-test using JMP software are presented in Figure 34 and Table 16.

The mean difference in Table 16 corresponds to the resilient modulus of the specimens made with the impact compaction minus the resilient modulus of the one made with gyratory compaction (SGC). The low p-value in all of the tests for the studied materials indicated that the resilient modulus of these two sets of data were not the same. The results indicated that samples produced by gyratory compactor showed higher mean

of resilient modulus compared to the impact compaction for Waco, Atlanta, and San Antonio base course materials. However, specimens fabricated by the gyratory compactor showed lower mean of resilient modulus compared to the impact compaction for Pharr base course material. It is in accordance with the observation mentioned before form the estimation of the resilient modulus in Table 13.

Table 16. Paired t-test on the Resilient Modulus of the Materials Fabricated with Different Compaction Methods

Material	Mean Difference (ksi)	Standard Error (ksi)	Degree of Freedom	t-ratio	p-value
Atlanta Base	-11.62	2.49	28	-4.67	< 0.0001 (prob <t)
Waco Base	-13.39	6.07	27	-2.21	0.018 (prob <t)
San Antonio Base	-85.19	16.39	20	-5.20	< 0.0001 (prob <t)
Pharr Base	2.35	0.46	29	5.11	< 0.0001 (prob >t)

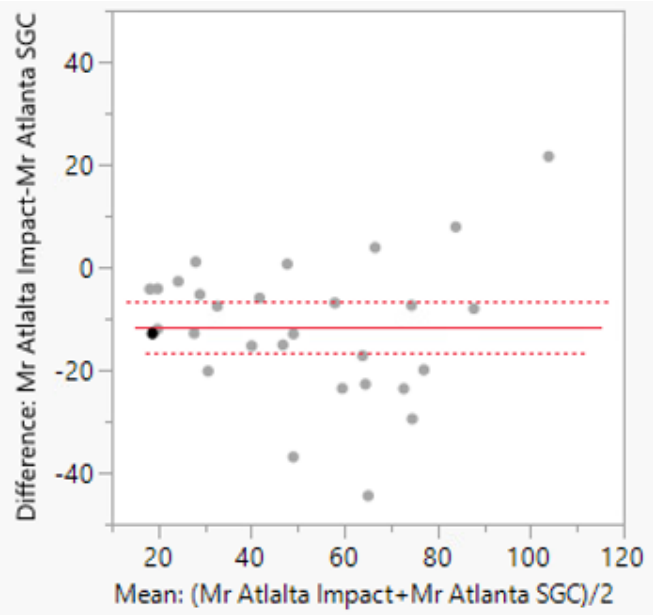

(a) Atlanta Base

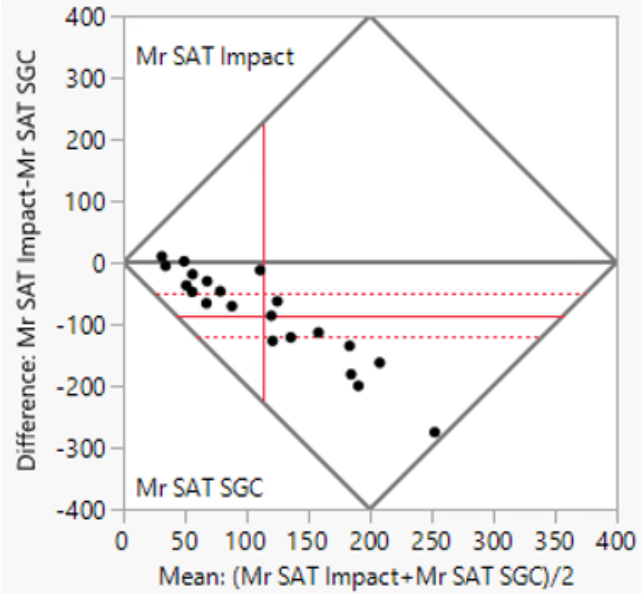

(b) San Antonio Base

Figure 34. Statistical Analysis on the Resilient Modulus of the Materials Made with Different Fabrication Methods

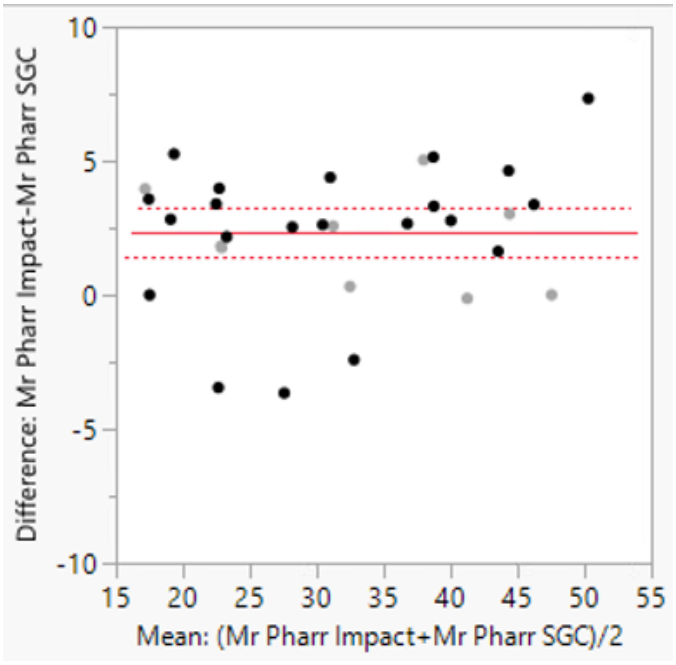

(c) Pharr Base

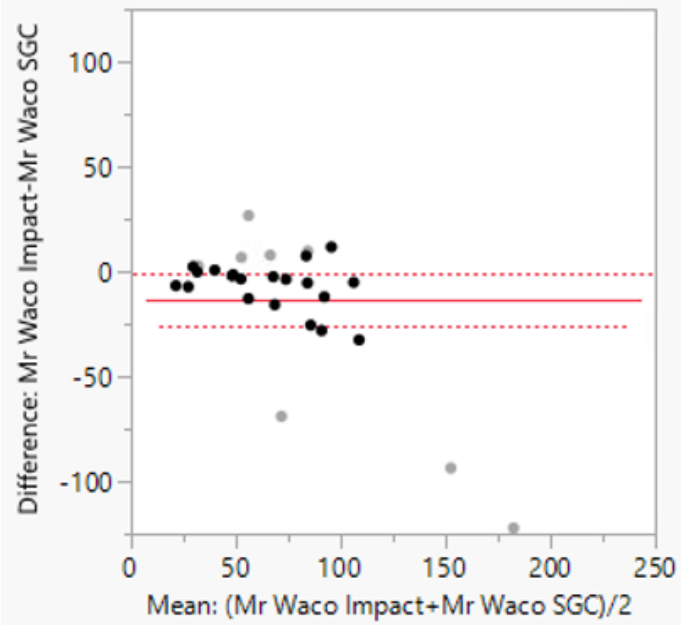

(d) Waco Base

Figure 34. Continued

3.12. Compaction Energy

Different materials may require different levels of compaction energy for compaction in the laboratory and the field, since they may have different aggregate structure and physical properties. The study of laboratory compaction energy was conducted to provide a potential indicator of the compaction energy and compaction effort that would be required in the field. Compaction is achieved by the combined action of gyration and normal pressure in the gyratory compactor. The sample volume decreases with each gyration in the gyratory compaction process. The experimental data of the gyratory compaction obtained from SGC was reviewed. The SGC can record the change of height of the sample over the number of gyrations during the gyratory compaction. The mathematical shape of the curve, plotting height of the specimen versus number of gyrations led to derive a mathematical equation which could model the decrease of height with the number of gyrations. Therefore, the volume change could be modeled. Thus, an equation has been developed for the gyratory compaction curve to predict the decrease of materials volume in the gyratory compaction process, and to predict the volume of sample as a function of number of gyration [25] as shown in the following equation:

$$V = \frac{V_e N^{\alpha} + V_1 \gamma (N_0 - N)^{\alpha}}{N^{\alpha} + \gamma (N_0 - N)^{\alpha}} \quad (3\text{-}21)$$

where, V= volume of sample,

V_e= volume of sample at the end of compaction,

V_1= volume of sample at the beginning of compaction;

N= number of gyrations;

N_0= number of gyrations at the end of compaction; and

α, and γ= regression coefficients.

It was assumed that the volume of the sample at the beginning of the compaction and end of compaction were known in the development of this equation. These data could be obtained from the SGC machine. It is assumed that the materials in the mold had a constant surface area as the surface area of the mold within the whole height of the sample. The volume of the sample at the end of compaction was obtained with the target height or final height recorded in the SGC at the last gyration. The height of the sample at the beginning of compaction was recorded at the gyration number equal to zero when the machine started to compact, which might be a little different from the real initial sample height. The proposed equation worked well with the experimental data. Using this equation, the following expression has been developed for the calculation of relative compaction energy in SGC compaction [25]:

$$CE = -p\left(V_0 - \frac{V_1+\gamma\, V_e(N_0-1)^{\alpha}}{1+\gamma(N_0-1)^{\alpha}}\right) \quad (3\text{-}22)$$

where CE = the estimated compaction energy, and

p = the compressive pressure applied in the SGC.

Using the experimental data, the coefficients α, and γ, and relative compactive energy for the studied base materials have been obtained and presented in Table 17 and Figure 35. The term relative is selected, because this variable does not provide the

absolute compaction energy, and is used for comparing the comacption energy between different materials.

Table 17. Gyratory Compaction Curve Coefficients and Compaction Energy

Material	α	γ	Compactive Energy (N-m)
San Antonio	0.968	0.156	364.815
Pharr	0.883	0.095	356.528
Waco	0.977	0.163	340.724
Atlanta	0.892	0.150	278.519
Amarillo	0.919	0.161	182.768

As observed in the results, San Antonio, Pharr base, and Waco materials required higher compaction energy to achieve the target density compared to Atlanta and Amarillo base materials. As shown in Figure 1, San Antonio and Waco have the least well-graded particle size distribution, and they are expected to require higher compaction energy. The San Antonio and Waco base course materials have highest values of gradation shape parameter, a_G, and lowest gradation scale parameter, λ_G, as shown in Figure 20 and Figure 21, respectively. It also confirms that these materials have the least well-graded particle size distribution among the studied materials. Pharr material contains some clayey materials. Amarillo requires the lowest compaction

energy among the studied materials. Amarillo base is a sandy material with non-plastic fines and needed lower compaction effort in the lab. Therefore, gyratory compactor could assist in providing the data for modeling the resistance of the material to deformation during the compaction process. It could capture the difference between the behavior of different materials in compaction and the energy required to reach a certain level of compaction. This difference could be explained by material properties.

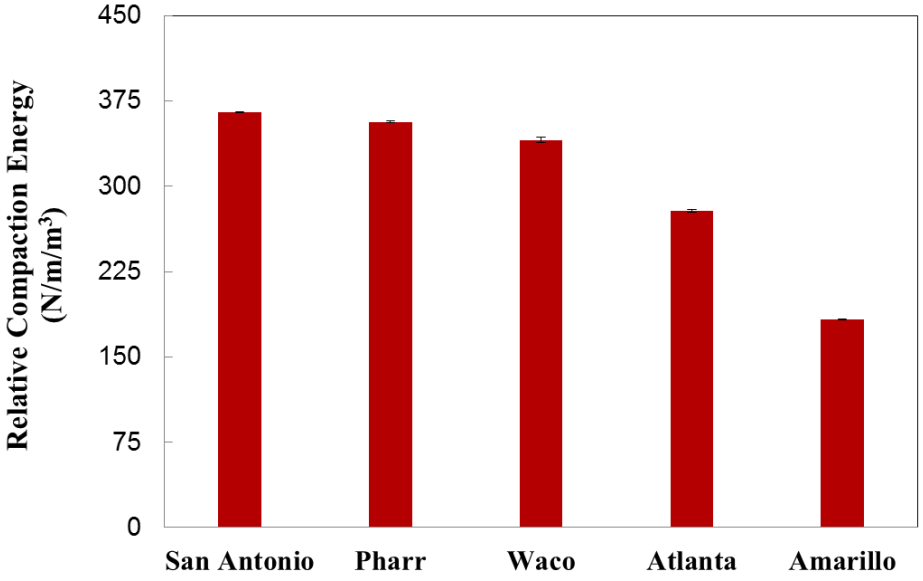

Figure 35. Calculated Compaction Energy in Gyratory Compaction

4. NONDESTRUCTIVE TESTING TECHNIQUES

4.1. Introduction

The non-destructive testing was performed using Computed Tomography (CT) scanning and the Percometer measurements of dielectric constant. CT scanning assists with understanding and comparison of the internal structure of the unbound materials in both the gyratory and impact hammer compaction methods. Dielectric constant of soil and granular materials is measured with Percometer. Suction is measured with filter paper test. This measured data along with the form of equation developed for the relationship between these two test properties can lead to find the relation between these properties for the studied material. Then, these relationships can be used to estimate the conditions of the soil and other properties by having the data from the nondestructive evaluation techniques.

In this chapter, the CT scanning results are presented. Then, the dielectric constant measured from the Percometer and predicted with CRIM model is investigated. Then, the relationship between soil suction and dielectric constant is investigated. This can help have an evaluation of the soil suction in the filed using Ground Penetrating Radar (GPR) as a nondestructive testing technique. Having an estimation of the soil suction can help with the evaluation and estimation of the properties of granular materials in the field dependent on suction and moisture conditions.

4.2. Computed Tomography (CT) Scanning

The results of the CT scanning on Pharr base course, and the subgrade soil material are presented herein. The CT scan images of the cross sections and porosity distribution curves through the height of the specimens are presented. Two series of samples were tested and investigated in this study, samples fabricated with the gyratory compactor and the impact hammer.

The distribution of porosity through the height of the specimens compacted with gyratory compactor and impact hammer for the Pharr base course material is demonstrated in Figure 36. The porosity versus height curve indicated that the specimen compacted with the gyratory compactor had a more uniform distribution of pores compared than the hammer compacted sample. The boundaries and layer interface between lifts are clearly observed in the CT scan images of sections of the specimens compacted with impact hammer, as shown in Figure 37. These observations indicated that the gyratory compactor provided more uniform aggregate structure through the height of the specimen. Moreover, higher porosity at the bottom of each lift in the specimen compacted with the impact hammer was observed, while the porosity was lower at the top of each lift.

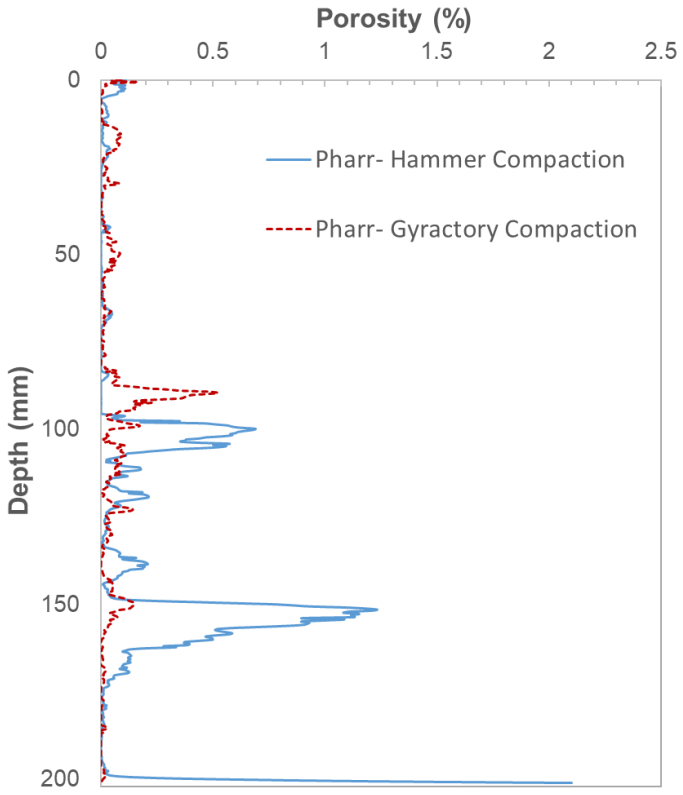

Figure 36. Porosity vs. Depth of the Specimens of Pharr Base Course Compacted with Gyratory and Impact Hammer Compaction Obtained from CT Scanning

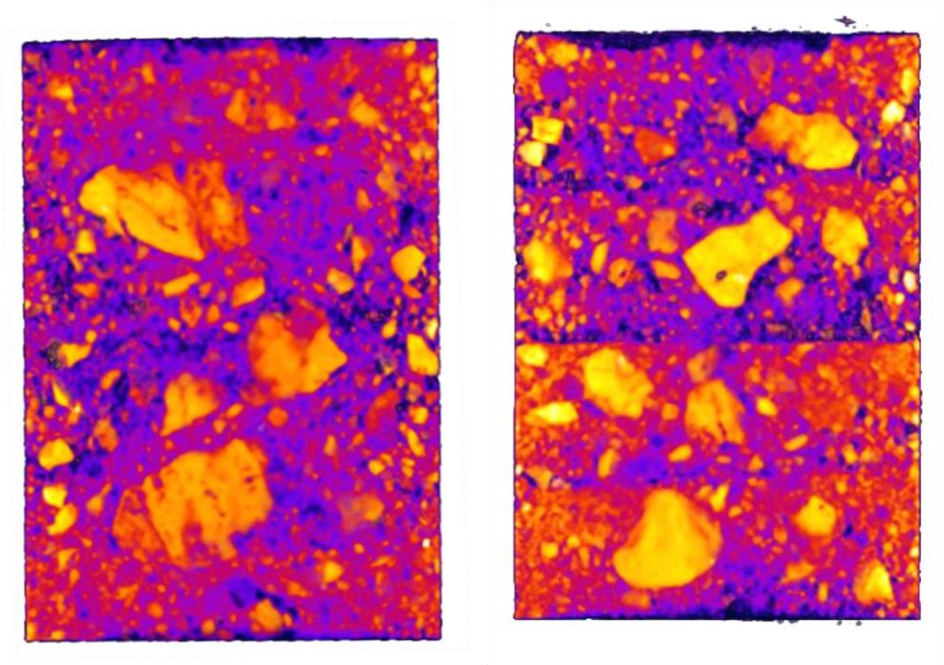

(a) (b)

Figure 37. Cross Sections of Pharr Base Course Compacted with a) Gyratory and b) Impact Hammer Compaction Obtained from CT Scanning

The porosity distribution of the specimens compacted with gyratory compactor and impact hammer for the subgrade soil is shown in Figure 38. The porosity curve indicated that the specimen compacted with the gyratory compactor had a more uniform distribution of pores compared to the hammer compacted sample. The boundaries and layer interface between lifts in the specimens compacted with impact hammer are clearly observed in the CT scan images of sections shown in Figure 39. These observations indicated that the gyratory compactor provided more uniform aggregate structure

through the height of the specimen. Moreover, higher porosity at the bottom of each lift in the specimen compacted with the impact hammer was observed, while the porosity was lower at the top of each lift.

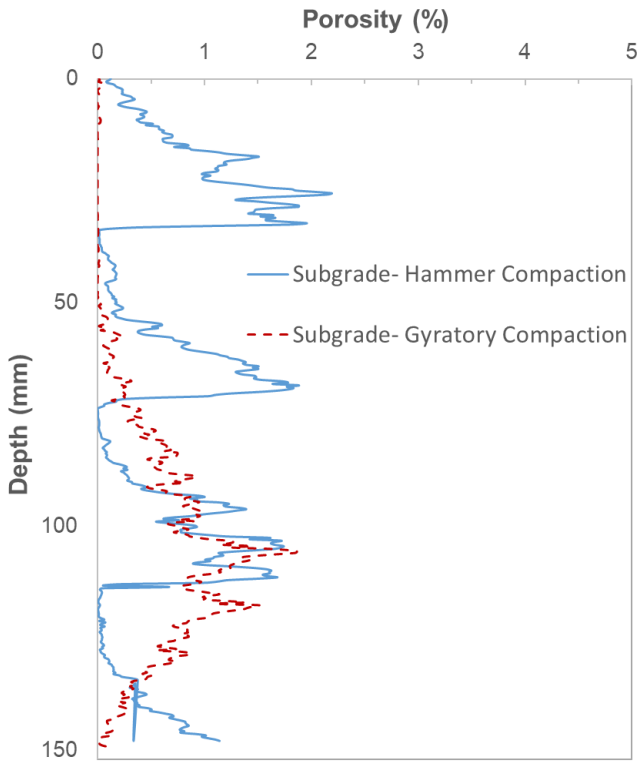

Figure 38. Porosity vs. Depth of the Specimens of Subgrade Soil Compacted with Gyratory and Impact Hammer Compaction Obtained from CT Scanning

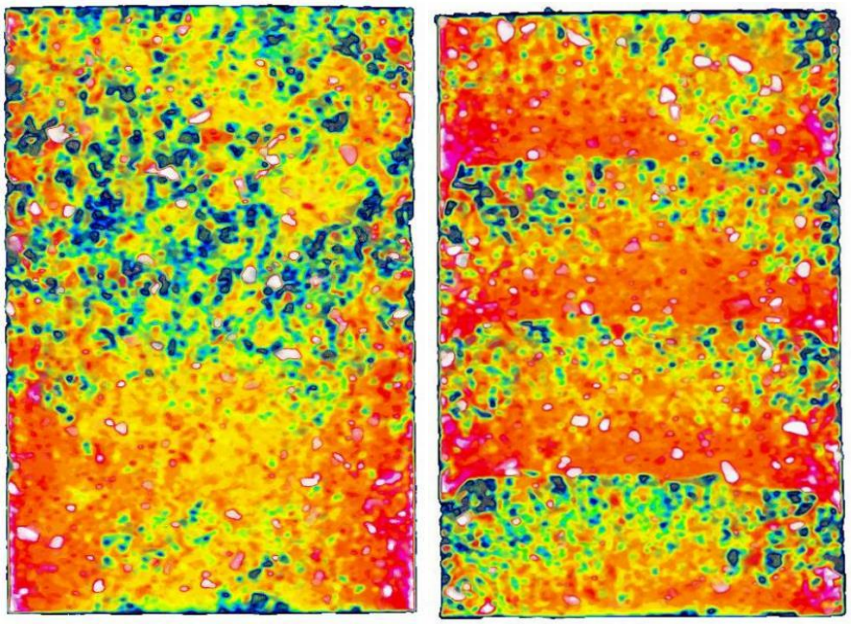

(a) (b)

Figure 39. Cross Sections of Subgrade Soil Compacted with a) Gyratory and b) Impact Hammer Compaction Obtained from CT Scanning

4.3. Nondestructive Evaluation Techniques Using Dielectric Constant

The dielectric constant of the specimens was measured using the Percometer for the materials compacted at optimum moisture content (OMC) with both gyratory compactor and impact hammer compaction. Then, some other samples with a moisture content drier than OMC were tested with the Percometer. These samples are the same samples prepared for filter paper test. The values of dielectric constant of the samples with OMC and drier than OMC are presented in Table 18.

Since soils and base course materials are mixtures of solid particles, water, and air, the dielectric constant of these materials is composite dielectric constant of solid particles, water, and air. In this study, the Complex Refraction Index model (CRIM) model has been used for soils as a multiphase mixture to calculate the dielectric constant of the solid particles. The CRIM model is expressed in the following equation to calculate the dielectric constant of a material composed of different components:

$$\varepsilon^n = \sum_{i=1}^{m} \varepsilon_i^n \, a_i \tag{4-1}$$

where, ε= dielectric constant of the material with m components,

ε_i= dielectric constant of component i, and

a_i= volumetric concentration of component i.

For soils as multiphase materials, n equal to 0.5 is the most common value. Therefore, we write the CRIM model with the following equation for soils:

$$\sqrt{\varepsilon} = \sqrt{\varepsilon_s}\,\theta_s + \sqrt{\varepsilon_w}\,\theta_w + \sqrt{\varepsilon_a}\,\theta_a \tag{4-2}$$

where, ε= dielectric constant of the soil, ε_s= dielectric constant of the soil solid particles, ε_w= dielectric constant of water, ε_a= dielectric constant of air, θ_s = volumetric content of solid particles, θ_w= volumetric water content, and θ_a= volumetric air content. Since, we have from soil mechanics that $\theta_a = 1 - (\theta_s + \theta_w)$, and the dielectric constant of air is almost 1.0, we can re-write the CRIM model equation:

$$\sqrt{\varepsilon} = \left(\sqrt{\varepsilon_s} - 1\right)\theta_s + \left(\sqrt{\varepsilon_w} - 1\right)\theta_w + 1 \tag{4-3}$$

Therefore, the dielectric constant of solid particles can be estimated using the CRIM model mentioned above, the measured dielectric constant of specimens at different moisture contents, specific gravity, and dry density. Dielectric constant of the solid particles has been estimated and is presented in Table 18.

Table 18. Measured Dielectric Constant of Materials and the Calculated Dielectric Constant of Solid Particles

Material	Compaction Method	Moisture Conditions	Dielectric Constant (ε)	Moisture Content (%)	ε_s
San Antonio	Gyratory	OMC	10.37	7.87	4.111
San Antonio	Gyratory	OMC- ωi	5.90	3.2	4.286
San Antonio	Hammer	OMC	13.61	6.5	8.525
San Antonio	Hammer	OMC- ωi	11.46	4.8	8.494
Atlanta	Gyratory	OMC	6.60	6.9	2.165
Atlanta	Gyratory	OMC- ωi	3.57	3.02	2.143
Atlanta	Hammer	OMC	8.90	6.7	4.260
Atlanta	Hammer	OMC- ωi	7.38	5.9	3.605
Pharr	Gyratory	OMC	17.47	13.58	6.886
Pharr	Gyratory	OMC- ωi	13.69	7.74	10.335
Pharr	Hammer	OMC	18.50	12.8	10.330
Pharr	Hammer	OMC- ωi	15.67	11	9.535

Table 18. Continued

Material	Compaction Method	Moisture Conditions	Dielectric Constant (ε)	Moisture Content (%)	ε_s
Waco	Gyratory	OMC	13.76	8.96	6.522
Waco	Gyratory	OMC- ωi	7.35	2.35	7.347
Waco	Hammer	OMC	14.90	8.2	8.679
Waco	Hammer	OMC- ωi	10.44	6.75	5.954

4.4. Suction Dielectric Characteristic Curve

A relationship between soil suction and dielectric constant can lead to having an estimation of the soil suction and consequently the moisture conditions of the soil with having the dielectric constant of the soil. The volumetric water content can be estimated using the soil water characteristic curve with having the matric suction. A relationship between soil suction and the dielectric constant has been developed:

$$\varepsilon = \frac{\varepsilon_{sat} + \alpha\, \varepsilon_{dry}\, h^{\gamma}}{1 + \alpha\, h^{\gamma}} \tag{4-3}$$

where, ε= dielectric constant of the soil, ε_{sat}= dielectric constant in the saturated conditions, particles, ε_{dry}= dielectric constant in the dry conditions, α, γ= model

coefficients. The dielectric constant in the saturated and dry conditions, ε_{sat} and ε_{dry} can be estimated for each material using the following expressions:

$$\sqrt{\varepsilon_{sat}} = \theta_s\sqrt{\varepsilon_s} + \theta_w\sqrt{\varepsilon_w} + \theta_a\sqrt{\varepsilon_a} \quad (4\text{-}4)$$

where θ_s = 1-n , θ_w=n , θ_a=0, and n=porosity.

$$\sqrt{\varepsilon_{dry}} = \theta_s\sqrt{\varepsilon_s} + \theta_w\sqrt{\varepsilon_w} + \theta_a\sqrt{\varepsilon_a} \quad (4\text{-}5)$$

where θ_s = 1-n , θ_w=0, θ_a=n and n=porosity.

The calculated dielectric constant of saturated conditions and dielectric constant dry conditions are presented in Table 19. The dielectric constant of saturated conditions and dry conditions are compared in Figure 40 for samples compacted with gyratory compactor and impact hammer.

Table 19. Estimated Dielectric Constant of Materials at Saturated Conditions and Dry Conditions

Material	Compaction	Moisture Conditions	e	n	θs	θw	θ_{air}	$\varepsilon_{saturated}$	ε_{dry}
San-Antonio	Gyratory	Saturated	0.240	0.193	0.807	0.193	0.000	11.518	-
	Gyratory	Dry	0.240	0.193	0.807	0.000	0.193	-	3.408
	Hammer	Saturated	0.244	0.196	0.804	0.196	0.000	16.885	-
	Hammer	Dry	0.244	0.196	0.804	0.000	0.196	-	6.459

Table 19. Continued

Material	Compaction	Moisture Conditions	e	n	θ_s	θ_w	θ_{air}	$\varepsilon_{saturated}$	ε_{dry}
Atlanta	Gyratory	Saturated	0.271	0.213	0.787	0.213	0.000	9.459	-
	Gyratory	Dry	0.271	0.213	0.787	0.000	0.213	-	1.871
	Hammer	Saturated	0.282	0.220	0.780	0.220	0.000	12.448	-
	Hammer	Dry	0.282	0.220	0.780	0.000	0.220	-	3.121
Pharr	Gyratory	Saturated	0.451	0.311	0.689	0.311	0.000	23.217	-
	Gyratory	Dry	0.451	0.311	0.689	0.000	0.311	-	5.445
	Hammer	Saturated	0.524	0.344	0.656	0.344	0.000	26.644	-
	Hammer	Dry	0.524	0.344	0.656	0.000	0.344	-	5.818
Waco	Gyratory	Saturated	0.302	0.232	0.768	0.232	0.000	16.904	-
	Gyratory	Dry	0.302	0.232	0.768	0.000	0.232	-	5.081
	Hammer	Saturated	0.312	0.238	0.762	0.238	0.000	17.666	-
	Hammer	Dry	0.312	0.238	0.762	0.000	0.238	-	5.286

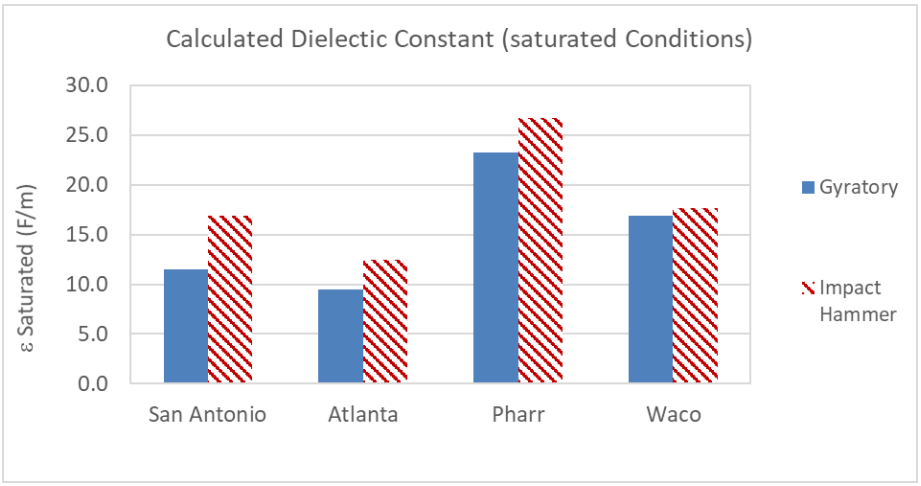

(a)

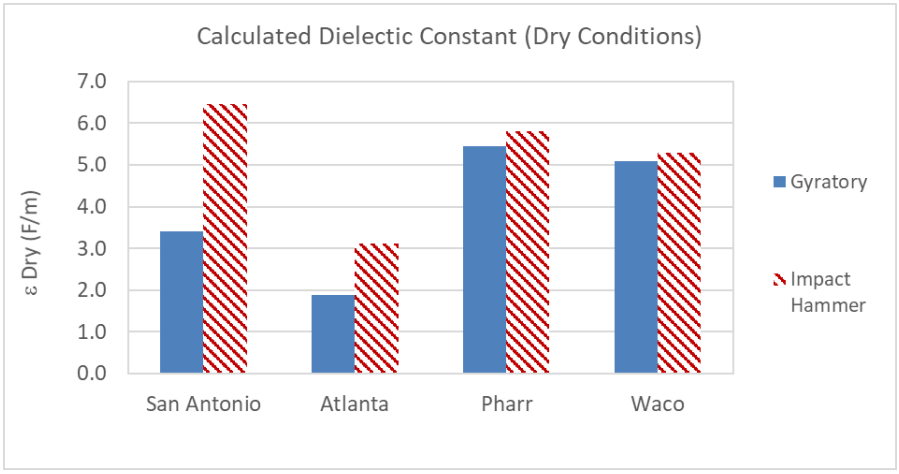

(b)

Figure 40. Dielectric Constant of and Saturated and Dry Conditions Obtained Using CRIM Model

The dielectric constant of the saturated and dry conditions for each material and each compaction method has been used in the soil suction versus dielectric constant

curve. Furthermore, the matric suction values and measured dielectric constant values at optimum moisture content and the moisture content drier than the optimum have been used in this equation.

The matric suction can be obtained from Soil water characteristic curve (SWCC). In this study, the same samples were used for measurement of matric suction and dielectric constant. Thus, the measured values of matric suction and dielectric constant have been used in the suction versus dielectric constant curve. Therefore, we have two data points on the suction dielectric constant curves thus far for two moisture conditions. Another point would be the suction of pF=7 or 1,000,000 kPa for dry conditions and the corresponding value of dielectric constant at the dry conditions, ε_{dry}. Another point would be the suction of 0 for saturated conditions and the corresponding value of dielectric constant at the saturated conditions, ε_{sat}. Thus, the curve-fitting with least mean square error would result in the parameters α and γ in the suction- dielectric constant curve. These values are presented in Table 20.

Table 20. Coefficients of Suction Dielectric Characteristic Curve for Materials Fabricated with the Gyratory and Impact Hammer Compaction Methods

Base Material	Compaction Method	α	ϒ
Pharr	Hammer	0.0144	0.7070
	SGC	0.0741	0.3457
Waco	Hammer	0.0751	0.6616
	SGC	0.0014	0.8054
Atlanta	Hammer	0.2859	0.2876
	SGC	0.0316	0.5507
San Antonio	Hammer	0.3054	0.2781
	SGC	0.0177	0.5817

The suction versus dielectric constant curves have been plotted in Figure 42 to Figure 44 for each material and each compaction method using the model parameters obtained from regression analysis. These curves can be applied in the prediction of matric suction of the soil structure with having the dielectric constant of the soil matrix. Then, the matric suction can be used in the SWCC curve to predict the volumetric water content and subsequently the moisture content of the soil matrix. These are distinctively different curves for the different compaction methods.

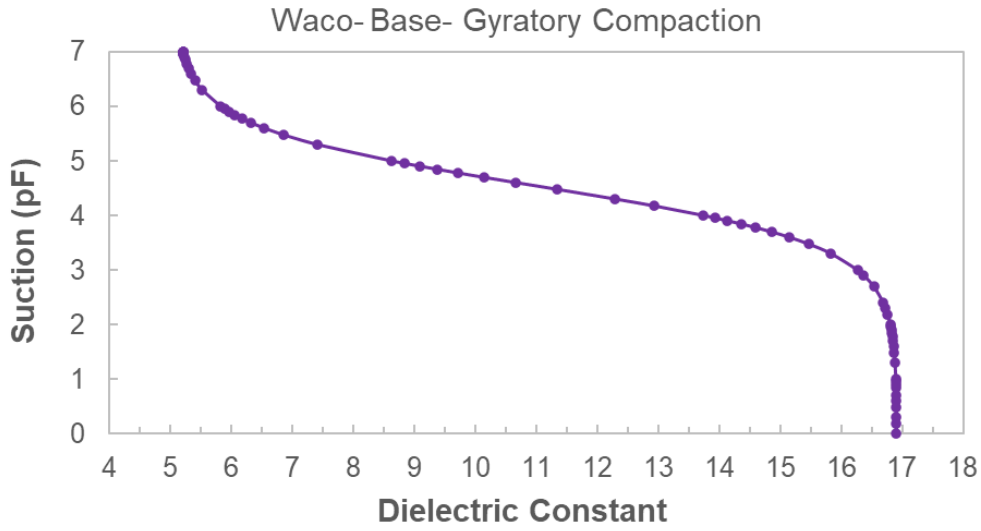

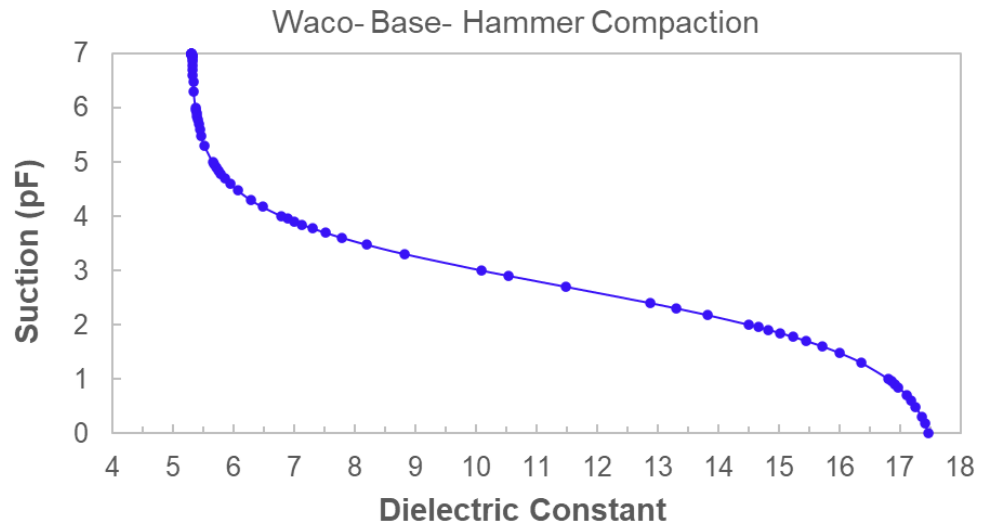

Figure 41. Suction Dielectric Constant Curve for Waco Base Course Compacted with Gyratory Compactor and Impact Hammer

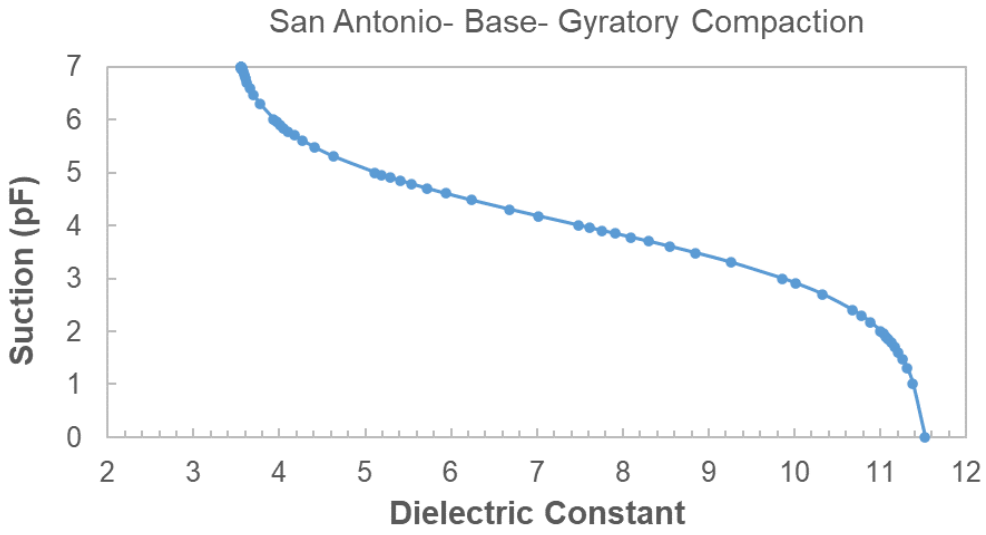

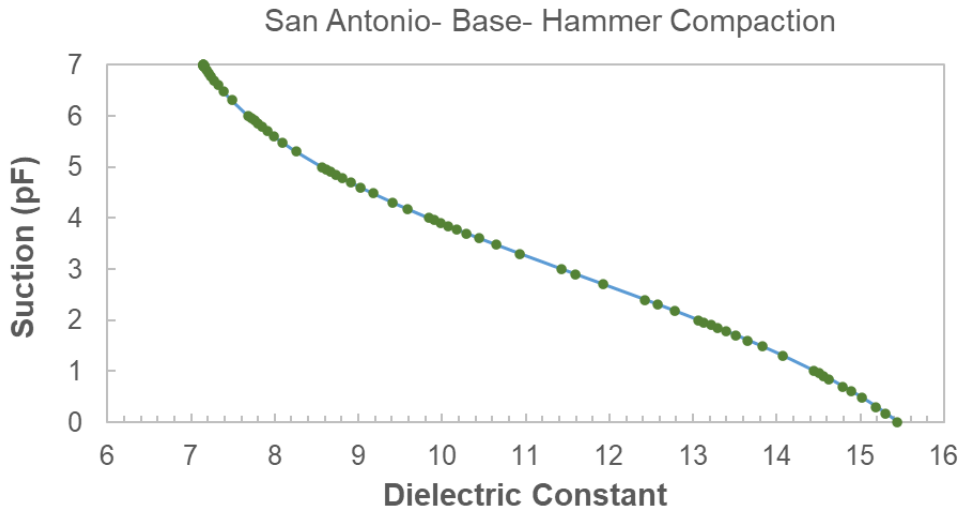

Figure 42. Suction Dielectric Constant Curve for San Antonio Base Course Compacted with Gyratory Compactor and Impact Hammer

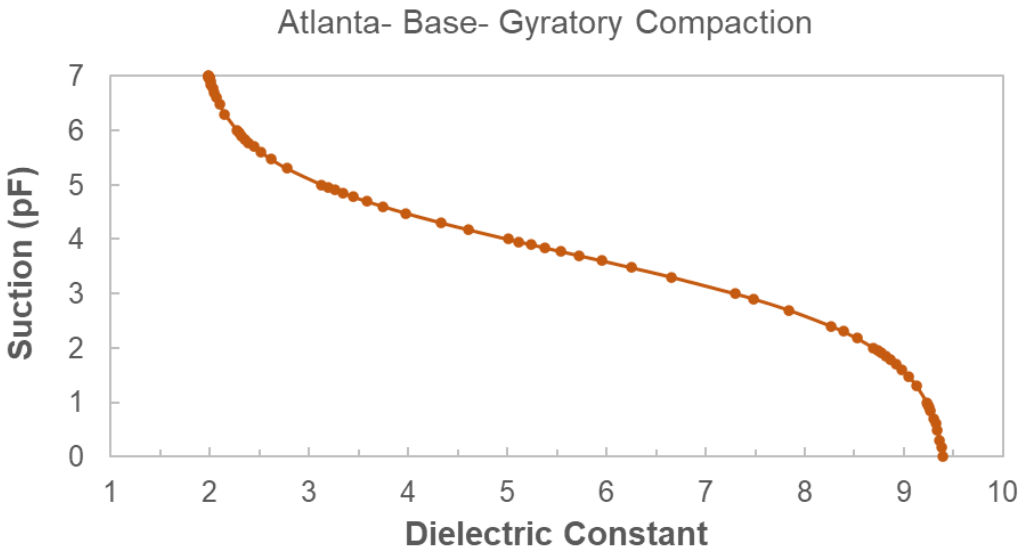

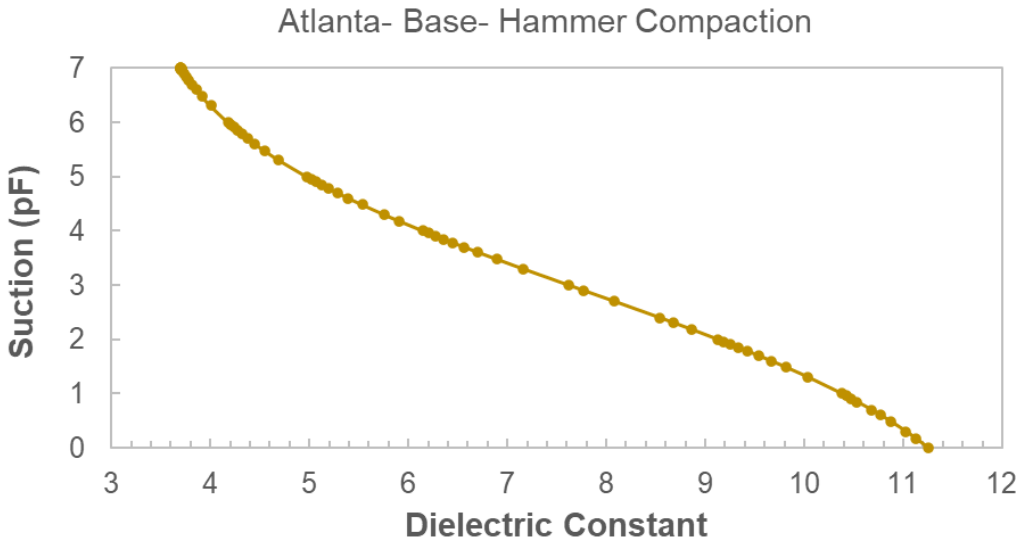

Figure 43. Suction Dielectric Constant Curve for Atlanta Base Course Compacted with Gyratory Compactor and Impact Hammer

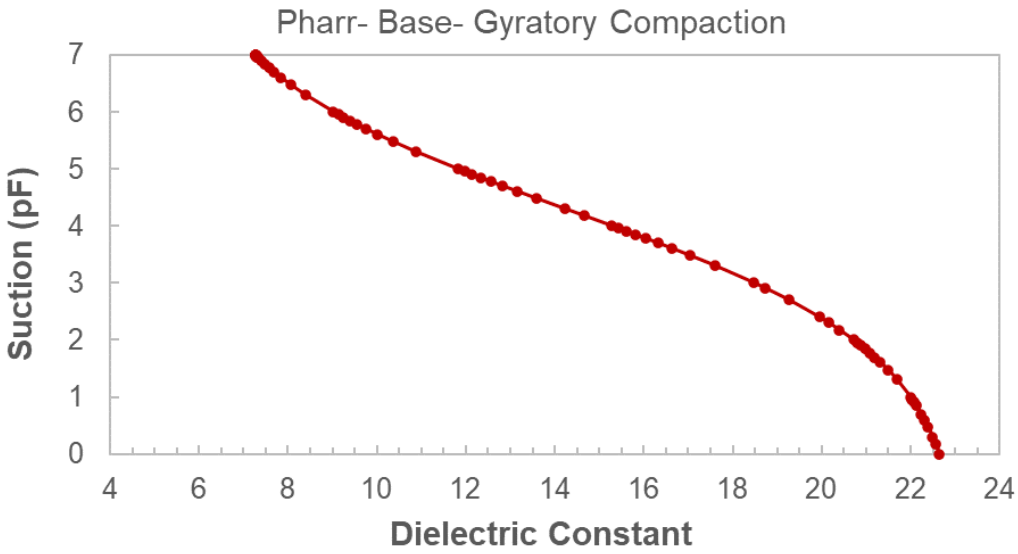

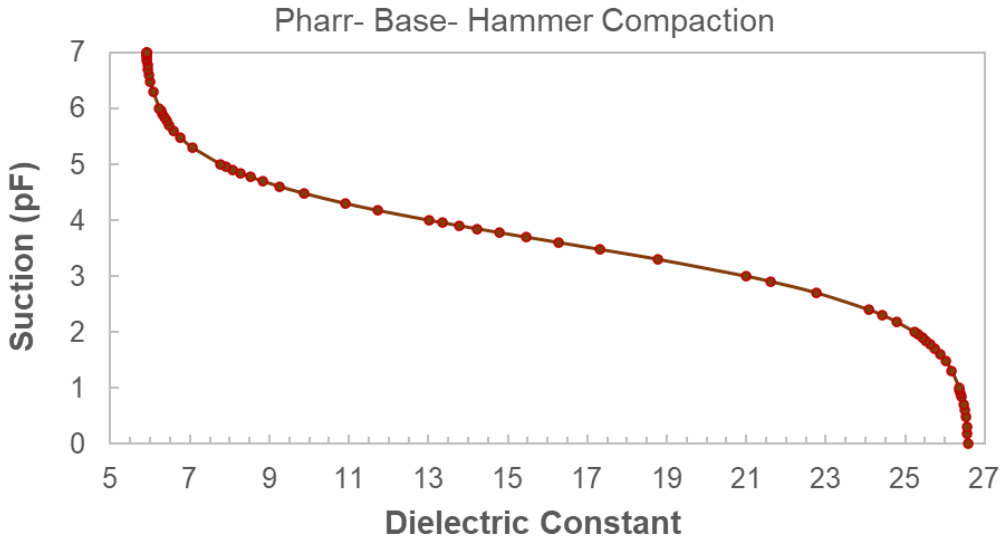

Figure 44. Suction Dielectric Constant Curve for Pharr Base Course Compacted with Gyratory Compactor and Impact Hammer

Having the soil suction versus dielectric constant can help engineers have an estimation of the suction, and moisture conditions using the Ground Penetrating Radar (GPR). GPR is a nondestructive testing technique that can used in the field for evaluation of the geometry of pavements, forensic analysis [19, 55, 56], and identification of damage to the pavement structure [55, 57]. The GPR measures the dielectric constant in the field. Using the curves developed in this study along with the measurements of the dielectric constant in the field with GPR can result in an estimation of the soil suction in the field. Then, the volumetric water content in the field can be estimated using the soil water characteristic curves described and generated in the previous chapter. Furthermore, the properties of soils such as resilient modulus and permanent deformation can be estimated using these properties. They can be useful tools for the evaluation of pavement conditions and forensic analysis. They can assist with early identification of pavement distresses and pavement needs for repair and maintenance and rehabilitation. The evaluation of the pavement conditions and application of the right treatments at the right time for the right pavement is very essential to keep the pavement network in satisfactory conditions and saves a lot of materials and resources [58, 59, 60, 61]. The tools in this study along with the GPR can help with the early notification of pavement problems and also the suitable time to proceed with the maintenance and rehabilitation.

5. CONCLUSIONS AND RECOMMENDATIONS

5.1. Summary and Conclusions

A series of experimental tests have been performed to investigate the engineering properties of the specimens of soils and granular materials compacted with the impact hammer and gyratory compaction methods in the laboratory. The results indicated that the gyratory compactor may offer a method to improve precision of the compressive strength test for unbound granular materials. Statistical analysis for equality of variance, *F*-test on the pooled variance, indicated that lower variance was observed in the compressive strength results of the specimens prepared with the gyratory compaction compared to the impact hammer compaction. Based on the unconfined strength test data, lower COV was also observed in the gyratory-compacted specimens than the impact hammer-compacted ones. Increasing the precision of the strength test can reduce the potential for disputes in test results among laboratories. The data showed that the optimum moisture content, OMC, obtained from the moisture dry density curve of the gyratory compaction was higher than the one determined from the impact hammer compaction by an average of almost one percent. Moreover, the maximum dry density, MDD, obtained from the gyratory compaction was slightly higher than the MDD determined from the impact hammer for the base course materials.

Furthermore, the material characteristics used in the mechanistic- empirical design of pavements are investigated in this study. Resilient modulus and permanent

deformation of materials have a significant effect on the long-term performance of layers and the pavement structure. The permanent deformation and resilient modulus tests showed that the gyratory-compacted samples had lower permanent strain values and higher resilient modulus compared to the hammer-compacted specimens for three of the four tested base materials with coarser aggregate structure, classified as gravel. Tseng-Lytton model and VESYS model were used for prediction of the permanent strain of base materials under cyclic loading. The generalized model and also the resilient model incorporating the matric suction and saturation conditions and stress states were used for prediction of the resilient modulus. Since resilient modulus is affected by the stress state and moisture and saturation conditions of the materials, the model which incorporates both of these factors was investigated.

The prediction models of the coefficients of the resilient modulus model were studied. The prediction models for the coefficients of the resilient modulus model were developed for the laboratory compaction methods used in this study and the different materials in this research. These models are dependent on the performance related properties, not just the empirical results. The prediction models for the coefficients of the resilient modulus model k_1, k_2, and k_3, were developed using multivariable regression analysis for the studied materials and compaction methods.

The parameters considered in this regression analysis were the maximum dry density, percent fines content (pfc), Methylene Blue Value (MBV), cumulative Weibull distribution parameters of AIMS parameters, i.e., angularity, texture, and sphericity. Parameters of cumulative Weibull distribution of AIMS results were the angularity

scale parameter and shape parameter, λ_A and a_A, respectively, texture scale parameter and shape parameter, λ_T and a_T, respectively, and sphericity scale parameter and shape parameter, λ_S and a_S, respectively. The parameters that were used in the developed equations for coefficients k_1, k_2, and k_3, of the resilient modulus model were maximum dry density, percent fines content (pfc), angularity scale parameter, λ_A, texture scale parameter, λ_T, and sphericity scale parameter λ_S. Two series of prediction models for coefficients of the resilient modulus model, k_1, k_2, and k_3, were developed for the specimens produced by the gyratory compactor and the impact hammer. It was discussed how these parameters could contribute to the coefficients of the resilient modulus model and ultimately to predict resilient modulus for each series of samples produced by impact hammer and gyratory compaction. The rise in angularity scale parameter, λ_A, generally increases the resilient modulus model. It is in accordance with the findings in the literature that increasing the angularity enhances the aggregate interlock and ultimately raises the resilient modulus.

It was also observed in the prediction model how the texture scale parameter, λ_T, can affect the coefficient k_3 in the resilient modulus model, and ultimately increase the resilient modulus. It is in accordance with the general presumption that the rise in the texture index can result in higher friction and resilient modulus. The coefficient k_3 impacts the role of the octahedral shear stress, τ_{oct}, in the resilient modulus model, as the exponent to the normalized octahedral shear stress. The gyratory compacted samples are subjected to shear stresses during the motions of the compaction process. The texture scale parameter, λ_T, has more contribution in the prediction model of k_3 for the

specimens compacted with gyratory compaction compared to impact hammer compaction.

The suction of the materials was also measured using filter paper test, and the soil water characteristic curve (SWCC) was also investigated in this study. The suction was measured for both samples prepared with the gyratory compaction and impact hammer compaction. The SWCC was developed for both of these samples through finding the SWCC model coefficients using the regression analysis and the experimental data. The SWCC for the gyratory compacted samples was generally above the SWCC for impact hammer compacted samples This indicated that the suction values are higher in the samples compacted with gyratory compaction than the ones made by impact hammer for the same volumetric water content. Thus, for a given water content, the higher suction in the gyratory-compacted samples generally produce a higher resilient modulus and lower permanent deformation, as were observed in the test results for three of the base course materials. The soil suction influences the behavior of the base course, and the SWCC can be used in prediction of most of the important properties of materials.

Furthermore, the equation for the relative compaction energy can help to quantify and distinguish between the compaction energy used for the compaction of different materials. All of the results substantiate the fact that the gyratory compaction produces a different mechanism of compaction from the impact hammer compaction. Totally transferring to the gyratory compaction would require some adjustments to the field

compaction targets. Considering all of these points, gyratory compaction can be a viable option for the laboratory compaction method.

In addition, nondestructive testing techniques were also used in this study. The CT scanning of the compacted specimens captured the voids between layers and the interface between the lifts in the specimens compacted with the impact hammer in some materials. The CT scans demonstrated that the gyratory compactor generally produced more uniform specimens.

Moreover, nondestructive test methods were performed through measurements of the dielectric constant of the materials. The dielectric constant of the materials was measured with Percometer for two series of materials fabricated with these two compaction methods. Using the CRIM model, the dielectric constant of the saturated and dry condition was estimated. Then, a function for the relationship between dielectric constant and suction was developed using the estimated saturated and dry dielectric constants. This relationship can ultimately help with estimation of the soil suction and soil moisture content using dielectric constant for both samples fabricated with the gyratory compactor and impact hammer. Therefore, we can have a method for predictions of properties of granular materials having an estimation of suction and moisture conditions. Many properties of soils are dependent on soil water content and soil suction. Moreover, determination of whether the gyratory compaction can simulate field conditions more accurately can be decided with non-destructive pavement evaluation techniques.

5.2. Recommendations for Future Work

The findings of this study can be used in the future research works to tie the laboratory results to the field data, and find which laboratory compaction method simulates the field conditions more realistically and accurately. In this study, precision of the strength test was investigated. The accuracy of data can also be studied. There are several research approaches that can be used to compare and associate the laboratory results with the field data. In this study, the relationship between the matric suction and the soil dielectric constant was investigated for the two compaction methods. Therefore, having the dielectric constant, one can predict the matric suction and moisture conditions. The volumetric water content can also be predicted using the soil water characteristic curves. The dielectric constant of the soil and granular materials in the field can be measured with Ground Penetrating Radar (GPR) as a nondestructive evaluation technique. The measured dielectric constant can be used in the suction versus dielectric constant curve, developed in this study, to estimate the matric suction of the soil in the field. Each of the curves of suction versus dielectric constant for samples compacted with the gyratory compaction and impact hammer can be used to estimate the soil suction in the field. Therefore, two curves or two series of matric suction values can be obtained using the dielectric constant measured by GPR using these two sets of developed curves. Then, these values of matric suction and corresponding volumetric water content can be used in the resilient modulus model to predict the resilient modulus in the field. Therefore, two sets of resilient modulus data are generated using the model and the two series of predicted suction data, one for the gyratory compaction and one for

the impact hammer compaction. Moreover, the resilient modulus of granular materials in pavement layers in the field can be estimated using the Falling Weight Deflectometer (FWD). Thus, the resilient modulus of the field materials obtained from the FWD data can be compared with the two series of resilient modulus data mentioned before, predicted by using the estimated soil suction and the resilient modulus model. Comparison of the resilient modulus from the FWD and the ones that are predicted with the resilient modulus model can help decide which sets of predicted resilient modulus are closer to the field conditions. It can be observed which compaction method results in the suction versus dielectric constant curve which ultimately results in the more accurate predicted resilient modulus/ suction. Therefore, it can be decided which compaction method can produce materials closer to the field conditions, and simulate the field conditions more realistically, by using nondestructive testing techniques.

Another approach is to measure the suction of the soils in the field. Then, this data can be compared with the two series of suction data estimated by using the dielectric constant obtained from GPR. One series of these suction values are estimated using the suction versus dielectric constant of the samples compacted with the gyratory compaction, and the other one uses the curve for samples compacted with impact hammer, as mentioned before. This comparison can help investigate whether the matric suction data in the field is closer to the suction estimated from suction versus dielectric constant curve for the gyratory compaction or impact hammer compaction. Therefore, it can be decided which curve and compaction method better represent the field conditions. Furthermore, there are some methods developed in the research group to predict the

water content and density of the soil by using the dielectric constant. Therefore, using the dielectric constant obtained with GPR in the field, the moisture content and the density can be estimated. These values can be compared with the density moisture content curves generated for impact hammer compaction and gyratory compaction in the laboratory. This comparison can assist with the determination of which compaction method can provide more realistic data and simulate field conditions better.

The material characteristics used in the mechanistic empirical design of pavements are investigated in this study. Resilient modulus and permanent deformation characteristics of materials have a significant effect on the long-term performance of materials and pavement structure. Using pavement management data and historical pavement performance data, if available, may also help decide which sets of characteristics result in a more realistic pavement performance prediction.

Further research is also recommended to investigate the compaction of sands with the SGC, especially the ones that have fines with high plastic fines. Determination of whether the gyratory compaction can more accurately simulate the field conditions can also be decided with measurements of a pavement in a full-scale test that, is currently under construction and uses gyratory compactor for the target values.

REFERENCES

1. Selig, E.T. Compaction Procedures, Specifications, and Control Considerations. Transportation Research Record 897, Transportation Research Board, National Research Council, 1982, pp. 1-8.

2. Proctor, R.R. Design and Construction of Rolled-Earth Dams, *Engineering News* Record, *Vol*. 3, 1933.

3. Sebesta, S., W. Liu, and P. Harris. Improving Lab Comapction Specifications for Flexible Bases within The Texas DOT, Publication FHWA/TX-09/0-5135-3. Texas Department of Transportation, Austin, TX, 2009.

4. Cominsky, R. j., G.A. Huber, T. W. Kennedy, and M. Anderson. The Superpave Mix Design Manual for New Construction and Overlays. Publication SHRP-A-407. Strategic Highway Research Program, National Research Council. Washington D.C., 1994.

5. Superpave Mix Design, Superpave Series No. 2 (SP-2). Asphalt Institute, Lexington, KY, 2001.

6. Ping, W. V., Z. Yang, M. Leonard, and S. Putcha. Laboratory Simulation of Field Compaction Characteristics on Sandy Soils. Transportation Research Record: Journal of the Transortation Research Board, No. 1808, 2002, pp. 84-95. https://doi.org/10.3141/1808-10

7. Developmentof the Gyratory Testing Machine and Procedures for Testing Bituminous Paving Mixtures. Technical Report No. 3-595, U.S. Army Corps of Engineers, Waterways Experiment Station, 1962.

8. Gyratory Compaction Method for Determining Density Requirements for Subgrade and Base of Flexible Pavements, Miscellaneous Paper No. 4-494, U.S. Army Corps of Engineers, Waterways Experiment Station, 1962.

9. Li, C., White, D. J., and Vennapusa, P. Moisture- Density- Strength- Energy Relationships for Gyratory Compacted Geomaterials. Geotechnical Testing Journal, 38 (4), 2015, pp. 461-473.

10. Mokwa, R., E. Cuelho, and M. Browne. Laboratory Testing of Soil Using the Superpave Gyratory Compactor. *Proceedings of Transportation Research Board 2008 Anuual Meeting*, Washington, D.C., 2008.

11. Epps, J., S. Sebesta, B. Hewes, H. Sahin, R. Luo, J. Button, R. Lytton, C.A. Herrera, R. Hatcher, F. Gu. Development of a Specification for Flexible Base Construction. Publication FHWA/TX-13/0-6621, Texas Department of Transportation (TxDOT), Austin, TX, 2014.

12. Tseng K., and R. Lytton. Prediction of Permanent Deformation in Flexible Pavement Materials, Implication of Aggregastes in the Design, Construction, and Performance of Felxible Pavememts. *ASTM STP 1016*, 1989, pp. 154-172.

13. Guide for Mechanistic-Empirical Design of New and Rehabilitated Pavement Structures, NCHRP 1-37A. National Cooperative Highway Research Program, Transportation Research Board, Washington, D.C., 2004.

14. Harmonized Test Methods for Laboratory Determination of Resilient Modulus for Flexible Pavement Design. NCHRP 1-28 A, National Cooperative Highway Research Program, Transportation Research Board, Washington, D.C., 2003.

15. Kenis, W. J. Predictive design procedures, VESYS users' manual: An interim design method for flexible pavements using the VESYS structural subsystem. Final Report Federal Highway Administration, Washington, D.C., 1978.

16. Korkiala-Tanttu, L. Verification of Rutting Calculation for Unbound Road Materials. Proceedings of the Institution of Civil Engineers, Transport, 162, 2009. pp. 107-114.

17. Sahin, H., F. Gu, and R. Lytton. Development of Soil-Water Characteristic Curve for Flexible Base Materials Using the Methylene Blue Test, Journal of Materials in Civil Enginering, 27, 2014.

18. Gu, F., H. Sahin, X. Luo, R. Luo, and R. Lytton. Estimation of Resilient Modulus of Unbound Aggregates Using Performance-Related Base Course Properties. Journal of Materials in Civil Engineering, 27, 2014.

19. Sahin, H., Nondestructive Test Methods for Rapid Assessment of Flexible Base Performance in Transportation Infrastructures. Ph.D. Dissertation. Texas A&M University, College Station, TX, 2014.

20. Fredlund, D.G., H. Rahardjo and M.D. Fredlund. Unsaturated Soil Mechanics in Engineering Practice. John Wiley Sons, Inc., Hoboken, NJ, 2012.

21. Chow, L., D. Mishra, and E. Tutumluer. Framework for Development of an Improved Unbound Aggregate Base Rutting Model for Mechanistic-Empirical Pavement Design. Transportation Ressearch Record: Journal of the Transortation Research Board, No. 2401 (1), 2014, pp. 11-21.

22. Gu, F., Y. Zhang, C. Droddy, R. Luo, and R. L. Lytton. Development of a New Mechanistic Empirical Rutting Model for Unbound Granular Material. Journal of Materials in Civil Engineering, 28 (8), 2016. DOI: 10.1061/(ASCE)MT.1943-5533.0001555.

23. Lytton, R. L. Foundations and Pavements on Unsaturated Soils. *1st* International. *Conference on Unsaturated Soils, Vol. 3, International Society*, Paris, France, 1995.

24. Osouli, A., S. Salam, and E. Tutumluer. Effect of Plasticity Index and Dust Ratio on Moisture-density and Strength Characteristics of Aggregates. Journal of Transportation Geotechnics, 9, 2016. pp. 69-79.

25. Arabali, P., S.I. Lee, S. Sebesta, M.S. Sakhaeifar, and R.L. Lytton. Application of Superpave Gyratory Compactor for Laboratory Compaction of Unbound Granular Materials. *International Conference on Transportation and Development*. Pittsburgh, PA, 2018.

26. Test Procedure for Triaxial Compression for Disturbed Soils and Base Materials, TEX-117-E. Texas Department of Transportation (TxDOT), Austin, TX, 2010.

27. Lee, S.I., S. Sebesta, P. Arabali, R. Lytton, and M. Sakhaeifar. Application of Superpave Gyratory Compactors for Flexible Base and Subgrade. Federal Highway Administration. Texas Department of Transportation, Austin, TX. 2019.

28. Standard Practice for Use of the Terms Precision and Bias in ASTM Test Methods, ASTM E177-14, ASTM International, West Conshohocken, PA, 2014.

29. Standard Practice for Comparing Test Methods, ASTM D 4855-97. ASTM International,West Conshohocken, PA, 2014.

30. Ott, R.L., and M. Longnecker. An Introduction to Statistical Methods and Data Analysi. Brooks/ Cole, Cengage Learning, Belmont, CA, 2016.

31. Test Procedure for Laboratory Compaction Characteristics and Moisture-Density Relationship of Base Materials, Tex-113-E. Texas Department of Transportation (TxDOT), Austin, TX., 2016.

32. Test Procedure for Laboratory Compaction Characteristics and Moisture-Density Relationship of Subgrade, Embankment Soils, and Bsckfil Material, Tex-114-E. Texas Department of Transportation (TxDOT), Austin, TX, 2011.

33. Arabali, P., S.I. Lee, S. Sebesta, R. L. Lytton, and M.S. Sakhaeifar. Comparison of Superpave Gyratory Compactor and Impact Hammer for Compaction of Unbound Granular Materials. 98th Transportation Research Board (TRB) Annual Meeting, Washington, D.C., 2019.

34. Salehi Ashtiani, R. Anisotropic Characterization and Performance Prediction of Chemically and Hydraulically Bounded Pavement Foundations, Ph.D. Dissertation. Texas A&M University, College Station, TX, 2009.

35. Fredlund D. and A. Xing, Equations for the Soil-water Characteristic Curve. Canadian Geotechnical. Journal, 31, 1994. pp. 521-532.

36. Saha, S., F. Gu, X. Luo and R.L. Lytton. Prediction of Soil-Water Characteristic Curve for Unbound Material Using Fredlund–Xing Equation-Based ANN Approach. *Journal of Materials in Civil Engineering*, 30 (5), 2018.

37. Bulut, R., C. Aubeny, and R. Lytton. Unsaturated Soil Diffusivity Measurements. International Symposium on Advanced Experimental Unsaturated Soil Mechanics, CRC Press, 2005.

38. Al-Rousan T., E. Masad, E. Tutumluer and T. Pan, Evaluation of Image Analysis Techniques for Quantifying Aggregate Shape Characteristics. *Construction and Building Materials*, vol. 21, no. 5, pp. 978-990, 2007.

39. Masad, E. A., Aggregate Imaging System (AIMS): Basics and Applications. Texas A&M Transportation Institute, Texas Department of Transportation, Austin, TX, 2005.

40. Mahmoud, E., L. Gates, S. Erdogan, and E. Garboczi. Comprehensive Evaluation of AIMS Texture, Angularity, and Dimension Measurements. Journal of Materials in Civil Engineering, 22 (4), 2010. pp. 369-379.

41. Pine Instrument. Aggregate Image Measurement System Manual. Pine Instrument Company, Grove City, PA, 2009.

42. R Core Team. R: A language and environment for statistical. R Foundation for Statistical Computing, Vienna, Austria., 2019. http://www.R-project.org/.

43. RStudio Team. RStudio: Integrated Development for R. RStudio, PBC, Boston, MA, 2019. http://www.rstudio.com/.

44. Gu, F., Y. Zhang, X. Luo, S. Sahin, and R. L. Lytton. Characterization and Prediction of Permanent Deformation Properties of Unbound Granular Materials for Pavement ME Design. Construction and Building Materials, 155, 2017. pp. 584-592.

45. Barksdale, R.D., and S. Y. Itani. Influence of Aggregate Shape on Base Behavior. Transportation Research Record, Journl of Transportation Research Board, No. 1227, 1989. pp. 173-182.

46. Tutumluer, E. and T. Pan. Aggregate Morphology Affecting Strength and Permanent Deformation Behavior of Unbound Aggregate Materials, Journal of Materials in Civil Engineering, 20 (9), 2008. pp. 617-627.

47. AASHTO. Mechanistic-empirical Pavement Design Guide: A Manual of Practice. American Association of State Highway and Transportation Officials, Washington, D.C., 2008.

48. Heath, A. C., J.M. Pestana, J.T. Harvey, and M. O. Bejerano. Normalizing Behavior of Unsaturated Granular Pavement Materials. Journal of Geotechnical and Geoenvironmental Engineering, 130 (9), 2004. pp. 896–904. 10.1061/(ASCE)1090-0241(2004).

49. Uzan, J. Characterization of Granular Material. Transportation Research Record, Transportation Research Board, 1022. 1985. pp. 52-59.

50. Saha, S., F. Gu, X. Luo, and R. L. Lytton. Use of an Artificial Neural Network Approach for the Prediction of Resilient Modulus for Unbound Granular Material. Transportation Research Record, Journal of Transportation Research *Board,* 2672 (52), 2018. pp. 23-33.

51. Huang, B., X. Chen, X. Shu, E. Masad, and E. Mahmoud. Effects of Coarse Aggregate Angularity and Asphalt Binder on Laboratory-measured Permanent Deformation Properties of HMA. International Journal of Pavement Engineering. 10 (1), 2009. pp. 19-28.

52. Allen, J. The Effect of Non-constant Lateral Pressures of the Resilient Response of Granular Materials, Ph.D. Thesis. University of Illinois at Urbana-Champaign, 1973.

53. Rao, C., E. Tutumluer, and I. Kim. Quantification of Coarse Aggregate Angularity based on Image Analysis, Transportation Research Record, Journal of Transportation Research Board, No. 1787, 2002. pp. 117-124.

54. *JMP*, *Version <15>*, Cary, NC,: AS Institute Inc., 1989-2020.

55. AL-Qadi, I. and S. Lahouar. Measuring layer thicknesses with GPR– Theory to practice. Construction and Building Materials, 19, 2005. pp. 763–772.

56. Shangguan, P. and I. L. Al-Qadi. Calibration of FDTD Simulation of GPR Signal for Asphalt Pavement Compaction Monitoring, IEEE Transsactions on Geoscience and Remote Sensing, 53 (3), 2015. pp. 1538-1548.

57. Morovatdar, A., S. R. Ashtiani, C. Licon, and C. Tirado. Development of a Mechanistic Approach to Quantify Pavement Damage using Axle Load Spectra from South Texas Overload Corridors. Geo-Structural Aspects of Pavements, Railways, and Airfields Conference (GAP 2019), Colorado Springs, CO, 2019.

58. Arabali, P., M. Sakhaeifar, T. J. Freeman, B.T. Wilson, and J.D. Borowiec. Decision-making Guideline for Preservation of Flexible Pavements in General Aviation Airport Management. Journal of Transportation Engineering, Part B: Pavements, 143 (2), 2017. DOI: 10.1061/JPEODX.0000002.

59. Peshkin, D., K. L. Smith, A. Wolters, J. Krstluovich, J. Moulthrop, and C. Alvarado. Guidelines for the preservation of highvolume-traffic roadways. Transportation Research Board, S2-R26-RR-2, Washington, D.C., 2011.

60. Arabali, P., M. Sakhaeifar, T. Freeman, B. Wilson, and J. Borowiec. Decision-making Tool for the Selection of Pavement Preservation Treatments in General Aviation Airport Pavements. International Conference on Transportation and Development, Houston, TX, 2016.

61. Shahin, M. Y. Pavement Management for Airports, Roads, and Parking Lots. Springer, New York, NY. 2005.

APPENDIX A.

THE RESILIENT MODULUS DATA FOR THE STUDIED MATERIALS TESTED UNDER THE REPEATED LOAD TRIAXIAL TESTS

Table A.1. Resilient Modulus Data for Atlanta Base Course Material Compacted with Gyratory Compactor

Loading Sequence No.	Resilient Modulus (ksi)	Loading Sequence No.	Resilient Modulus (ksi)
1	14.02	16	20.39
2	26.84	17	35.17
3	42.39	18	50.05
4	59.79	19	64.16
5	-	20	75.25
6	15.43	21	24.50
7	28.79	22	40.09
8	44.18	23	54.68
9	60.50	24	67.88
10	74.44	25	78.00
11	18.04	26	28.02
12	32.22	27	44.13
13	47.32	28	58.56
14	62.26	29	71.33
15	74.35	30	81.04

Table A.2. Matric Suction and Volumetric Water Content for Atlanta Base- Gyratory

Suction at Optimum Moisture Content (kPa)	Volumetric Water Content
-209.694	0.1498

Table A.3. Resilient Modulus Data for Atlanta Base Course Material Compacted with Impact Hammer Compaction

Loading Sequence No.	Resilient Modulus (ksi)	Loading Sequence No.	Resilient Modulus (ksi)
1	12.31	16	17.76
2	20.60	17	28.90
3	30.57	18	42.55
4	42.87	19	55.32
5	-	20	67.11
6	13.84	21	22.93
7	21.29	22	38.79
8	32.43	23	54.49
9	47.76	24	70.74
10	59.84	25	83.82
11	16.09	26	28.58
12	26.30	27	48.05
13	39.23	28	68.53
14	53.14	29	87.87
15	60.96	30	114.70

Table A.4. Matric Suction and Volumetric Water Content for Atlanta Base- Impact

Suction at Optimum Moisture Content (kPa)	Volumetric Water Content
-8.224	0.1442

Table A.5. Resilient Modulus Data for San Antonio Base Course Material Compacted with Gyratory Compactor

Loading Sequence No.	Resilient Modulus (ksi)	Loading Sequence No.	Resilient Modulus (ksi)
1	26.39	16	69.71
2	48.42	17	123.53
3	-	18	196.55
4	117.13	19	275.42
5	-	20	390.27
6	37.07	21	100.52
7	65.72	22	184.65
8	-	23	290.57
9	156.29	24	289.17
10	-	25	-
11	79.80	26	83.09
12	101.90	27	126.24
13	163.12	28	-
14	215.02	29	-
15	251.05	30	-

Table A.6. Matric Suction and Volumetric Water Content for San Antonio- Gyratory

Suction at Optimum Moisture Content (kPa)	Volumetric Water Content
-44.100	0.1739

Table A.7. Resilient Modulus Data for San Antonio Base Course Material Compacted with Impact Hammer

Loading Sequence No.	Resilient Modulus (ksi)	Loading Sequence No.	Resilient Modulus (ksi)
1	36.19	16	32.56
2	50.30	17	52.73
3	68.18	18	75.12
4	104.82	19	94.06
5		20	114.94
6	31.58	21	34.44
7	46.62	22	57.57
8	67.43	23	90.66
9	93.49	24	126.69
10	119.20	25	
11	32.10	26	52.78
12	55.36	27	
13	76.97	28	
14	101.48	29	
15	115.90	30	

Table A.8. Matric Suction and Volumetric Water Content for San Antonio- Impact

Suction at Optimum Moisture Content (kPa)	Volumetric Water Content
-2.199	0.1432

Table A.9. Resilient Modulus Data for Pharr Base Course Material Compacted with Gyratory Compactor

Loading Sequence No.	Resilient Modulus (ksi)	Loading Sequence No.	Resilient Modulus (ksi)
1	21.17	16	17.20
2	25.85	17	21.20
3	29.49	18	29.50
4	32.95	19	37.14
5	-	20	42.24
6	21.30	21	-
7	22.19	22	-
8	26.90	23	30.15
9	34.81	24	35.59
10	41.78	25	42.83
11	17.67	26	-
12	20.58	27	-
13	28.79	28	-
14	37.05	29	-
15	41.83	30	-

Table A.10. Matric Suction and Volumetric Water Content for Pharr Base- Gyratory

Suction at Optimum Moisture Content (kPa)	Volumetric Water Content
-104.558	0.2575

Table A.11. Resilient Modulus Data for Pharr Base Course Material Compacted with Impact Hammer

Loading Sequence No.	Resilient Modulus (ksi)	Loading Sequence No.	Resilient Modulus (ksi)
1	12.86	16	16.65
2	20.12	17	24.25
3	27.57	18	30.94
4	34.95	19	36.73
5	-	20	41.02
6	13.74	21	18.90
7	21.12	22	26.55
8	28.37	23	32.90
9	35.25	24	38.21
10	40.67	25	42.07
11	15.30	26	20.74
12	22.82	27	28.38
13	29.76	28	34.51
14	35.97	29	39.55
15	40.66	30	43.21

Table A.12. Matric Suction and Volumetric Water Content for Pharr Base- Impact

Suction at Optimum Moisture Content (kPa)	Volumetric Water Content
-215.293	0.2310

Table A.13. Resilient Modulus Data for Waco Base Course Material Compacted with Gyratory Compactor

Loading Sequence No.	Resilient Modulus (ksi)	Loading Sequence No.	Resilient Modulus (ksi)
1	41.02	16	29.04
2	39.47	17	49.17
3	55.49	18	69.06
4	58.62	19	79.88
5	73.54	20	94.56
6	17.14	21	30.84
7	30.34	22	49.28
8	74.84	23	68.59
9	62.63	24	90.63
10	77.88	25	109.85
11	32.78	26	33.02
12	53.50	27	54.88
13	76.52	28	78.27
14	70.26	29	102.70
15	86.39	30	123.95

Table A.14. Matric Suction and Volumetric Water Content for Waco Base- Gyratory

Suction at Optimum Moisture Content (kPa)	Volumetric Water Content
-19.573	0.1895

Table A.15. Resilient Modulus Data for Waco Base Course Material Compacted with Impact Hammer

Loading Sequence No.	Resilient Modulus (ksi)	Loading Sequence No.	Resilient Modulus (ksi)
1	18.02	16	30.73
2	40.28	17	48.03
3	49.56	18	66.61
4	72.93	19	87.26
5	-	20	101.41
6	23.66	21	33.44
7	47.19	22	56.01
8	60.68	23	70.31
9	76.83	24	89.20
10	92.49	25	121.34
11	31.54	26	37.25
12	50.67	27	69.41
13	72.07	28	105.74
14	86.18	29	149.68
15	103.65	30	-

Table A.16. Matric Suction and Volumetric Water Content for Waco Base- Impact

Suction at Optimum Moisture Content (kPa)	Volumetric Water Content
-2.408	0.1721